Theoretical Studies of the Nonlinear Optical Properties of Organic Materials

Thesis by

Daqi Lu

In Partial Fulfillment of the Requirements

for the Degree of

Doctor of Philosophy

California Institute of Technology

Pasadena, California

2000

(Submitted Nov 19, 1999)

To my parents

Acknowledgements

I would like to thank the following people:

1. Mentor Bill Goddard for his guidance and support.

2. Prof. Guanhua Chen, Prof. Seth Marder and Prof. Jason Perry for the cooperation on this project.

3. Group members, Guanghua Gao, Jinsong Hu, Xinlei Hua, Rick Muller, Yuejin Guo, Ersan Demiralp, Siddharth Dasgupta, Mario Blanco, Tahir Cagin, Matt Carlson, Derek Debe,Cecco Faglioni, Darryl Willick, and Yongchun Tang for their help.

4. IQC coworkers, Eric Wu, Derek Xu, Bill Larsen, C. J. Stoltman, John Busby, Li Ping, Scott Louie, and Connie Chan for going through the frustration and happiness of an Internet startup with me.

5. My wife, Winnie Wang, for her patience and understanding.

Contents

List of Figures

List of Tables

Chapter 1 Introduction

There is a great deal of interest in developing organic nonlinear optical (NLO) materials[1] for use in

1. optical processing of data/images,
2. optical storage of data/images
3. optically based telecommunications, and
4. optically based computers.

The important properties for these applications are the hyperpolarizabilities, which describe how the dipole moment (μ) depends on an applied electric field ($\mathcal{E}$),

$$\mu_i(\mathcal{E}) = \mu_i + \alpha_{ij}\mathcal{E}_i + \beta_{ijk}\mathcal{E}_j\mathcal{E}_k + \gamma_{ijkl}\mathcal{E}_j\mathcal{E}_k\mathcal{E}_l + ... \tag{1.1}$$

Here α, β, and γ are the polarizability, first hyperpolarizability, and second hyperpolarizability, respectively.

The properties of most interests are β and γ which control

1. frequency doubling (better focus, more data),
2. changes in refractive index (electro-optical switches for telecommunications), and
3. frequency mixing.

Currently $LiNbO_3$ is the material of choice for these applications[1]. However, polymers would provide great advantages in ease of processing and for tailoring the properties to match precise requirements.

Recent advances in developing new high β, γ organic materials[2-3] include the development of such materials such as polymer in Figure 1.1. The general pattern

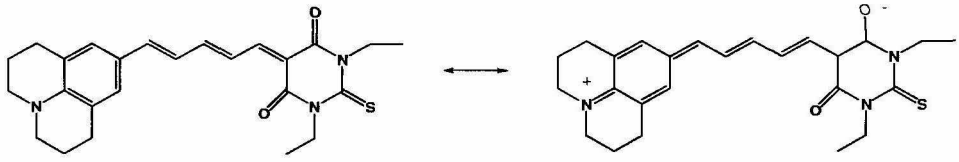

Figure 1.1: Molecule with high β

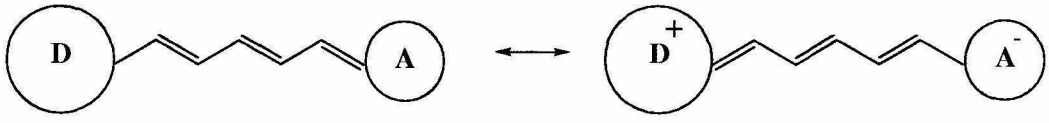

Figure 1.2: Donor acceptor type molecule

for good NLO materials are donor acceptor type molecules with a conjugated chain in between (Figure 1.2).

A typical approach for predicting polarizabilities involves summing over intermediate states formed from molecular orbitals. Thus for a laser frequency ω, the polarizability and hyperpolarizabilities have the form (2.31) - (2.33). Given a good description of the excited states, this sum-over-states approach can be used to predict accurate values of α, β, and γ. However,there are two problems:

1. It rapidly becomes complicated and expensive as system size increases.

2. There is no obvious relationship between α,β,γ or between these properties and other properties of the system.

We have developed a new approach (denoted VB-CT) for predicting NLO properties. There are four models in this approach to describe the relationship between the NLO properties and the linker (VB-CT-E), the structure (VB-CT), the solvent (VB-CT-S), and the temperature (VB-CT-T). For the past few years, this model has gained vast popularity and has become the standard model for predicting the NLO properties of conjugated system. A partial list of the papers that reference VB-CT model is in reference 10-60.

In order to accurately predict the NLO properties, we also did *ab initio* calculations on long polyacetylene chain[8] and polymers[9] with the best NLO properties at both Hartree Fock and DFT level. The results agree well with the experiment.

1.1 Valence-Bond Charge-Transfer Exciton (VB-CT-E) Model[4]

In Chapter 2, we develop a theory to predict the polarizability (α), second hyperpolarizability (γ), and the saturation lengths for nine polymeric materials. The theory (VB-CT-E) is based on a valence-bond view on the ground and excited states and considers the excited states as charge transfer excitons. It involves just two parameters which can be extracted from simple molecular orbital calculations and/or from experimental values of bandgap and bandwidth. For the one system (oligothiophenes) with experimental data on saturation length, the predicted L_γ and L_α are in good agreement with experiment.

1.2 Valence-Bond Charge-Transfer (VB-CT) Model[5]

In Chapter 3, we describe the nonlinear optical properties of charge-transfer organic materials in the framework of a simple valence-bond charge-transfer model. This model leads to analytic formulas for the absorption frequency, hyperpolarizabilities, and bond length alternation, all of which are described in terms of two parameters, V, and t related to the bandgap, and bandwidth. This model provides a clear physical picture for the dependence of the hyperpolarizabilities on the structure of charge-transfer molecules and leads to good agreement with the trends predicted by the AM1 calculations.

1.3 Valence-Bond Charge-Transfer Solvent (VB-CT-S) Model[6]

In Charpter 4, we develop a model to precit the solvation effect on the NLO properties of charge transfer organic materials such as 1,1 dicyano,6-(di-butyl amine) hexatriene.

This model is based on the VB-CT framework, using a continuum description of the solvent. The resulting model leads to analytic formulas for the absorption frequency, the hyperpolarizabilities, and the bond length alternation with only one solvent dependent parameter ϵ (the dielectric constant of the solution). The theory involves just four solvent-independent parameters, V_0, t, S_F, and Q, which are related to the bandgap, bandwidth, geometry, and dipole moment of the CT molecule. The results are in good agreement with experiment.

1.4 Valence-Bond Charge-Transfer Temperature (VB-CT-T) Model[7]

In Chapter 5, we predict the temperature effect on the NLO properties of the charge transfer organic materials. This model is based on the valence-bond charge-transfer (VB-CT) framework, but considers the effect of finite temperatures on the hyperpolarizabilities. This leads to *analytic* formulae for the hyperpolarizabilities as the function of temperature. Both electronic and vibrational contributions to the hyperpolarizabilities are discussed in this model.

1.5 Saturation of the Second Hyperpolarizability for Polyacetylenes[8]

Polyacetylene (PA) polymers $-(-CH=CH-)_N-$ lead to large second hyperpolarizabilities (γ) that increase with N. For small N the increase is quite rapid, eventually saturating (becoming linear in N) for $N \geq N_{sat}^{\gamma}$. Both experimental and theoretical attempts have been made to estimate N_{sat}^{γ}. In 1994 this led to two *Science* papers, one obtaining $N_{sat}^{\gamma} = 20$ (semiempirical theory) and the other obtaining $N_{sat}^{\gamma} = 125$ (experiment, but on a substituted disordered form of PA)! In Chapter 6, we did *ab initio* calculations up through $N = 49$ ($C_{98}H_{100}$) and show that $N_{sat}^{\gamma} = 45 \pm 5$. The much larger experimental value, $N_{sat}^{\gamma} = 125$, is explained in terms of the structural defects and disorder introduced by the synthetic method.

1.6 *ab initio* Predictions of Large Hyperpolarizabilities Push-Pull Polymers[9]

Recently significant advances have been made in engineering push-pull organic chromophores to have very large hyperpolarizabilities (β), leading to materials with $\mu \cdot \beta$ as high as 15,000 10^{-48} esu. Such developments have been slow and costly because of difficulties in synthesis, purification, and measurement. As an alternative we have developed a new Quantum Mechanical program (Jaguar/NLO) which provides predictions of β for such molecules far faster than previously possible. In Chapter 7, We have applied Jaguar/NLO to predicting α, β, and γ for the high β push-pull organics and find excellent agreement with experiment.

In summary, VB-CT model provides a qualititive framework, and *ab initio* calculation provides an accurate prediction for the NLO properties of organic materials. Combined together, these methods can be used as an effective tool for developing new nonlinear optical materials.

1.7 References

1. Prasad, P. N.; Williams, D. J. Eds, *Introduction to Nonlinear Optical Effects in Molecules and Polymers*; Wiley: New York, 1991.

2. Marder, S. R. *et al.*, *Science* **263**, 511(1994).

3. Marder, S. R.; Torruellas, W. E.; Blancharddesce, M.; Ricci, V. *et al.*, *Science* 1997, **276**, 1233.

4. Lu, D.; Chen, G.; Goddard, W. A. III, *J. Chem. Phys.* **101**, 4920 (1994).

5. Lu, D.; Chen, G.; Perry, J.; Goddard, W. A. III, *J. Am. Chem. Soc.* **116**, 10679 (1994).

6. Chen, G.; Lu, D.; Goddard, W. A. III, *J. Chem. Phys.* **101**,5860 (1994).

7. Lu, D.; Chen, G.; Goddard, W. A. III, *J. Phys. Chem.* Submitted.

8. Lu, D.; Marten, B.; Freisner, R. A.; Goddard, W. A. III, *Chem. Phys. Lett.* **257**, 224 (1996).

9. Lu, D.; Marten, B.; Cao, Y.; Ringnalda, M.; Freisner, R. A.; Goddard, W. A. III, *Chem. Phys. Lett.* **242**, 543 (1995).

10. Bartkowiak, W.; Lipinski, J., *Chem. Phys. Lett.* **292**, 92 (1998)

11. Bartkowiak, W.; Lipinski, J., *J. Phys. Chem.* **A 102**, 5236 (1998)

12. Barzoukas, M.; Runser, C.; Fort, A. *et al.*, *Chem. Phys. Lett.* **257** 531 (1996)

13. Bishop, D. M.; Champagne, B.; Kirtman, B., *J. Chem. Phys.* **109** 9987 (1998)

14. Bublitz, G. U.; Ortiz, R.; Marder, S. R., *et al.*, *J. Am. Chem. Soc.* **119** 3365 (1997)

15. Chen, G.; Mukamel, S., *J. Chem. Phys.* **103**, 9355 (1995)

16. Castiglioni, C.; DelZoppo, M.; Zerbi, G., *Phys. Rev.* **B 53**, 13319 (1996)

17. Cho, M.; Kim, H. S.; Jeon, S. J., *J. Chem. Phys.* **108**, 7114 (1998)

18. Cho, M., *J. Chem. Phys.* **106**, 7550 (1997)

19. Cho, M., *J. Phys. Chem.* **A 102**, 703 (1998)

20. Cho, M., *J. Phys. Chem.* **A 103**, 4712 (1999)

21. Dehu, C.; Meyers, F.; Hendrickx, E. *et al.*, *J. Am. Chem. Soc.* **117**, 10127 (1995)

22. Del Zoppo, M.; Castiglioni, C.; Gerola, V. *et al.*, *J. Opt. Soc. Am.* **B 40**, 308 (1998)

23. Del Zoppo, M.; Castiglioni, C.; Zuliani, P. *et al.*, *J. Appl. Polym. Sci.* **70**, 1311 (1998)

24. Fanti, M.; Fowler, P. W.; Orlandi, G. *et al.*, *J. Chem. Phys.* **107**, 5072 (1997)

25. Fanti, M.; Zerbetto, F., *Chem. Phys. Lett.* **285**, 180 (1998)

26. Gao, J. L.; Alhambra, C., *J. Am. Chem. Soc.* **119**, 2962 (1997)

27. Geskin, V. M.; Bredas, J. L., *J. Chem. Phys.* **109**, 6163 (1998)

28. Kamos, D. R. *et al.*, *J. Phys. Chem.* **99**, 11061 (1995)

29. Kim, H. S.; Cho, M. H.; Jeon, S. J., *J. Chem. Phys.* **107**, 1936 (1997)

30. Kim, S. Y.; Lee, M.; Boo, B. H., *J. Chem. Phys.* **109**, 2593 (1998)

31. Kryachko, E. S., *J. Phys. Chem.* **A 103**, 4368 (1999)

32. Luo, Y.; Agren, H.; Koch, H. *et al.*, *Phys. Rev.* **B 51**, 14949 (1995)

33. Lee, H.; An, S. Y.; Cho, M. H., *J. Phys. Chem.* **B 103**, 4992 (1999)

34. Lee, Y. K.; Jeon, S. J.; Cho, M. H., *J. Am. Chem. Soc.* **120**, 10921 (1998)

35. Lipinski, J.; Bartkowiak, W., *Chem. Phys.* **245**, 263 (1999)

36. Marder, S. R.; Kippelen, B. *et al.*, *Nature* **388**, 845 (1997)

37. Markovic, R.; Baranac, M., *J. Am. Chem. Soc.* **64**, 311 (1999)

38. Martin, R. E.; Diederich, F., *Angew. Chem. Int. Edit.* **38**, 1350 (1999)

39. Matyushov, D. V.; Ladanyi, B. M., *J. Phys. Chem.* **A 102**, 5027 (1998)

40. Matyushov, D., *Chem. Phys.* **211**, 47 (1996)

41. Moura, G.; Simas, A. M.; Miller, J., *Chem. Phys. Lett.* **257**, 639 (1996)

42. Perry, J. W.; Marder, S. R.; Meyers, F. *et al.*, *Acs. Sym. Ser.* **601**, 45 (1995)

43. Painelli, A., *Chem. Phys.* **245**, 185 (1999)

44. Painelli, A., *Synthetic. Met.* **101**, 218 (1999)

45. Painelli, A., *Chem. Phys. Lett.* **285**, 352 (1998)

46. Remacle, F., *Chem. Phys. Lett.* **291**, 453 (1998)

47. Remacle, F.; Collier, C. P.; Markovich, G. *et al.*, *J. Phys. Chem.* **B 102**, 7727 (1998)

48. Sujatha, K.; Ravichandran, G.; Govindan, K., *J. Indian. Chem. Soc.* **75**, 37 (1998)

49. Szablewski, M.; Thomas, P. R.; Thornton, A. *et al.*, *J. Am. Chem. Soc.* **119**,3144 (1997)

50. Thompson, W. H.; Blanchard-Desce, M.; Alain, V. *et al.*, *J. Phys. Chem.* **A 103**, 3766 (1999)

51. Thompson, W. H.; Blanchard-Desce, M.; Hynes, J. T., *J. Phys. Chem.* **A 102**, 7712 (1998)

52. Torii, H.; Tasumi, M., *J. Phys. Chem.* **B 101**, 466 (1997)

53. Torii, H.; Furuya, K.; Tasumi, M., *J. Phys. Chem.* **A 102**, 8422 (1998)

54. Tykwinski, R. R.; Gubler, U.; Martin, R. E. *et al.*, *J. Phys. Chem.* bf B 102, 4451 (1998)

55. Wortmann, R.; Bishop, D., *J. Chem. Phys.* **108**, 1001 (1998)

56. Xie, R.; Rao, Q., *Appl. Phys. Lett.* **72**, 2358 (1998)

57. Yang, M.; Kim, J. Y.; Jung, Y. *et al.*, *J. Chem. Phys.* **108**, 4013 (1998)

58. Zuliani, P.; Delzoppo, M.; Castiglioni, C. *et al.*, *J. Chem. Phys.* **103**, 9935 (1995)

59. Zhang, Y.; Lu, Z., *Theochem. Mol. Struc.* **467**, 233 (1999)

60. Zyss, J.; Nicoud, J., *Curr. Opin. Solid. St. M* **1**, 533 (1996)

Chapter 2 The Valence-Bond Charge-Transfer-Exciton ($VB - CTE$) Model for Predicting Nonlinear Optical Properties of Polymeric Materials

2.1 Introduction

Nonlinear optical (NLO) properties are important in numerous applications from lasers to optical switches and electronics.[1] Some of the best NLO properties are displayed by organic materials, for example charge-transfer type organic molecules where contributions to NLO come mostly from charge resonance between the donor and acceptor.[2] However, for molecules with a long polylene bridge, the bridge can also contribute significantly, leading to even better nonlinear optical properties. Thus S. Marder and coworkers[3] have shown that crystal (Figure 2.1) lead to $\gamma = 10^{-34}$ esu.

Although NLO properties improve with increasing length of the polymer bridge, experiments[4] indicate that it saturates near 7 units for oligothiophenes (Figure 2.2).

In order to design and optimize such materials, it is of interest to predict the NLO properties as a function of donor and acceptor, as a function of the nature and length of the polymer bridge, and as a function of solvent. There have been many recent theoretical[5–8] and experimental[3] studies directed at understanding and

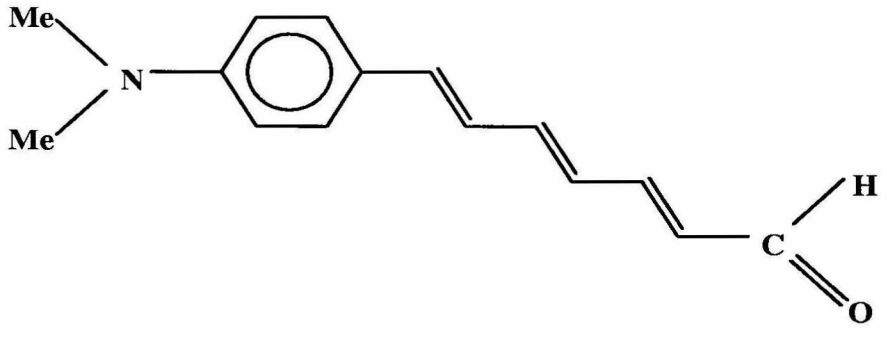

Figure 2.1: Molecule with good NLO properties

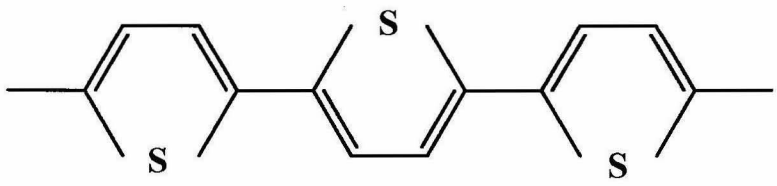

Figure 2.2: Polymer oligothiophene

optimizing the NLO properties of organic compounds. The conventional method of calculating hyperpolarizabilities consists of calculating the occupied and excited molecular orbitals of a molecule and summing over the excited states,[9] equations (2.31) to (2.33). These methods work well for small molecules; however, for large and complex molecules, such methods rapidly become extremely tedious and compute intensive.

We develop here an alternate approach based on a valence-bond view of the bonding and a charge-transfer-exciton view of the excited states. This method allows very rapid calculations and leads to results in good agreement with experiment. With an additional approximation it leads to analytical formulae that provide physical insight into the factors determining the magnitude of α and γ and the saturation length.

2.2 The Valence-Bond Charge-Transfer-Exciton (VB-CTE) View of Polymer Excited States

2.2.1 The Hamiltonian

As a prototype we will use a rigid-chain polymer with N monomers and take N to be odd for convenience. We assume that the most important states of the polymer can be discribed with a valence-bond (VB) description using only the highest-occupied molecular orbital (HOMO) and the lowest-unoccupied molecular orbital (LUMO) of each monomer unit. In the ground state the HOMO is doubly occupied and the LUMO is empty. Now consider the excitation of a monomer (site p) near the middle of a long polymer. The occupied LUMO may be considered as on the same monomer

(leading to a covalent excitation energy ΔE_c), or on adjacent monomers (sites $p\pm$ 1), or on sites farther away (sites $p \pm 2$, $p \pm 3$, etc.). We let ϕ_{pq} denote the many electron charge-transfer-exciton wavefunction in which an electron at site p is excited to a monomer q units the right of p leaving a hole at site p. Considering a fixed site p for the hole, the Hamiltonian matrix between various ϕ_{pq} becomes

$$H^{(o)} = \begin{pmatrix} \ddots & & & & & & & & \\ & \ddots & & & & & & & \\ & & \ddots & & & & & & \\ & & -t & V_{-2} & -t & & & & \\ & & & -t & V_{-1} & at & & & \\ & & & & at & 0 & -at & & \\ & & & & & -at & V_1 & -t & \\ & & & & & & -t & V_2 & -t \\ & & & & & & & & \ddots \\ & & & & & & & & \ddots \\ & & & & & & & & & \ddots \end{pmatrix}, \tag{2.1}$$

where matrix elements are kept only between adjacent sites. The diagonal matrix elements V_q are the energy required to remove one electron from the LUMO of one monomer and place it in the HOMO of the monomer q units away. They become

$$V_q = \langle \phi_{pq} | \mathcal{H} | \phi_{pq} \rangle = IP - EA - \frac{e^2}{\epsilon |q| R_o}, \tag{2.2}$$

where IP is the ionization potential of the monomer, EA is the electron affinity of the monomer, R_o is the distance between the nearest monomer centers, and q is the number of monomers between the donor and acceptor states ($q = \pm 1, \pm 2$, etc.). The transfer matrix elements are

$$-t = \langle \phi_{pq} | \mathcal{H} | \phi_{p,q+1} \rangle \qquad if \qquad |q| > 1 \tag{2.3}$$

$$-at = \langle \phi_{p0} | \mathcal{H} | \phi_{p1} \rangle \qquad if \qquad q = 1 \tag{2.4}$$

$$at = \langle \phi_{p,-1} | \mathcal{H} | \phi_{p0} \rangle \qquad if \qquad q = -1 \tag{2.5}$$

where the opposite sign of the matrix elements for $q = \pm 1$ arise from the antisymmetric LUMO and HOMO of butadiene (see Appendix A and Fig. A.1). We have ignored the covalent excitation at $q = 0$ because it does not contribute to changes in the dipole moment.

The evaluation of the matrix element t and constant a is discussed in Appendix A where we find that for the butadiene unit of thiophene

$$t = 0.36\beta \tag{2.6}$$

$$a = \sqrt{2} \tag{2.7}$$

where β is the resonance integral between the adjacent sp^2 carbon orbitals.

2.2.2 Dipole Moment

Writing the dipole operator as $\mu = \sum_l q_l R_l$ where q_l is the charge on monomer l,the Hamiltonian in an electric field $\mathcal{E}$ becomes

$$H = H^0 - \mu \cdot \mathcal{E}. \tag{2.8}$$

In order to examine the polarizability and hyperpolarizability, we need matrix elements of the dipole operators.

$$P_{ij,\alpha} = \langle \phi_{pi} | \mu_\alpha | \phi_{pj} \rangle \tag{2.9}$$

where α is the component (x, y, or z). Assuming that only the component along the polymer axis (say z) is important, this leads to

$$P_{ij,z} = \langle \phi_{pi} | \sum_l q_l R_l | \phi_{pj} \rangle = \delta_{ij}(-eR_i) \tag{2.10}$$

and the dipole moment matrix becomes

$$P_z = \begin{pmatrix} \ddots & & & & & & & \\ & \ddots & & & & & & \\ & & \ddots & & & & 0 & \\ & & & -2eR_0 & & & & \\ & & & & -eR_0 & & & \\ & & & & & 0 & & \\ & & & & & & eR_0 & \\ & & 0 & & & & & 2eR_0 \\ & & & & & & & & \ddots \\ & & & & & & & & & \ddots \\ & & & & & & & & & & \ddots \end{pmatrix}. \tag{2.11}$$

For a finite electric field $\mathcal{E}$, the energy of the ground state becomes

$$E^0 = \langle 0 | H^o - P \cdot \mathcal{E} | 0 \rangle, \tag{2.12}$$

leading to the static polarizability and hyperpolarizability

$$\alpha_{zz} = -\frac{d^2 E^0}{d\mathcal{E}_z^2} \tag{2.13}$$

$$\beta_{zzz} = -\frac{1}{2}\frac{d^3 E^0}{d\mathcal{E}_z^3}, \tag{2.14}$$

$$\gamma_{zzzz} = -\frac{1}{6}\frac{d^4 E^0}{d\mathcal{E}_z^4}. \tag{2.15}$$

The above analysis is for a fixed site p. The total values are approximately N times as large.

2.2.3 Neglect of Coulomb Interactions

Although the Coulomb correction in (2.2) may be large, we will first consider the simple approximation where these terms are ignored, leading to

$$V_q^{N_0 Q} = V = IP - EA. \tag{2.16}$$

The energy of ground state $|0\rangle$ is calculated by using the following perturbation formulas[11]. The Hamiltonian in an electric field $H = H^o - P \cdot \mathcal{E}$ can be written as $H = H_o + W$ where H_o

$$H_0 = \begin{pmatrix} \cdot & & & & & & & & \\ & \cdot & & & & & & & \\ & & \cdot & & & & & & \\ & & & V & & & & & \\ & & & & V & & & & \\ & & & & & 0 & & & \\ & & & & & & V & & \\ & & & & & & & V & \\ & & & & & & & & \cdot \\ & & & & & & & & & \cdot \\ & & & & & & & & & & \cdot \end{pmatrix} \tag{2.17}$$

is the unperturbed Hamiltonian matrix and

$$W = \begin{pmatrix} \ddots & & & & & & & & \\ & \ddots & & & & & & & \\ & & \ddots & & & & & & \\ & & -t & 2eR_0\mathcal{E}_z & -t & & & & \\ & & & -t & eR_0\mathcal{E}_z & at & & & \\ & & & & at & 0 & -at & & \\ & & & & & -at & -eR_0\mathcal{E}_z & -t & \\ & & & & & & -t & -2eR_0\mathcal{E}_z & -t \\ & & & & & & & & \ddots \\ & & & & & & & & & \ddots \end{pmatrix} \tag{2.18}$$

is considered as the perturbation Hamiltonian matrix.

Using the standard perturbation formulas (Appendix B) leads to

$$\alpha_{zz} = \frac{4a^2e^2R_0^2\eta^2}{V}A(\eta) \tag{2.19}$$

$$\beta_{zzz} = 0 \tag{2.20}$$

$$\gamma_{zzzz} = \frac{8a^2e^4R_0^4\eta^2}{V^3}G(\eta) \tag{2.21}$$

where

$$A(\eta) = \sum_{i=0}^{\infty} A_{2i}\eta^{2i} \tag{2.22}$$

$$G(\eta) = \sum_{i=0}^{\infty} G_{2i}\eta^{2i} \tag{2.23}$$

and

$$\eta = \frac{t}{V} \tag{2.24}$$

is the dimensionless energy dominating the saturation length.

As shown in Appendix C, t is related to the bandwidth (B) by

$$B \approx 4t \tag{2.25}$$

while V is related to the energy gap (E_g) by

$$E_g \approx V - 2t. \tag{2.26}$$

Thus

$$\eta = \frac{t}{V} = \frac{\frac{B}{4}}{E_g + \frac{B}{2}} \tag{2.27}$$

We will see that a large t leads to a larger saturation length while large V or bandgap leads to a smaller η and a small saturation length. For $E_g = 0$, (2.27) comes to $\eta = \frac{1}{2}$. Thus the range of η is 0 to $\frac{1}{2}$.

2.3 Saturation Length

2.3.1 Empirical Formula for Saturation Lengths

As shown in Appendix A, $a \sim \sqrt{2}$, so the polynomials in (2.22) and (2.23) are functions of only one parameter $\eta = \frac{t}{V}$. Consequently, the saturation length is a function only of $\eta = \frac{t}{V}$. The length dependence of α and γ are shown for various values of η in Figure 2.3 (scaled by the limiting values). We will define the the saturation length L_α and L_γ as the length for which α and γ, respectively, attain 95% of the limiting value. To a good approximation we find (Figure 2.3.b) that

$$L_\gamma \sim 1 + 38\frac{t}{V} \tag{2.28}$$

for $\eta = 0.1$ to 0.4. Similarly the saturation length for polarizability is approximated by

$$L_\alpha \sim 1 + 20\frac{t}{V} \tag{2.29}$$

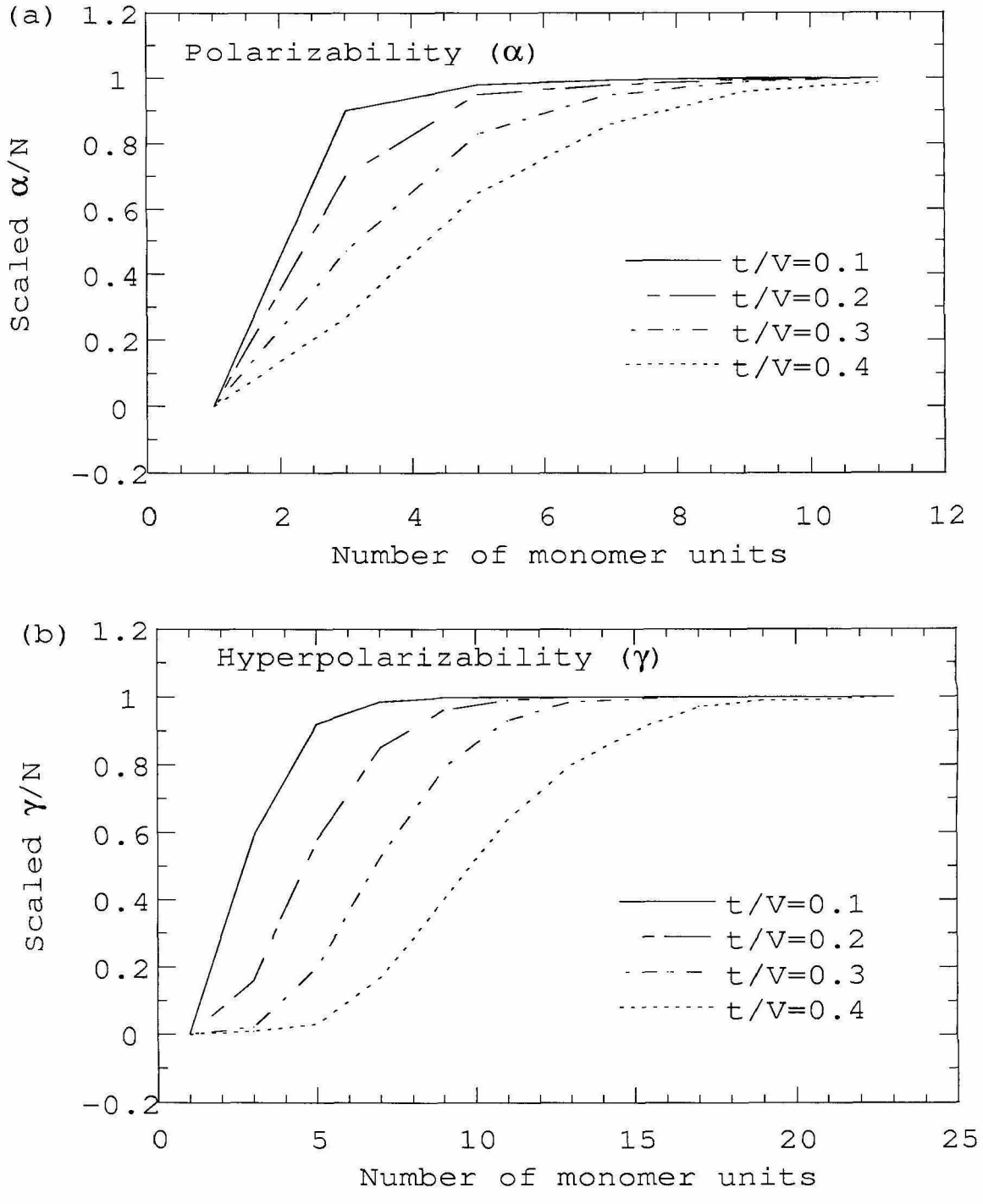

Figure 2.3: Dependence of saturation behavior on $\eta = t/V$ for (a) polarizability and (b) hyperpolarizability

as shown in Figure 2.3.a. Combining (2.28) and (2.29) leads to

$$L_\gamma \sim 1.9 L_\alpha - 0.9. \tag{2.30}$$

N	Excitation Energy[a] (eV)	$\langle\alpha\rangle^b(10^{-23}esu)$ NoQ	Q	$\langle\gamma\rangle^c(10^{-34}esu)$ NoQ	Q
3	2.47	3.20	8.38	3.10	5.56
5	2.00	8.39	22.83	30.51	75.07
7	1.86	12.98	35.62	84.90	236.01
9	1.82	16.97	46.61	136.78	385.49
11	1.81	20.79	57.09	177.73	498.88
13	1.80	24.58	67.48	212.91	596.08
15	1.80	28.36	77.87	246.28	688.98
17	1.80	32.15	88.25	279.23	781.02

Table 2.1: Theoretical properties of polyacetylene as a function of polymer length, N. Q indicates the use of (2.2) whereas NoQ indicates the use of (2.16). All cases use zero frequency. The monomer is butadiene. [a] Using $V = 2.85eV$. [b] $\langle\alpha\rangle = \frac{1}{3}\langle\alpha_{zz}\rangle$. [c] $\langle\gamma\rangle = \frac{1}{5}\langle\gamma_{zzzz}\rangle$.

2.3.2 Effects of Coulomb Interation and Frequency of Electromagnetic Fields

The results in Section 2.2.3 and Section 2.3.1 are approximate since the Coulomb interaction in (2.2) is ignored. Including the Coulomb interactions between electrons and holes [using (2.2) instead of (2.16)] prevent us from obtaining analytical results as in Section 2.2.3. Also for frequency dependence polarizabilities we again cannot get analytical formulas.

So we use sum-over-state approach in which the polarizability and hyperpolarizability have the form

$$\alpha_{ij}(-w, w) = 2I_{-w,w}\left(\frac{e^2}{\hbar}\right)\sum_n{}' \frac{r^i_{gn} r^j_{ng}}{w_{ng} - w} \tag{2.31}$$

$$\beta_{ijk}(-w_\sigma; w_1, w_2) = 3K(-w_\sigma; w_1, w_2)\left(\frac{e^3}{\hbar^2}\right) I_{-\sigma;1,2} \sum_{m,n}{}' \left\{ \frac{r^i_{gn}\bar{r}^j_{nm}r^k_{mg}}{(w_{mg} - w_\sigma)(w_{ng} - w_1)} \right\} \tag{2.32}$$

$$\gamma_{ijkl}(-w_\sigma; w_1, w_2, w_3) = 4K(-w_\sigma; w_1, w_2, w_3)\left(\frac{e^4}{\hbar^3}\right) I_{-\sigma;1,2,3} \left[\sum_{m,n,p}{}' \frac{r^i_{gp}\bar{r}^j_{pn}\bar{r}^k_{nm}r^l_{mg}}{(w_{pg} - w_\sigma)(w_{ng} - w_1 - w_2)(w_{mg} - w_1)} - \sum_{mn}{}' \frac{r^i_{gm}r^j_{mg}r^k_{gn}r^l_{ng}}{(w_m - w_\sigma)(w_{ng} - w_1)(w_{ng} + w_2)} \right]. \tag{2.33}$$

Here

(i) g indicates the ground state and $\sum'$ indicates that g is excluded from the sum.

(ii) r^i_{kl} indicates the dipole matrix element for component i between states l and k and $\bar{r}^i_{kl} = r^i_{kl} - r^i_{gg}$.

(iii) $\omega_\sigma = \sum_i \omega_i$.

(iv) $K(-\omega_\sigma; \omega_1, \omega_2, \omega_3)$ is a numerical factor determined by the nature of the nonlinear optical process[9].

(v) $I_{-\sigma;1,2,3}$ denotes the average of all terms generated by permuting σ,ω_1,ω_2,ω_3.

The excitation energy are obtained by diagonalizing the Hamiltonian matrix (2.1) and the dipole matrix elements can be obtained by transformation of matrix (2.11). The resulting values of α and γ are listed in Table 2.1 and 2.2 for polyacetylene and oligothiophene respectively. Tables 2.1 an 2.2 show that Coulomb interactions *do* affect the magnitude of α and γ. Thus including Coulomb interactions leads to α_{zz} 2 to 3 times larger and to γ_{zzzz}, 2 to 3 times larger. However, as shown in Figure 2.4, the saturation length is nearly identical. The reason for this is that at the point

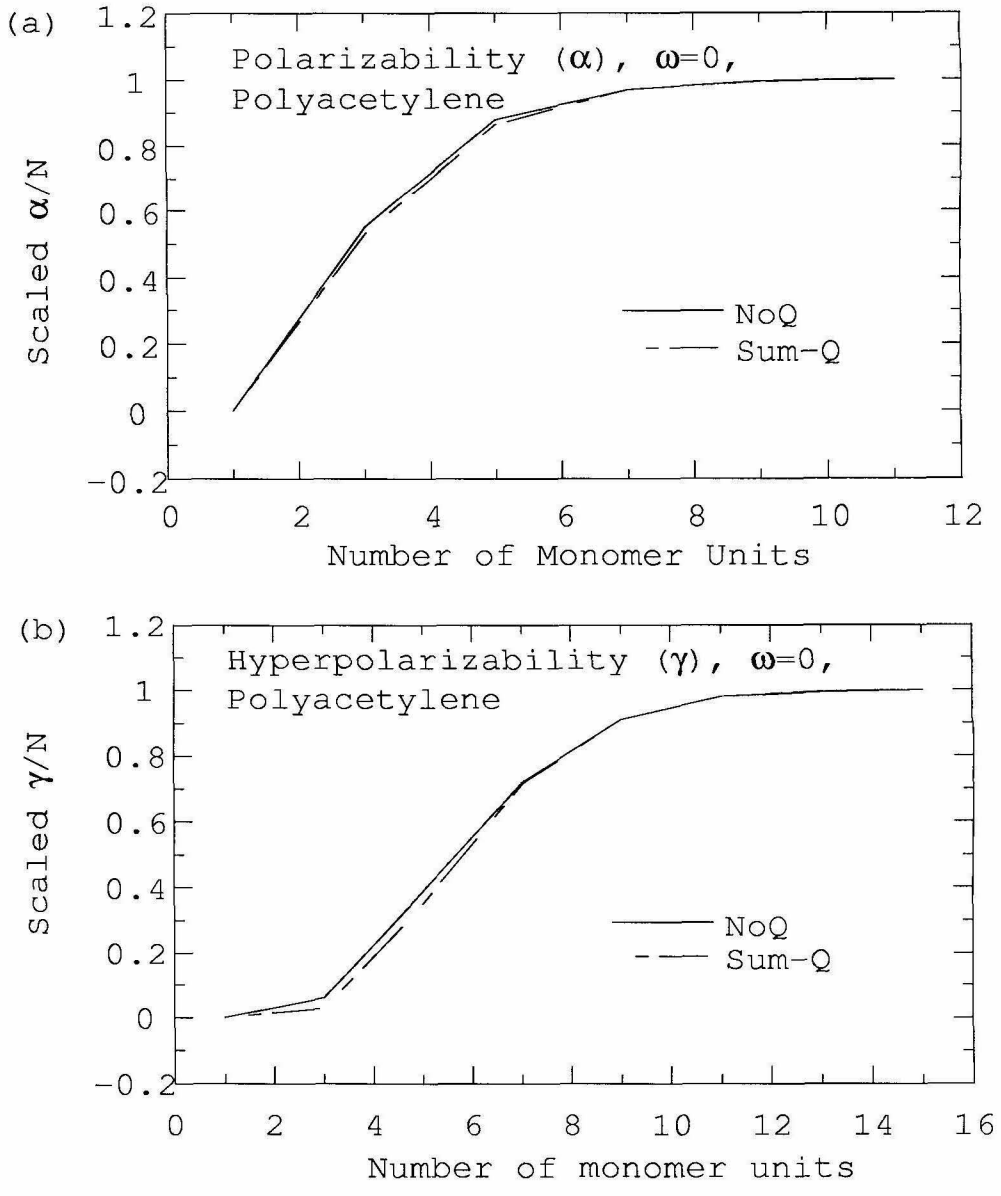

Figure 2.4: The saturation behavior of polyacetylene for (a) polarizability and (b) hyperpolarizability. The solid line (NoQ) uses sum-over-state or perturbation without Coulomb interaction. The dashed line (Sum-Q) uses sum-over-state with Coulomb interaction

where the separation between the electron and hole is approximately the saturation length, the Coulomb interaction is much less than V and thereby has negligible affect on exciton size.

The frequency also affects the magnitude and saturation length of α and γ. When the frequency is near resonance, the magnitude and saturation length change a great deal. Thus from Table 2.2, the magnitude of γ_{zzzz} increases by a factor of 10. This is because $w = 1.16eV$ is near the resonance frequency of $w = 1.4eV$. The saturation length also increases by 2 units (Figure 2.5.b). However, for frequencies far from resonance, the change in saturation length is negligible (Figure 2.5), and the change in magnitude is about one order of magnitude.

2.4 Calculations of the Saturation Lengths for Oligothiophenes and Polyacetylene

For oligothiophenes, the saturation length of α and γ with chain length has recently been observed experimentally[4]. We will use the above theory to predict the saturation properties of polyacetylene and oliogthiophenes.

2.4.1 Oliothiophenes, Comparison to Experiment

To estimate the NLO properties of oligothiophenes,we evaluate a and t by ignoring the sulfur and using Hückel theory (MO's for butadiene in Figure A.1). The analysis in Appendix A comes to

$$t = 0.36\beta. \tag{2.34}$$

A fit to the band states of polyacetylene[12] leads to

$$\beta = 2.4(1.0 \pm 0.7\delta)eV \tag{2.35}$$

where δ is the bond length alternation (half the difference in bond length between double and single bonds). Butadiene leads to $2\delta = (1.47 - 1.34) = 0.13$Å, and hence we take

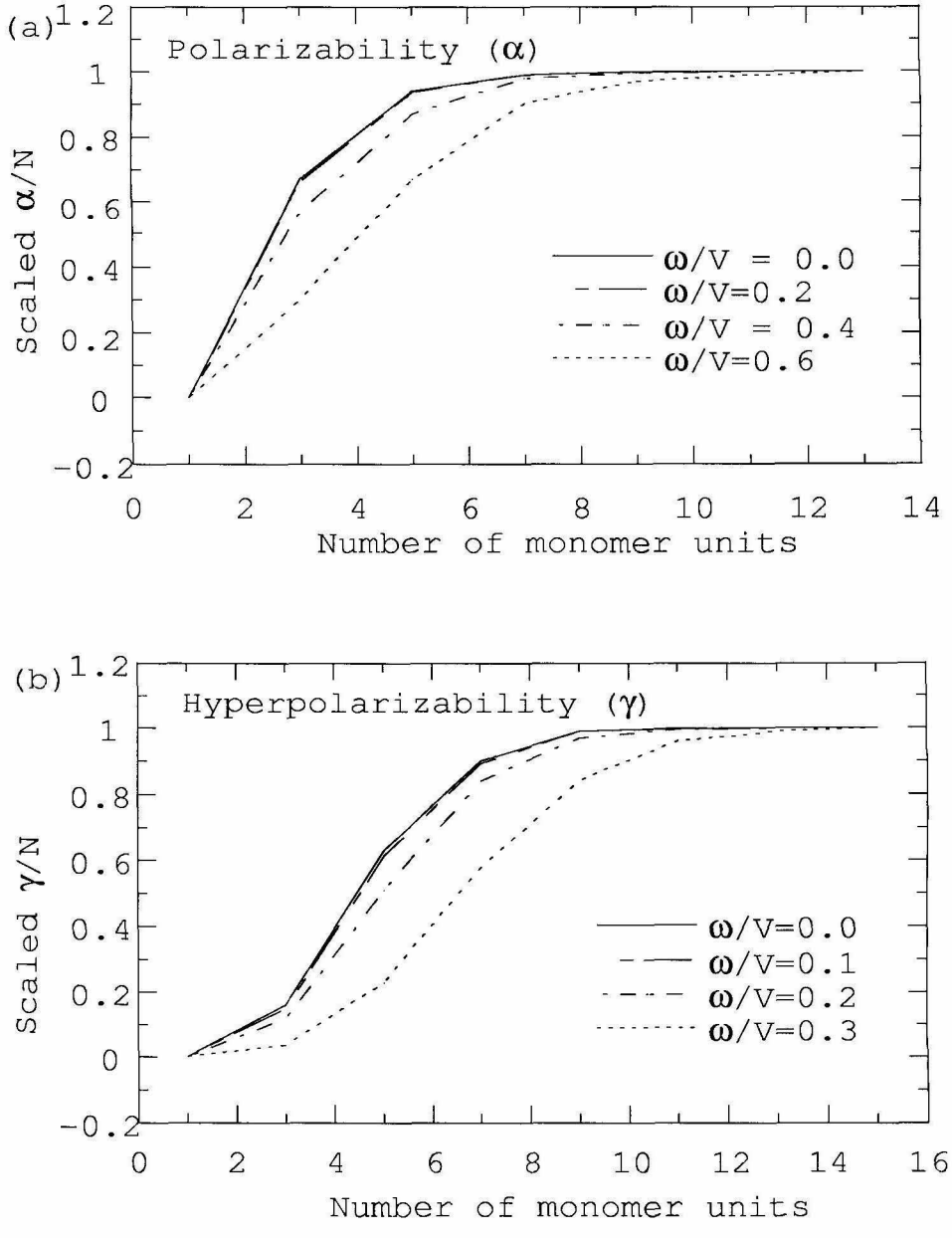

Figure 2.5: Effect of frequency on the saturation behavior of (a) polarizability and (b) hyperpolarizability. The resonance frequency of α is 2.8 eV (corresponding to $\omega/\mathrm{V} = 0.49$) whereas the resonance frequency of γ is 1.4 eV (corresponding to $\omega/\mathrm{V} = 0.24$).

$$\delta = 0.065\mathring{A}. \tag{2.36}$$

With (2.6) and (2.34), (2.35) leads to

$$t = 0.83eV. \tag{2.37}$$

We solved for the eigenvalues of (2.1) as a function of chain length (see Table 2.2) and find that

$$V = 4.09eV \tag{2.38}$$

leads not only to the experimental energy gap[4] $E_g = 2.77eV$ for saturation, but also an excellent fit with the observed transitions for shorter polymers. From Appendix C,

$$V \approx E_g + 2t \tag{2.39}$$

which would lead to $V = 2.77 + 1.67 = 4.44eV$, in reasonable agreement with the more exact calculation of 4.09 eV. Equations (2.37) and (2.38) lead to $t/V = 0.20$, suggesting saturation lengths of $L_\alpha = 5$ monomers and $L_\gamma = 8.6$ monomers, which are in excellent agreement with the experiment $L_\alpha \sim 5$ and $L_\gamma \sim 8$[4]. Using the above parameters and including Coulomb interaction leads to the α and γ in Figure 2.6 (using experimental[4] frequencies). The results are in excellent agreement with experiment except for $N = 7$. Experimently α/N and γ/N are greater than the values for larger N whereas experiment and caculations show that α/N and γ/N increase monotonically with N. Consequently, we suggest there may be an experimental artifact at $N = 7$.

The $w = 0$ values for α and γ calculated from formulas (2.22) and (2.23) and from the sum-over-state (2.31) and (2.33) are listed for comparison in Table 2.2. The calculated γ at $w = 1.16eV$ is off from the experiment by 6% for $N = 11$ and by 13% for $N = 9$. However, the caculated α at $\omega = 1.95eV$ is about 3 to 4 times the observed values.

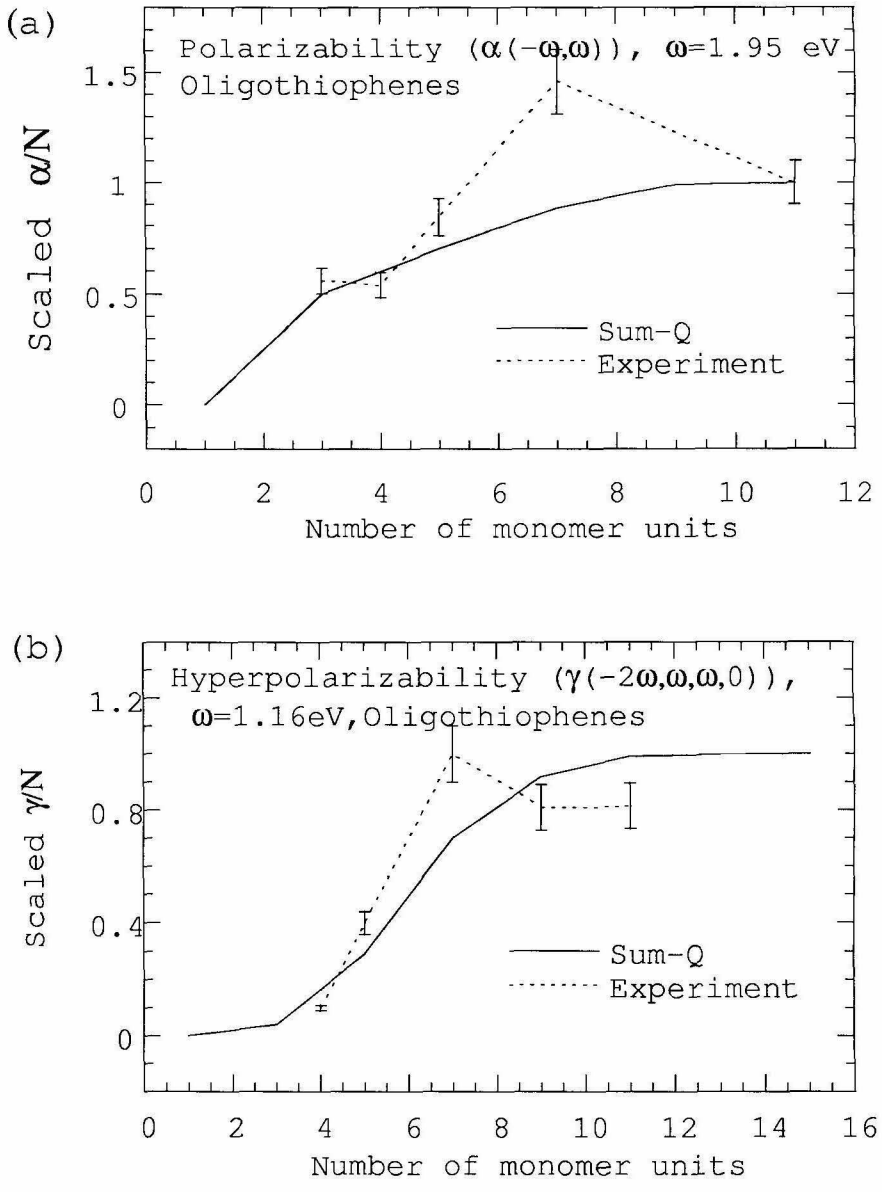

Figure 2.6: Comparison of theory and experiment for saturation behavior of oliogthiophene. (a) polarizability (ω =1.95 eV) and (b) hyperpolarizability (ω =1.16 eV). Dashed line with error bar uses experiment data. The solid line uses sum over states with Coulomb interaction.

	Excitation Energies (eV)		$\langle\alpha_{zz}(10^{-23}esu)\rangle$ Calculation		Expt[a]	$\langle\gamma_{zzzz}(10^{-34}esu)\rangle$ Calculation		Expt[a]
N	Calc[b]	Expt	$\omega=0$	$\omega=1.95$		$\omega=0$	$\omega=1.16$	
3	3.52	3.67	2.71	3.90	1.1	2.10	5.39	9.9
5	2.99	3.01	6.36	10.93	2.6	12.8	60.3	107
7	2.84	2.81	9.35	17.13	6.6	26.5	188.4	360
9	2.79	2.78	12.09	22.45	...	37.11	321.78	370
11	2.77	2.77	14.78	27.51	7.0	45.98	429.2	460

Table 2.2: Experimental and theoretical properties of oligothiophenes as a function of polymer length, N. N_oQ indicates the use of (2.16) whereas Q indicates the use of (2.2). $\omega = 0$ indicates the static case whereas $\omega \neq 0$ indicates finite frequency. $\omega = 1.95eV$ for $\langle\alpha(-\omega,\omega)\rangle$ and $\omega = 1.16eV$ for $\langle\gamma(-2\omega;\omega,\omega,0)\rangle$. [a]See reference 4. [b]Using $V = 4.09eV, t = 0.83eV$ and $a = \sqrt{2}$.

2.4.2 Polyacetylene

Next we consider the case of a simple trans polyene (polyacetylene). We still use butadiene as the monomer comes to

$$t = 0.83eV \tag{2.40}$$

$$a = \sqrt{2} \tag{2.41}$$

just as for oligothiophenes.

We solved for the eigenvalues of matrix (2.1) as a function of chain length and chose V so that excitation energy for large N equals the experimental bandgap, $E_g = 1.8eV$. This leads to

$$V = 2.85eV. \tag{2.42}$$

In comparison use of (2.39) with the observed gap leads to $V = 3.47eV$, in fair agreement with the calculated value.

Equations (2.40) and (2.42) lead to $t/V = 0.29$ which from (2.28) and (2.29) suggest $L_\alpha \approx 6.8$ and $L_\gamma \approx 12$. That means that saturation length of α is about 14

double bonds and the saturation length for γ is about 24 double bonds. This result is in agreement with other theoretical results[14] (21 double bonds). The saturation length for γ of oligothiphenes is 16 double bonds, considerably shorter than that of polyacetylene. This results primarily from the higher value of V and hence the bandgap arise from the the sulfur in oligiothiophenes.

2.5 Discussion

2.5.1 Comparision with Experiment

Considering the simplicity of this $VB - CTE$ model, the predicted results are excellent. Important approximations which may cause discrepancies are:

1. This model is derived for the long chain limit and should hold for short chain length.
2. The hole is assumed fixed.
3. For the nearest neighbors interaction, the expressions for Coulomb interaction should be corrected for sheilding.
4. The covalent (same site) exciton is neglected.
5. The correlation between electron-hole pair is neglected.

2.5.2 Predictions for Other Materials, Design Considerations

The analytical results (2.19)-(2.27) (obtained for a static external field with neglect of Coulomb interactions) indicate that the magnitudes of α and γ for this class of polymers are determined by two parameters:

t - the monomer hopping matrix element (one quarter the bandwidth, B)

V - the exciton excitation energy ($\simeq E_g + 4t \simeq E_g + B/2$)

Polymer[f]	B[a] (eV)	E_g[b] (eV)	t[g] (eV)	V[g] (eV)	η	L_α[c]	L_γ[c]	α_{zz}[d,e]$/N$ (10^{-23}esu)	γ_{zzzz}[d,e]$/N$ (10^{-34}esu)
a	3.9	2.1	1.0	4.1	0.24	5.8	10.1	2.41	11.30
b	3.5	3.4	0.9	5.1	0.17	4.4	7.5	1.13	2.54
c	2.8	3	0.7	4.4	0.16	4.2	7.1	2.49	15.93
d	3.8	3.2	0.95	5.1	0.19	4.8	8.2	1.13	2.55
e	2.5	2.2	0.6	3.4	0.18	4.6	7.8	3.88	44.90
f	3.3	3.3[a]	0.8	5.0	0.16	4.2	7.1	0.40	0.51
g	2.7	5.4[a]	0.7	6.8	0.10	3.0	4.8	0.083	0.020
h	1.3	3.1[a]	0.3	3.8	0.08	2.6	4.0	1.09	3.45
j	-	2.77	0.83[h]	4.09	0.20	5.0	9.0	1.77	6.87
i	-	1.8	0.83[h]	2.85	0.29	6.8[i]	12.0[i]	5.65	82.06

Table 2.3: Predicted saturated values polarizability (α), hyperpolarizability (γ), and saturation lengths (L_α, L_γ) of polymers. Based on equation (2.19) and (2.21) with $\omega = 0$. [a]Calculated values from reference 15. [b]Experimental values from reference 15. [c]Calculated using (2.28) or (2.29). [d]Using $a = \sqrt{2}$. [e]Values at saturation using (2.19) and (2.21) and $\omega = 0$. An approximate correction for finite frequency is to multiply $\alpha(-\omega,\omega)$ by $E_g/(E_g - \omega)$ and to multiply $\gamma(-3\omega;\omega,\omega,\omega)$ by $E_g{}^3/(E_g - \omega)(E_g - 2\omega)(E_g - 3\omega)$. [f]See Figure 2.7. [g]Using (2.25) and (2.26) unless otherwise noted. [h]Derived in text rather than from B. [i]The entries in the table are in terms of butadiene monomers. The number of double bonds is 14 for α and 24 for γ.

In addition the monomer length R_o plays an obvious role. $a \approx 1/\sqrt{2}$ is nearly constant and hence has little effect. Thus we hope that these relations will provide experimental with insights in designing and developing new materials.

The saturation length depends only on one parameter, $\eta = t/V$. Inclusion of Coulomb interactions and finite frequency (far from resonance) leads to little change in the saturation length. These results lead to the simple empirical formulae (2.31) and (2.32) for relating saturation length to η. Thus to design new materials with longer saturation length and with larger magnitudes for α and γ, one should increase t and/or decrease V.

To predict α and γ for other materials we need only estimate t and V and substitute into (2.19) and (2.21). The value of t can be estimated from the bandwidth of the conduction band, $B \approx 4t$. Given t, the value for V can be estimated from

a. Polydiacetylene

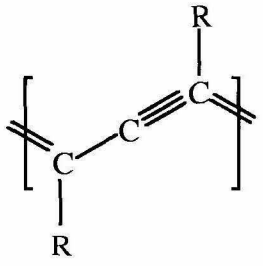

b. Polyparaphenylene

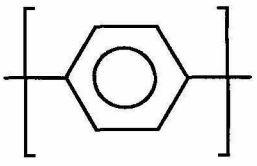

c. Polyparaphenylene vinylene

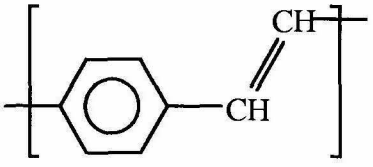

d. Polyprrople

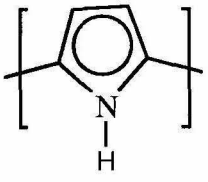

e. Polythiophene vinylene

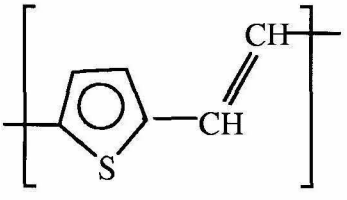

f. Polyvinylene sulfide

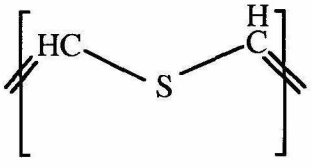

g. Polymethineimine

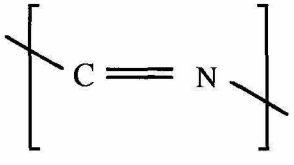

h. Polybenzothiophene

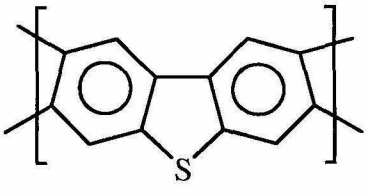

i. Polyacetylene (trans)

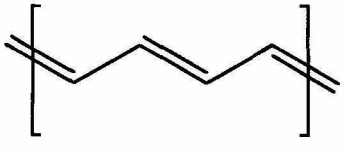

j. Polythiophene

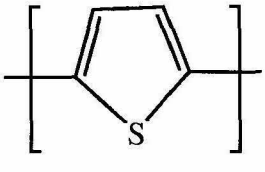

Figure 2.7: Repeating units for polymers of Table 2.3

the energy gap (between the conduction and valence bands) using equation (2.26), $V = E_g + 2t$. These values of B and E_g can be obtained either from experiment or theory. To illustrate the use of this approach we predict in Table 2.3 the values of α, γ, and the saturation lengths (L_α, L_γ) for a number of polymers (see Figure 2.7) based on published values is of the bandwidth (B) and bandgap (E_g).

2.5.3 Comparisons to Other Theory

Another recent approach to predicting NLO properties is by Mukamel and coworkers[14] who studied polyacetylene chains without donor acceptor groups. They used the Pariser-Parr-Pople (PPP) Hamiltonian and solved the equations of motion for pairs of electrons and holes by assuming pairs of different types are decoupled. This approach greatly simplifies the general calculation over a standard sum over molecular orbital states approach by allowing the motion of electron-hole, electron-electron and hole-holeairs. VB-CTE model further simplifies the calculation by considering only the electron-hole pairs (excitons) since the electron-electron and hole-hole pairs are much higher in energy.

2.6 Summary

By focusing solely on electron-hole pairs, we constructed a simple Hamiltonian for a conjugated polymer chain and solved for the properties using perturbation theory. Analytical formulae are derived for α and γ in terms of just two parameters: V and t plus the overall monomer length, R_o. These formulae predict the experimental values of α and γ within an order of a magnitude and show that α and γ can be increased by (i) decreasing the cost of creating an exciton (V) and (ii) once it is created by increasing the energy gain (t) of delocalizing it over many repeat units.

We find that the saturation length is determined by only single parameter: the ratio of t (the hopping matrix element between nearest monomers) and V (the exciton excitation energy). These two parameters are obtained easily from experiment or theory. In addition we obtained the simple empirical formula (2.31) and (2.32) for

predicting the saturation lengths. These results should be valuable for designing new materials and for interpreting experiments.

2.7 References

1. Prasad, P. N.; Williams, D. J. Eds., *Introduction to Nonlinear Optical Effects in Molecules and Polymers*, Wiley, New York, 1991.

2. Marder, S. R.; Beratan, D. N.; Cheng, L. T., *Science* **252**, 103 (1991).

3. Cheng, L. T.; Tam, W., Stevenson, S. H.; Meredith, G. R.; Rikken, G.; Marder, S. R., *J. Phys. Chem.* **95**, 10631 (1991).

4. Thinpont, H.; Rikken, G. R.; Meijer, E. W.; ten Hoeve, W.; Wynberg, H., *Phys. Rev. Lett.* **65**, 2141 (1990).

5. Beratan, D. N.; Onuchic, J. N.; Perry, J. W., *J. Phys. Chem.* **91**, 2696 (1987).

6. Shuai, Z.; Brédas, J. L., *Phys. Rev.* B **44**, 5962 (1991).

7. Heflin, J. R.; Wong, K. Y.; Zamani-khamiri, O.; Garito, A. F., *Phys. Rev.* B **38**, 1573 (1988).

8. Greene, B. I.; Orenstein, J.; Schmitt-Rink, S., *Science* **247**, 679 (1990).

9. Orr, B. J.; Ward, J. F., *Mol. Phys.* **20**, 513 (1971).

10. Pople, J. A.; Walmsley, S. H., *Faraday Soc. and Cont.* **15**, 441 (1962).

11. Corson, E. M., *Perturbation methods in the quantum mechanics of n-electron systems*,Hafner Publishing Company, New York.

12. Tavan, P.; Schulten, K., *Phys. Rev.* B **36**, 4337 (1987).

13. Fann, W. S.; Benson, S.; Madey, J. M. J.; Etemad, S.; Baker, G. L.; Kajzar, F., *Phys. Rev. Lett.* **62**, 1492 (1989).

14. Mukamel, S.; Wang, H. X., *Phys. Rev. Lett.* **69**, 65 (1992).

15. Skotheim, T. A. Eds., *Handbook of Conducting Polymers*,Vol 2. Marcel Dekker, Inc., p 859.

16. Mathematica, Version 2.0, Wolfram Research, Inc., Champaign, Illinois.

17. Richardson, C. H., *An Introduction to the Caculus of Finite Differences*, D.van Nostrand Company, Inc. 1954, p 108.

Chapter 3 The Valence-Bond Charge-Transfer Model (VB-CT) for Nonlinear Optical Properties of Charge-Transfer Organic Molecules

3.1 Introduction

Nonlinear optical (NLO) materials are playing an increasingly important role for a wide range of applications, including laser technology, telecommunications, data storage, and optical switches[1–4]. Exemplary NLO properties are exhibited by conjugated organic molecules with terminal electron donor and acceptor groups (Figure 3.1). Such molecules possess a low energy charge transfer (CT) state and exhibit large second and third order nonlinearities[5–7]. Marder, Perry, and coworkers[7] have studied the NLO properties of a series of such materials and have shown strong correlation between hyperpolarizabilities and bond length alternation (BLA) in the conjugated bridge. They used solvents of varying polarity to modify the BLA for the conjugated organic molecules and measured the corresponding hyperpolarizabilities. Gorman and Marder[7e] carried out finite-field semiempirical molecular orbital calculations (at the AM1 level) to obtain numerical relationships between the hyperpolarizabilities and the BLA, with results consistent with experimental trends. However, there is not yet a simple analytical model to explain the relationship between BLA and the various order polarizabilities.

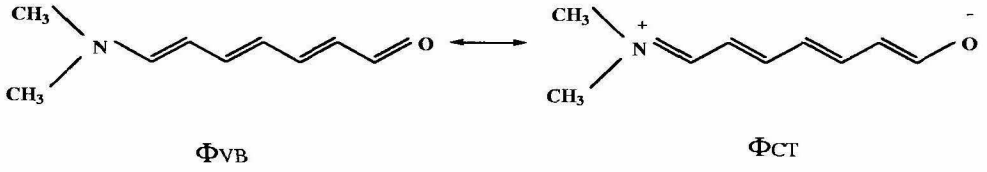

Figure 3.1: Donor acceptor type molecule

Here we start with the valence-bond charge-transfer model (VB-CT) previously used to describe the hyperpolarizabilities of polyenes[8] and extend it to systems terminated with donor and acceptor units. This VB-CT model is used to describe the polarizability and hyperpolarizabilities of charge-transfer type molecules. We derive analytic formulea that explain the relation of the polarizability and hyperpolarizabilities to BLA. Because of its basis in classical resonance theory, this VB-CT model provides insight into the factors determining α, β, and γ.

The basic theory is developed in Section 3.2 and predictions of hyperpolarizabilities are given in Section 3.3. Section 3.4 compares the VB-CT results to quantum chemical calculations (AM1) and shows how to use the theory in interpreting experimental results and predicting properties.

3.2 Theory

3.2.1 The VB-CT Model

We consider a molecule of the form in Figure 3.1 where Ψ_{VB} is the normal valence-bond configuration (no charge transfer between donor and acceptor). The second state Ψ_{CT} is obtained by moving an electron from donor to acceptor, leading to the alternative VB description of the intervening polyene unit. Taking the energy of Ψ_{VB} as the reference, the Hamiltonian matrix becomes

$$H_0 = \begin{pmatrix} E_{VB} & -t \\ -t & E_{CT} \end{pmatrix} = \begin{pmatrix} 0 & -t \\ -t & V \end{pmatrix}, \tag{3.1}$$

where $-t = \langle \Psi_{VB} | \mathcal{H} | \Psi_{CT} \rangle$ is the many-body charge transfer matrix element (t is positive),

$$V = E_{CT} - E_{VB}, \tag{3.2}$$

and we assume that $\langle \Psi_{VB} | \Psi_{CT} \rangle = 0$. V is determined by the nature of the donor and acceptor molecules, or the topology of the conjugated linker (which determines the change in aromaticity), and the effect of solvent polarity. Solving for the eigenvalues

of (3.1) leads to the energies

$$E_{gr} = \frac{1}{2}V - \frac{1}{2}\sqrt{V^2 + 4t^2}, \tag{3.3}$$

$$E_{ex} = \frac{1}{2}V + \frac{1}{2}\sqrt{V^2 + 4t^2}, \tag{3.4}$$

where gr and ex indicate the ground and excited states. The energy gap is

$$E_g = \sqrt{V^2 + 4t^2} \tag{3.5}$$

which can be related to the wavelength for the maximum in the absorption spectrum

$$\lambda_{max} = \frac{hc}{E_g}. \tag{3.6}$$

Denoting the fraction of the charge-transfer configuration in the ground state as f, we write the ground state eigenfuntion as

$$\Psi_{gr} = \sqrt{1-f}\Psi_{VB} + \sqrt{f}\Psi_{CT}. \tag{3.7}$$

From (3.1) and (3.3) we obtain

$$\Psi_{gr} = \frac{t}{\sqrt{t^2 + E_{gr}^2}}\Psi_{VB} + \frac{E_{gr}}{\sqrt{t^2 + E_{gr}^2}}\Psi_{CT}, \tag{3.8}$$

so that

$$f = \frac{E_{gr}^2}{t^2 + E_{gr}^2} = \frac{1}{2} - \frac{V}{2\sqrt{V^2 + 4t^2}}. \tag{3.9}$$

Also

$$f = \frac{\partial E_{gr}}{\partial V}. \tag{3.10}$$

3.2.2 Inclusion of the Bond Length Alternation (BLA) Coordinate

Since Ψ_{CT} and Ψ_{VB} involve alternate resonant descriptions of the intervening polyene unit, the increase of f from 0 to 1 will change each double bond ($R = 1.33$Å) of the polyene to a single bond ($R = 1.45$Å) and vice versa. [These distances are based on the experimental average bond lengths trans-1,3,5,7-octatetraene[9].] Thus the bond length alternation (BLA) coordinate changes from $q = -0.12$Å to $q = +0.12$Å as the CT fraction f goes from 0 to 1, leading to a one-to-one relationship. We will describe the bond length distortion as a vibrational coordinate by associating potentials (3.11) and (3.12) with the VB and CT states. The vibrational contributions to the Hamiltonian (3.1) are

$$E_{VB} = \frac{1}{2}k(q - q^0_{VB})^2, \tag{3.11}$$

$$E_{CT} = V_0 + \frac{1}{2}k(q - q^0_{CT})^2, \tag{3.12}$$

where q^0_{VB} and q^0_{CT} are equilibrium positions and V_0 is the *adiabatic* energy difference for these two states. For $f = 0$ the equilibrium BLA coordinate is $q^0_{VB} = -0.12$Å and for $f = 1$ it is $q^0_{CT} = +0.12$Å. Thus V and the ground state energy E_{gr} are replaced by

$$V = V_0 + \frac{1}{2}k\left[\left(q - q^0_{CT}\right)^2 - \left(q - q^0_{VB}\right)^2\right], \tag{3.13}$$

and

$$E_{gr} = \frac{1}{2}\left[V_0 + \frac{1}{2}k\left(q - q^0_{VB}\right)^2 + \frac{1}{2}k\left(q - q_{CT}\right)^2\right] - \frac{1}{2}\sqrt{V^2 + 4t^2}. \tag{3.14}$$

The equilibrium coordinate of Ψ_{gr}, q_{opt}, is obtained by solving

$$\frac{dE_{gr}}{dq} = 0. \tag{3.15}$$

This leads to

$$q_{opt} = \frac{1}{2}\left(q^0_{VB} + q^0_{CT}\right) + \frac{1}{2}\left(q^0_{VB} - q^0_{CT}\right)\frac{V}{\sqrt{V^2 + 4t^2}}$$

$$= q^0_{VB} - f\left(q^0_{VB} - q^0_{CT}\right)$$
$$= -0.12 + 0.24f. \tag{3.16}$$

Thus f and q_{opt} are linearly related to each other. We should note that the V in (3.13) is the vertical energy difference (3.2) for a *particular* value, q, whereas V_0 is the adiabatic energy difference with each surface at its minimum. Eqn (3.13) with $q = q_{opt}$ and eqn (3.16) leads to a nonlinear equation which we solve iteratively for q_{opt}.

Figure 3.2 illustrates the variation of the ground state potential surface and q_{opt} for $V_0 = 1.0, 0.0$, and $-1.0eV$ using

$$t = 1.1eV \tag{3.17}$$

[derived from the experimental data on molecule in Figure 3.1, see discussion in Section 3.4.4] and

$$k = 33.55eV/\text{Å}^2 = 773.7kcal/mol\text{Å}^2 = 5.38mdyn/cm \tag{3.18}$$

(from UFF[10]) for the force constant in (3.11) and (3.12). V_0 is determined by the nature of the donor, the acceptor, the conjugated linker, the solvent, etc. For $V_0 = 1eV$ (Figure 3.2.a), we obtain $q_{opt} = -0.069$Å. For $V_0 = 0$ (degenerate VB and CT), we obtain $q_{opt} = 0$ (Figure 3.2.b). Further stabilization of CT to $V_0 = -1eV$ (Figure 3.2.c) reverses the BLA to $q_{opt} = +0.069$Å.

3.2.3 Application of an Electric Field

For conjugated donor acceptor systems in Figure 3.1, the polarizability and hyperpolarizabilities are dominated by the z component (along the chain axis), and we will ignore all other components. Assuming that only Ψ_{CT} contributes to the dipole moment, we write

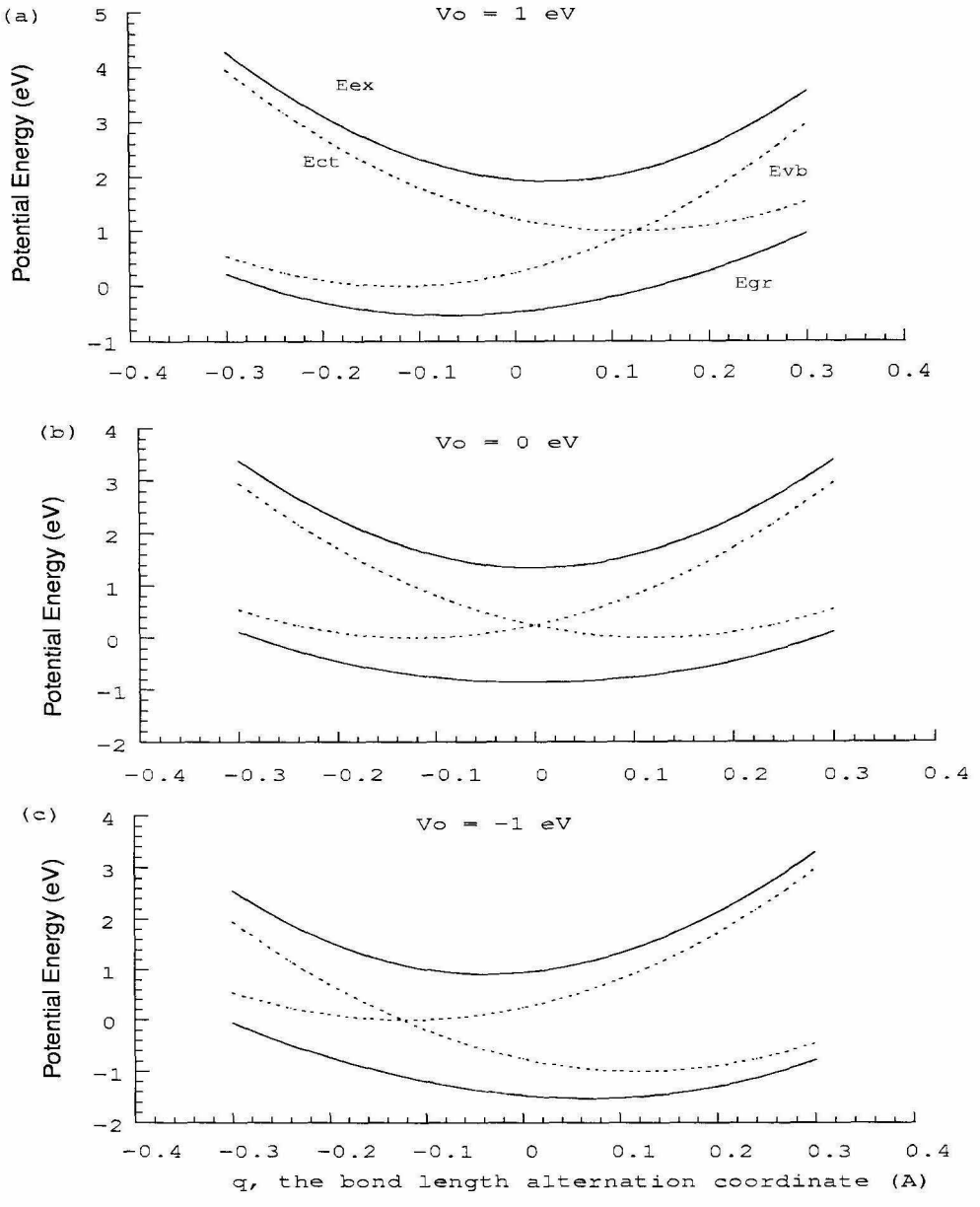

Figure 3.2: Energies of the ground (E_{gr}) and excited (E_{ex}) states as a function of bond length alternation (BLA), q. V_0 is the adiabatic difference between the pure VB and CT states and q_{opt} is the optimum BLA coordinate, q_{opt}. These calculations used k and t from (3.17). (a) $V_0 = 1eV$ leads to $q_{opt} = -0.069$Å, (b) $V_0 = 0$ leads to $q_{opt} = 0$, (c) $V_0 = -1eV$ leads to $q_{opt} = +0.069$Å.

$$\mu_{CT} = QeR_{DA} \tag{3.19}$$

where Q is the net charge transfer for Ψ_{CT}. In an applied external electric field, $\mathcal{E}$, as used in measurements of hyperpolarizabilities, the additional (optical) Hamiltonian is

$$H_1 = \begin{pmatrix} 0 & 0 \\ 0 & -\mu_{CT}\mathcal{E} \end{pmatrix}, \tag{3.20}$$

leading to

$$H = H_0 + H_1 = \begin{pmatrix} E_{VB} & -t \\ -t & E_{CT} - \mu_{CT}\mathcal{E} \end{pmatrix}. \tag{3.21}$$

Thus the relative energy V is replaced by

$$V_\mathcal{E} = V - \mu_{CT}\mathcal{E}. \tag{3.22}$$

Equations (3.1), (3.5) and (3.9) continue to apply for finite applied fields but with V replaced by $V_\mathcal{E}$. In particular the change in f due to the applied field is

$$\frac{df}{d\mathcal{E}} = \frac{df}{dV_\mathcal{E}}\frac{dV_\mathcal{E}}{d\mathcal{E}} = \frac{2t^2\mu_{CT}}{(V_\mathcal{E}^2 + 4t^2)^{3/2}} = \frac{2t^2\mu_{CT}}{E_g^3}. \tag{3.23}$$

3.2.4 Polarizabilities

Given the dependence of the ground state energy on the external electric field, the dipole moment of the ground state, P_z, is obtained from

$$P_z(\mathcal{E}) = -\frac{dE_{gr}}{d\mathcal{E}}. \tag{3.24}$$

Assuming that z is the direction along the chain and that $\mathcal{E}$ is in this direction, the polarizability and hyperpolarizabilities can then be obtained from

$$\alpha_{zz} = \frac{dP_z}{d\mathcal{E}}\,|_{\mathcal{E}=0}, \tag{3.25}$$

$$\beta_{zzz} = \frac{1}{2}\frac{d^2P_z}{d\mathcal{E}^2}\,|_{\varepsilon=0}, \tag{3.26}$$

$$\gamma_{zzzz} = \frac{1}{6}\frac{d^3P_z}{d\mathcal{E}^3}\,|_{\varepsilon=0}\,. \tag{3.27}$$

$$\delta_{zzzzz} = \frac{1}{24}\frac{d^4P_z}{d\mathcal{E}^4}\,|_{\varepsilon=0}\,. \tag{3.28}$$

Using (3.9), (3.14) and (3.16) we obtain

$$P_z = -\mu_{CT}\frac{dE_{gr}}{dV_\mathcal{E}}\,|_{\varepsilon=0} = f\mu_{CT} \tag{3.29}$$

$$\alpha_{zz} = -\mu_{CT}^2\frac{df}{dV_\mathcal{E}}\,|_{\varepsilon=0} = \frac{2t^2\mu_{CT}^2}{E_g^3} \tag{3.30}$$

$$\beta_{zzz} = \frac{\mu_{CT}^3}{2}\frac{d^2f}{dV_\mathcal{E}^2}\,|_{\varepsilon=0} = \frac{3t^2\mu_{CT}^3V}{E_g^5} \tag{3.31}$$

$$\gamma_{zzzz} = -\frac{\mu_{CT}^4}{6}\frac{d^3f}{dV_\mathcal{E}^3}\,|_{\varepsilon=0} = \frac{4t^2\mu_{CT}^4[V^2-t^2]}{E_g^7}, \tag{3.32}$$

$$\delta_{zzzzz} = \frac{\mu_{CT}^5}{24}\frac{d^4f}{dV_\mathcal{E}^4}\,|_{\varepsilon=0} = \frac{5t^2\mu_{CT}^5V[V^2-3t^2]}{E_g^9}. \tag{3.33}$$

The following discussions will omit the z subscripts.

3.3 Predictions of μ, α, β, and γ From VB-CT Theory

As f increases from $f = 0$ to $f = 1$, the VB-CT model leads to a structural evolution in which the polyene double bonds for Ψ_{VB} change to polyene single bonds in Ψ_{CT} and vice versa. Thus each bond decreases or increases by 0.12Å as f goes from 0 to 1. Since there is a linear relation (3.16) between f and q_{opt} [the ground state bond length alternation (BLA)], and since f determines the polarizability and hyperpolarizabilities, the polarizability and all hyperpolarizabilies are determined by a single BLA parameter, q_{opt}.

This has been anticipated by Marder[7] *et al.*, who pointed out that bond length alternation is a useful parameter to examine the structure-property relationships for

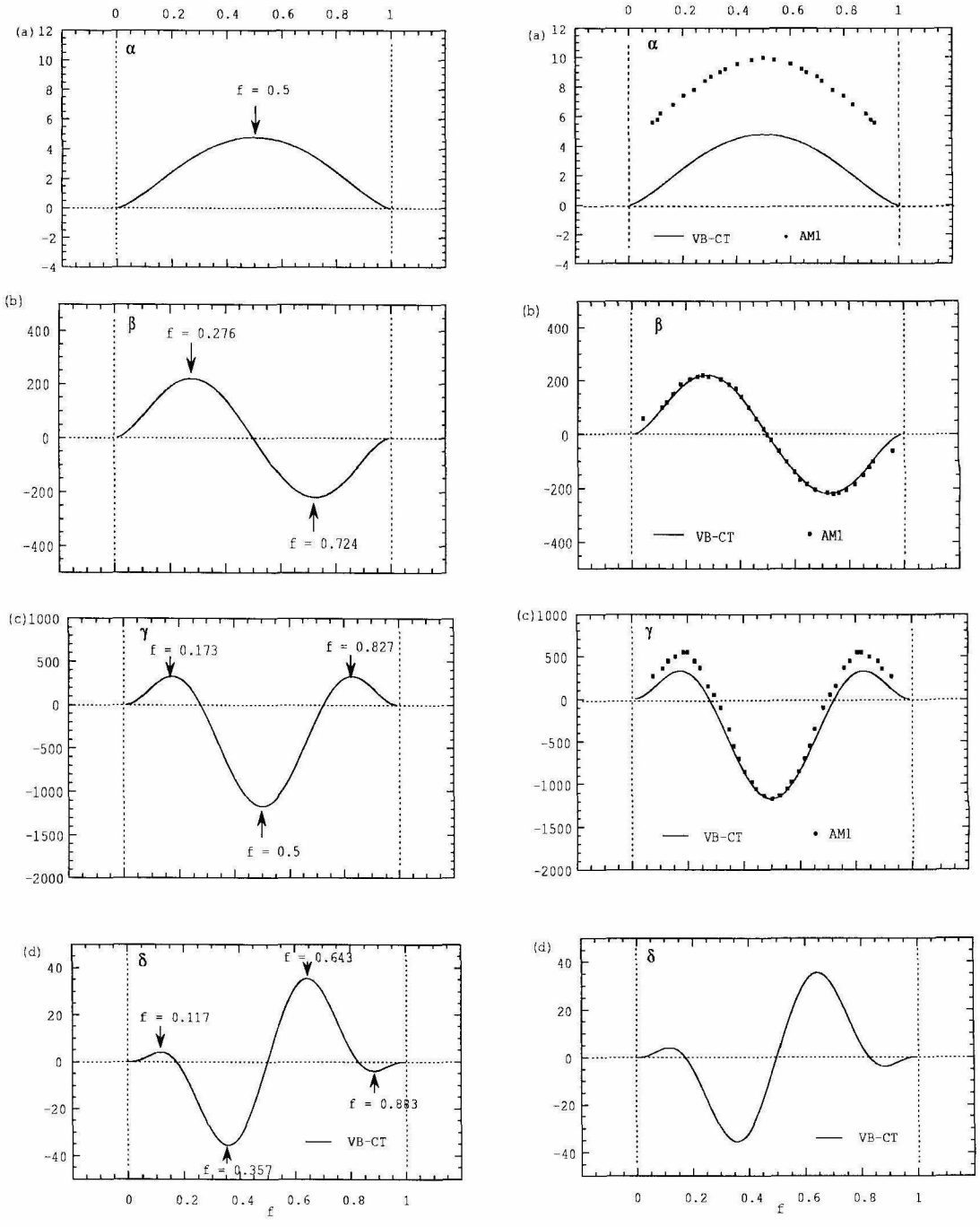

Figure 3.3: The relation between hyperpolarizability and charge transfer character (f). The right-hand side figures are the comparision between VB-CT caculation (solid line) and AM1 caculation (squares) (reference 9). (a) Polarizability, α, (b) hyperpolarizability, β, (c) second hyperpolarizability, γ, and (d) third hyperpolarizability, δ.

nonlinear optical materials. They showed that the β and γ values can be tuned through extrema and zero-crossings by varying BLA. In addition they carried out finite-field AM1 calculations[7e] on molecule in Figure 3.1 and showed the relationships of α, β and γ to q_{opt}. Their results provide a good test of VB-CT theory.

In order to illustrate the relationships as calculated using the VB-CT model, we used (3.9), (3.16), and (3.28)-(3.33) to calculate f, q_{opt}, α, β, γ, and δ as a function of V, all with the fixed values of t and k from (3.17 - 3.18). This allowed us to obtain α, β, and γ as a function of q_{opt}, Figure 3.3.

General observations from these relations are as follows:

1. α has a maximum for $f = \frac{1}{2}$, which is when all bond lengths in the polyene chain are equal.

2. β is related to the derivative of α with respect to f, leading to a maximum at $f = 0.276$, a minimum at $f = 0.724$, and a zero value at $f = \frac{1}{2}$. The maximum and minimum have the same magnitude.

3. γ is related to the derivative of β with respect to f, leading to the largest magnitude (a minimum) at $f = \frac{1}{2}$, with secondary maxima (about 1/4 the magnitude) at $f = 0.173$ and $f = 0.827$. $\gamma = 0$ at $f = 0.276$ and $f = 0.724$ where $|\beta|$ is a maximum.

4. δ is related to the derivative of γ with repect to f, leading to largest magnitudes at $f = 0.357$ (minimum) and $f = 0.643$ (maximum); secondary maxima in the magnitudes occur at $f = 0.117$ (maximum) and $f = 0.883$ (minimum). δ has zeroes at the places where $|\gamma|$ is a maximum ($f = 0.173$, $f = 0.5$, and $f = 0.827$).

These derivative relationships can be understood as follows: From (3.22), $V_{\mathcal{E}}$ is a linear function of $\mathcal{E}$, leading to

$$\frac{d}{d\mathcal{E}} = \frac{d}{dV_{\mathcal{E}}}\frac{dV_{\mathcal{E}}}{d\mathcal{E}} = -\mu_{CT}\frac{d}{dV_{\mathcal{E}}}. \tag{3.34}$$

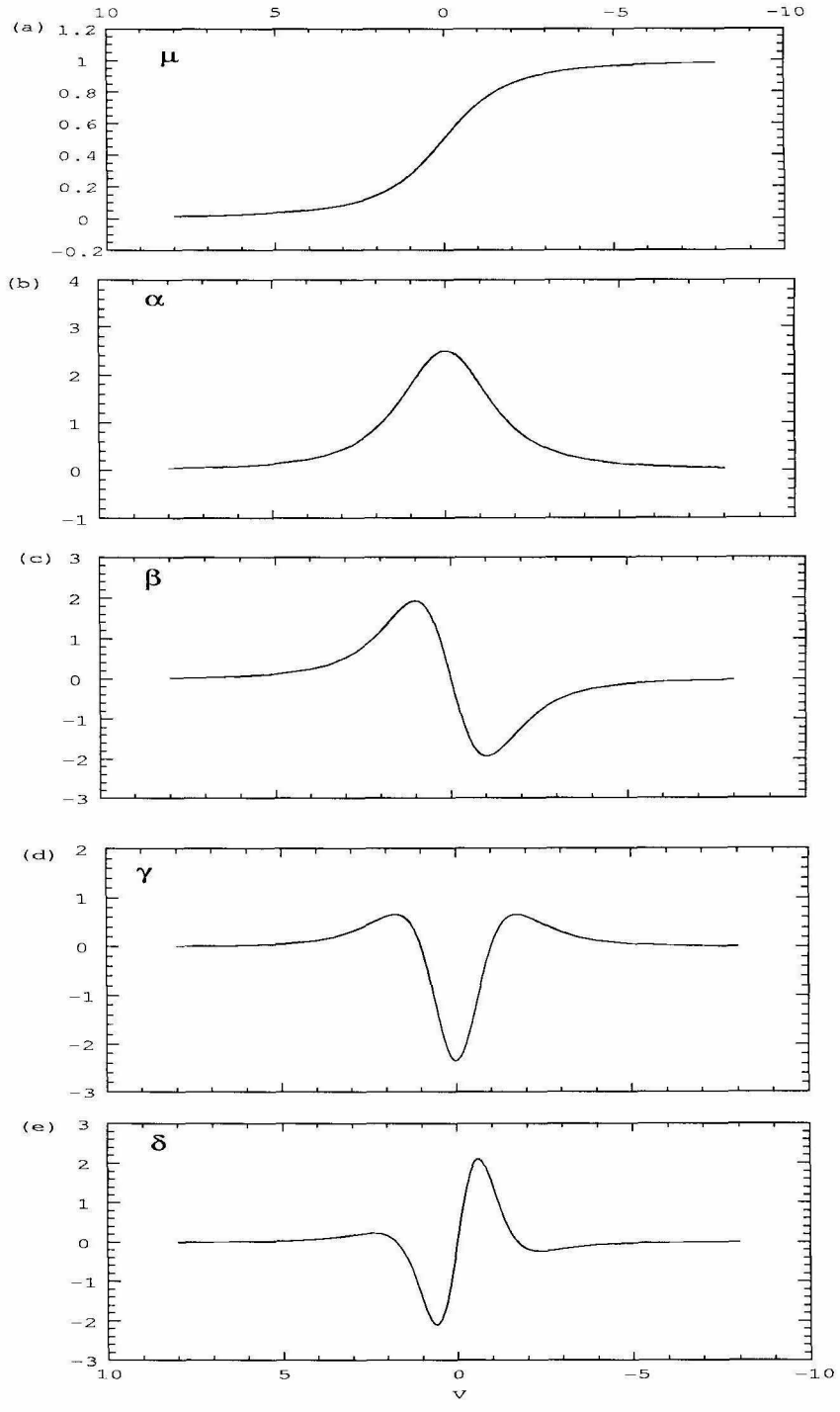

Figure 3.4: The relation between the dipole moment P_z (in units of μ_{CT}) and V (the VB-CT excitation energy). (a) polarizability, α, (b) hyperpolarizability, β, (c) second hyperpolarizability, γ, and (d) third hyperpolarizability, δ obtained from the derivatives of P_z with respect to $-V$ as shown by equations (3.30)-(3.33).

The relation between the dipole moment P_z and $V_\mathcal{E}$ is plotted in Figure 3.4.a. We assume that the dipole moment of Ψ_{VB} is zero, which corresponds to the limit with $V_\mathcal{E} = +\infty$. The dipole moment P of the charge transfer state is μ_{CT}, which corresponds to the limit with $V_\mathcal{E} = -\infty$. Taking the first, second, and third derivatives of the dipole moment with $-V_\mathcal{E}$ leads to α, β, γ, and δ as shown in Figure 3.4.b - 3.4.e. The relations between $V_\mathcal{E}$, f, and q_{opt} are expressed in (3.9) and (3.16). Changing variables from $V_\mathcal{E}$ to q_{opt} leads to

$$\frac{d}{dV_\mathcal{E}} = \frac{d}{dq_{opt}}\frac{dq_{opt}}{dV_\mathcal{E}} = -0.12\frac{df}{dV_\mathcal{E}}\frac{d}{dq_{opt}} \tag{3.35}$$

where the range of $V_\mathcal{E}$, *i.e.*, $[-\infty,\infty]$ is mapped onto the range of q_{opt}, [+0.12, -0.12]. Thus the shapes of the curves are similiar but the signs of α and γ change, as indicated by (3.29) and (3.30).

These results lead to the following observations:

When $V = 0$ (degenerate VB and CT states), we have

$$f = \frac{1}{2}, \tag{3.36}$$

$$q_{opt} = 0, \tag{3.37}$$

$$t = E_g/2. \tag{3.38}$$

At this point, α is a maximum, $\beta = 0$, and γ is a minimum (largest magnitude), and $\delta = 0$.

When $|V| = |t|$, we have

$$f = 0.276 \; or \; 0.724, \tag{3.39}$$

$$q_{opt} = \pm 0.0538\text{Å}, \tag{3.40}$$

$$t = \frac{E_g}{\sqrt{5}}. \tag{3.41}$$

Thus β takes its maximum (minimum) and $\gamma = 0$.

When $|V| = \sqrt{3}|t|$, we have

$$f = 0.173 \; or \; 0.827, \tag{3.42}$$

$$q_{opt} = \pm 0.0785\text{Å}, \tag{3.43}$$

$$t = \frac{E_g}{\sqrt{7}}. \tag{3.44}$$

Thus $|\gamma|$ is a maximum and $\delta = 0$.

When $|V| = 0.595|t|$, we have

$$f = 0.357 \; or \; 0.643, \tag{3.45}$$

$$q_{opt} = \pm 0.0343\text{Å}, \tag{3.46}$$

$$t = 0.479E_g. \tag{3.47}$$

Thus $|\delta|$ takes its largest maxima.

When $|V| = 2.376|t|$, we have

$$f = 0.117 \; or \; 0.883, \tag{3.48}$$

$$q_{opt} = \pm 0.0919\text{Å}, \tag{3.49}$$

$$t = 0.322E_g. \tag{3.50}$$

Thus $|\delta|$ takes its second largest maxima.

The shapes of the polarizability curves are relatively insensitive to the value t. Thus the salient factor for polarizability and hyperpolarizabilities is the bond length alternation.

3.4 Discussion

3.4.1 Comparison with AM1 Calculations

The VB-CT results are compared with AM1 calculations[7e] (squares) in Figure 3.3. [The AM1 calculations led to a limited bond length alternation of 0.108Å, whereas the experimental value for octatetraene led to 0.12Å; consequently for AM1 $q_{opt} = -0.108$ for $f = 0$ and $q_{opt} = +0.108$ for $f = 1$.] In Figure 3.3 we used Q values of 0.69, 0.51, 0.69, 0.69 to scale the curves for α, β, γ, and δ respectively.

The AM1 results for β and γ agree quite well with VB-CT theory. VB-CT has α going to zero as $f \rightarrow 0$ or 1, whereas the AM1 calculations lead to about half the maximum. This is probably because the current VB-CT calculations ignore the polarizability for a fixed VB or CT structure (it could have been included as an additive correction).

3.4.2 Comparison with Two-Level Models

Two-level models have been used widely to understand the nonlinear optical properties of materials[11]. In the absence of an external electric field, the system is described in terms of two eigenvectors corresponding to the ground and excited states. Upon applying an electric field $\mathcal{E}$, the additional Hamiltonian term, $-\mathcal{E} \cdot \mu$ is treated as a perturbation, where μ is the dipole moment matrix

$$\mu = \begin{pmatrix} \mu_{gg} & \mu_{ge} \\ \mu_{ge} & \mu_{ee} \end{pmatrix}. \tag{3.51}$$

This leads, for example, to a first hyperpolarizability β of the form

$$\beta \sim (\mu_{ee} - \mu_{gg}) \frac{\mu_{ge}^2}{E_{ge}^2} \tag{3.52}$$

where E_{ge} is the energy gap. This expression results from the change in ground state energy due to field, but does not account explicitly for the change in structure due to the modified equilibrium position of the ground state potential. Thus, it does not

Figure 3.5: Valence bond state of the bridge

provide a form for the higher polarizabilities, and does not provide an explicit picture for the structure/property relationships illustrated above.

The VB-CT model differs from such two-level models because the nonlinear optical properties are treated as due to the dependence of the dipole moment on the "field" on VB-CT adiabatic energy difference, V, which itself depends on the mixing of VB and CT and the resultant change in structure. This VB-CT picture leads itself easily to the calculation of changes in structure and of the structure-NLO property relationships with only a few chemically meaningful parameters. This leads to a direct relationship between α, β, γ, δ as the structure varying between a neutral polyene-like structure and a zwitterionic structure.

3.4.3 Additional Excited States

The VB-CT model assumes that all other excited states are much higher than the VB and CT states. In particular the resonant states (Figure 3.6) involving the bridge or linker must be much higher. For octatetraene (Figure 3.5) the absorption maxima is about 4 eV indicating that the resonant state of the linker in Figure 3.1 is about 4 eV above the VB state[12]. Since the donor acceptor molecules considered here have the CT state about 1 eV to 2 eV above the VB state, neglect of the resonant state should be a good approximation. When the energy of the resonance structure is close to those of VB and CT, the contributions from the linker resonant state must be included. This complicates the theory so that the results are no longer analytic. However, combining the current VB-CT theory for donor acceptor molecules with the VB-CT-E theory[8] for polymer linkers is straightforward and under development[13].

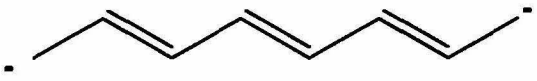

Figure 3.6: Charge transfer state of the bridge

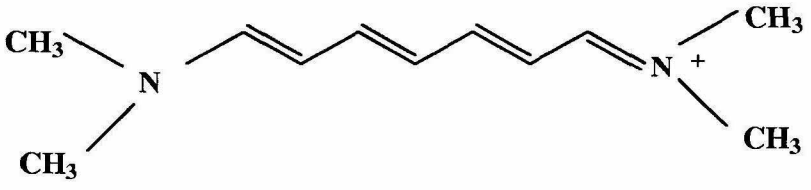

Figure 3.7: Molecule with $f = 0.5$

3.4.4 Applications to Various Molecules

To illustrate the application of the VB-CT model, we will consider the nonlinear polarizabilities of several donor acceptor molecules linked by a conjugated octatetraene chain. As described in Section 3.3, t can be explicitly related to λ_{max} for certain structural limits. Given t, one can use the expressions and the relationships given above to identify molecules that would have properties near the peak values or zero crossings of the polarizabilities.

For the case of the four double bond cyanine (Figure 3.7), λ_{max} was measured to be 516 nm in CH_3CN solvent, with $\gamma = -370 \times 10^{-36} esu$.[14] By symmetry this system has f =0.5, leading to $t = E_g/2$, and hence $t = 1.18eV$. From (3.41) we predict that a molecule of the same length and linker type but with $E_g = \sqrt{5}t$ would lead to $\gamma = 0$ and a positive maximum in β. Using $t = 1.18eV$ this would occur at $\lambda = 467$ nm. In fact, in the solvents C_6H_6 and dioxane, molecule in Figure 3.8 has $\lambda_{max} = 472$ nm and $\lambda_{max} = 468$ nm, respectively, and γ changes from $15 \times 10^{-36} esu$ to $-25 \times 10^{-36} esu$ with a positive peak in $\mu\beta$![15–16]

From (3.44), we expect γ to have a positive maximum when $E_g = \sqrt{7}t$, or $\lambda_{max} =$ 394nm. Experimentally, molecule in Figure 3.9 is observed[15] to have a positive peak in γ for solvent CH_3CN, as well as a $\lambda_{max} = 418$nm, close to the prediction from the

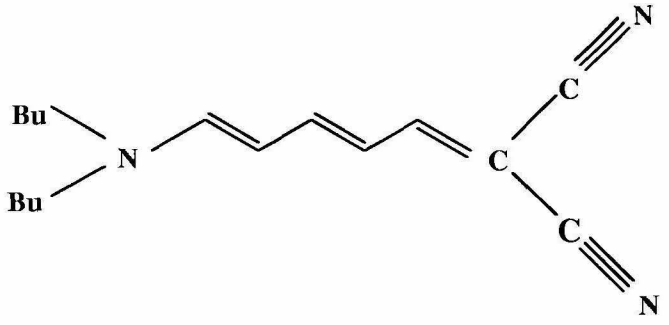

Figure 3.8: Molecule with the positive maximum in β

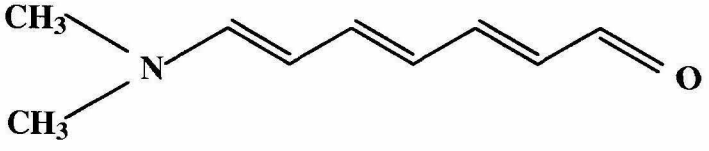

Figure 3.9: Molecule with the positive maximum in γ

VB-CT model. Thus, (55) has $t = E_g/\sqrt{7} = 1.10eV$.

Thus, spectroscopic measurements of λ_{max}, together with selected NLO data, can be utilized to predict structures and solvents needed to attain desired structure-NLO property relationships. Elsewhere[16] we will consider a more complete description of solvent effects.

3.5 Summary

We presented the valence-bond charge-transfer (VB-CT) model to provide a simple means for predicting nonlinear optical properties of charge transfer type organic molecules and for explaining in simple analytic terms the relationship between these properties and structure. The absorption frequency, hyperpolarizabilities, and bond length alternation (BLA) are expressed in term of analytic formulae with a total of four independent parameters, V, t, Q, and k. Here k is a force constant appropriate for the BLA coordinate of polyene linkers and should be similar for all such materials

(it might depend on polyene length; we used a k based on the universal force field)[10]. Q is the ratio of the actual dipole moment of the excited CT state to that expected for perfect charge transfer. This value will depend mainly on polyene length, but will be close to the values used here (Q = 0.5 to 0.7). V and t are related to bandgap (λ_{max}) and to bandwidth. The value of t is mainly determined by the length of the polyene spacer as well as the coupling of the donor and acceptor to the spacer. Thus, the variable most accessible to design is V which can be modified by changing the strength of the donor or the acceptor, the bridge topology, or the solvent polarity. We have shown how to estimate the polarizabilities for various materials by estimating V based on bandgap measurements.

We have shown how α, β, γ, and δ are related by derivatives with respect to f and how the design of molecules with an appropriate value of f can lead to optimization of particular properties, while minimizing the others.

3.6 References

1. Prasad, P. N.; Williams, D. J. Eds, *Introduction to Nonlinear Optical Effects in Molecules and Polymers* (Wiley, New York, 1991).

2. Kuhn, H.; Robillard, J. Eds, *Nonlinear Optical Materials* (CRC Press, Inc. 1992).

3. Ashwell, G. J.; Hargreaves, R. C.; Baldwin, C. E.; Bahra, G. S.; Brown, C. R., *Nature* **357**, 393 (1992).

4. Stegeman, G. I.; Burke, J. J.; Seaton, C. T., "*Nonlinear Integrated Optics,*" in "*Optical Engineering: Integrated Optical Components and Circuits.*" ed. by Huteheson, L. D.; Dekker, M., New York, 1987, Vol. 13.

5. Dulcic, A.; Flytzanis, C.; Tang, C. L.; Pepin, D.; Fetizon, M.; Hoppiliard, Y., *J. Chem. Phys.* **74**, 1559 (1981).

6. Cheng, L. T.; Tam, W.; Marder, S. R.; Stiegman, A. E.; Rikken, G.; Spangler, C. W., *J. Phys. Chem.* **95**, 10643 (1991).

7. (a) Marder, S. R.; Beratan, D. N.; Cheng, L. T., Science **252**, 103 (1991); (b) Marder, S. R.; Perry, J. W.; Bourhill, G.; Gorman, C. B.; Tiemann, B. G., *Science* **261**, 186 (1993); (c) Marder, S. R.; Gorman, C. B.; Tiemann, B. G.; Cheng, L. T., *J. Am. Chem. Soc.* **115**, 3006 (1993); (d) Marder, S. R. *et al.*, *J. Am. Chem. Soc.* **115**, 2524 (1993); (e) Gorman, C. B.; Marder, S. R.,*Proc. Natl. Acad. Sci.* **90**, 1129 (1993).

8. Lu, D.; Chen, G.; Goddard, W. A. III, *J. Chem. Phys.*, **101**, 4920 (1994).

9. Baughman, R. H.; Kohler, B. E.; Levy, I. J.; Spangler, C. W., *Synth. Met.* **11**, 37 (1985).

10. Rappé, A. K.; Casewit, C. J.; Colwell, K. S.; Goddard, W. A. III; Skiff, W. M., *J. Am. Chem. Soc.* **114**, 10024 (1992).

11. Oudar, J. L., *J. Chem. Phys.* **67**, 446 (1977).

12. Granvill, M. F.; Holtom, G. R.; Kohler, B. E., *J. Chem. Phys.* **72**, 4671 (1980).

13. Lu, D.; Chen, G.; Goddard, W. A. III, work in progress.

14. Bourhill, G.; Tiemann, B. G.; Perry, J. W.; Marder, S. R., *Nonlinear Optics*, in press.

15. Bourhill, G.; Cheng, L. T.; Gorman, C. B.; Lee, G.; Marder, S. R.; Perry, J. W.; Perry, M. J.; Tiemann, B. T., *Proc. SPIE* 2143 (1994).

16. Chen, G.; Lu, D.; Goddard, W. A. III, *J. Chem. Phys.*, **101**, 5860 (1994).

Chapter 4 The Valence-Bond Charge-Transfer Solvation Model (VB-CT-S) Nonlinear Optical Properties of Organic Molecules in Polar Solvents

4.1 Introduction

Lu *et al.*[1] (denoted as Paper I) recently proposed the valence-bond charge-transfer (VB-CT) model to predict polarizability (α) and hyperpolarizabilities (β, γ, and δ) of charge-transfer conjugated molecules. This simple model accounts for the dependence of the polarizabilities on the charge transfer energy (V) and shows that α, β, γ, and δ are all related to the bond-length alternation (BLA), which is in turn related to the fraction, f, of the wavefunction having CT character. This leads to a derivative relationship among α, β, γ and δ. In Section 4.2 we start with the VB-CT model and employ the Marcus solvation model[2] to predict how solvation affects the polarizabilities of molecule in Figure 4.1. This leads to the valence-bond charge-transfer-solvation (VB-CT-S) model in which the solvent is described as a continuous medium with dielectric constant ϵ and the donor and acceptor groups are represented by two spheres of radius r_D and r_A, respectively (see Figure 4.2). VB-CT-S describes how the absorption edge, BLA, and hyperpolarizabilities are related to the solvent properties.

In Section 4.3 VB-CT-S is employed to interpret and explain recent experimental

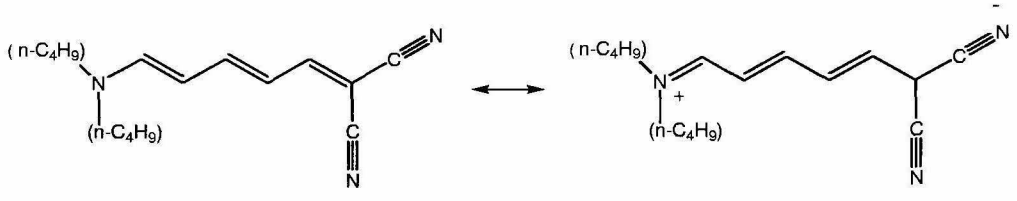

Figure 4.1: Molecule 1,1 dicyano, 6-(di-butyl amine) hexatriene

observations by Marder, Perry, and coworkers[3] on the effect of solvation on the second hyperpolarizability, γ. We also predict the values of α, β, and δ as a function of solvent polarity.

4.2 The VB-CT-S Model

4.2.1 No Solvent

The VB-CT model of Paper I assumes that the wavefunction of the molecule and all properties can be described as a linear combination

$$\Psi_{gr} = \sqrt{1-f}\ \Psi_{VB} + \sqrt{f}\ \Psi_{CT} \tag{4.1}$$

of the two valence bond configurations in Figure 3.1, Ψ_{VB} and Ψ_{CT}. Here Ψ_{VB} is the wavefunction for the valence bond ground state (no charge transfer from donor to acceptor) while Ψ_{CT} describes the state in which an electron is moved from donor to acceptor while readjusting the other bonds. The optimum resonance fraction, f, in (4.1) is determined by the relative energy of Ψ_{VB} and Ψ_{CT}, the coupling between them, the change in the dipole moments, and the solvent polarity.

Without solvent the Hamiltonian is

$$H_0 = \begin{pmatrix} 0 & -t \\ -t & V \end{pmatrix}, \tag{4.2}$$

where Ψ_{CT} and Ψ_{VB} are assumed to be orthogonal

$$\langle \Psi_{CT} | \Psi_{VB} \rangle = 0. \tag{4.3}$$

Here

$$-t = \langle \Psi_{CT} | \mathcal{H} | \Psi_{VB} \rangle \tag{4.4}$$

is the charge transfer matrix element (t is positive), and

$$V = \langle \Psi_{CT} | \mathcal{H} | \Psi_{CT} \rangle - \langle \Psi_{VB} | \mathcal{H} | \Psi_{VB} \rangle \tag{4.5}$$

is the difference in energy between Ψ_{CT} and Ψ_{VB}. This leads to a bandgap of

$$E_g = \sqrt{V^2 + 4t^2}. \tag{4.6}$$

Introducing the bond length alternation coordinate, q_{opt}, V is replaced by

$$V = V_0 + \frac{1}{2}k\left[\left(q - q^0_{CT}\right)^2 - \left(q - q^0_{VB}\right)^2\right], \tag{4.7}$$

and the bond length alternation can be written as

$$\begin{aligned} q_{opt} &= (1-f)\, q^0_{VB} + f q^0_{CT} \\ &= q^0_{VB} - f\left(q^0_{VB} - q^0_{CT}\right) \end{aligned} \tag{4.8}$$

where $q^0_{VB} = -0.12$Å and $q^0_{CT} = +0.12$Å.

4.2.2 Solvation Effects

Placing a CT molecule into a polar solvent leads to reorientation of both the solvent and solute molecules. This changes the relative energy of Ψ_{VB} and Ψ_{CT}, (4.5), which through (4.2) changes the optimum fraction, f, of CT character in the ground state (4.1). Assuming that only CT contributes, the dipole moment of the ground state becomes

$$\mu = f\mu_{CT} = fQeR_{DA} \tag{4.9}$$

where

$$\mu_{CT} = QeR_{DA}. \tag{4.10}$$

As shown in Chapter 3, the fraction of CT character in the ground state is

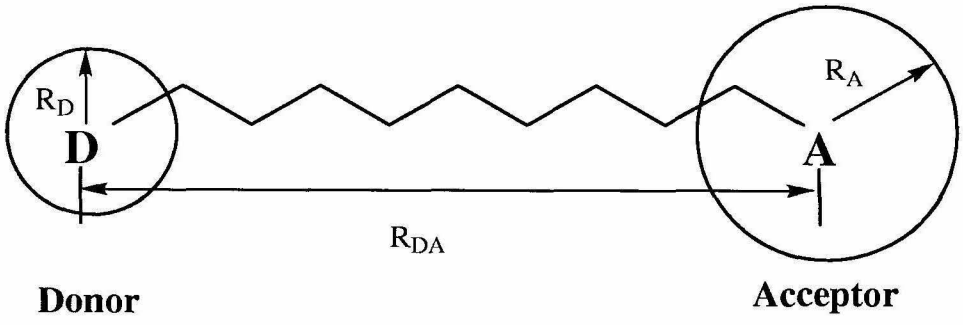

Figure 4.2: The Marcus solvation model. r_D and r_A are the radii of the donor and acceptor, respectively. R_{DA} is the distance between the donor and acceptor.

$$f = \frac{\sqrt{V^2 + 4t^2} - V}{2\sqrt{V^2 + 4t^2}} = \frac{1}{2} - \frac{\sqrt{E_g^2 - 4t^2}}{2E_g} \quad . \tag{4.11}$$

In the VB-CT-S model we assume that electronic states other than Ψ_{VB} and Ψ_{CT} have much higher energies and that t (the coupling between Ψ_{VB} and Ψ_{CT}) is independent of solvent. Thus quantitative evaluation of the solvation effects requires only the change in relative energy, (4.5),

$$V_S = V + \Delta V_S \tag{4.12}$$

due to the presence of solvent. Here V is the energy difference between Ψ_{VB} and Ψ_{CT} without solvent and ΔV_S is the change in the relative energy caused by the addition of solvent. Including BLA the final V is obtained from (4.12) using V_S in place of V.

To evaluate ΔV_S we approximate[2] the donor and acceptor by two spheres of radius r_D and r_A with charges distributed symmetrically as in Figure 4.2. For charges of Ze and $-Ze$ on the donor and accepter atoms, the electric displacement field $\mathbf{D}$ is

$$4\pi\mathbf{D} = \frac{Ze}{|\mathbf{x_s} - \mathbf{x_d}|^3}(\mathbf{x}_s - \mathbf{x}_d) - \frac{Ze}{|\mathbf{x}_s - \mathbf{x}_a|^3}(\mathbf{x}_s - \mathbf{x}_a), \tag{4.13}$$

where $\mathbf{x}_s$, $\mathbf{x}_d$, $\mathbf{x}_a$ are the displacement vectors for solvent, donor and acceptor, respectively. Assuming the relaxation time of solvent molecules is much longer than the time scale of charge transfer, the induced dipole moment density of solvent is always equal to its equilibrium value $\mathbf{P_{eq}}$, which is readily expressed as

$$\mathbf{P_{eq}} = \left(1 - \frac{1}{\epsilon}\right)\mathbf{D_{eq}} \tag{4.14}$$

where ϵ is the dielectric constant of the solvent, and $\mathbf{D_{eq}}$ is the electric displacement field at equilibrium [i.e., $Z = fQ$ in (15)]. For a static electric field, the energy is calculated as

$$E_\epsilon = \frac{1}{2}\int \mathbf{E}\cdot\mathbf{D}\, d^3\mathbf{r}. \tag{4.15}$$

The energy change upon the adding the solvent is

$$\Delta E = -\frac{1}{2\epsilon_0}\int \mathbf{P_{eq}}\cdot\mathbf{D}\, d^3\mathbf{r}. \tag{4.16}$$

Ignoring image charges, this leads to

$$\Delta V_S = -\frac{e^2}{4\pi\epsilon_0}\left(1 - \frac{1}{\epsilon}\right) fQ^2 S_F, \tag{4.17}$$

where

$$S_F = \frac{1}{2r_D} + \frac{1}{2r_A} - \frac{1}{R_{DA}} \tag{4.18}$$

depends only on the geometry.

From (4.17) we observe that strong solvation effects arise from:

1. large ϵ
2. small radii of donor or acceptor, and
3. large R_{DA}.

Given (4.12) and (4.17) expressing V in terms of V_0, S_F, and ϵ, we can use (4.6) to determine the energy gap, E_g, as a function of solvent polarity. We assume that the energy gap is given by the absorption edge $\lambda_{max} = hc/E_g$.

The polarizabilities have the form (see 3.30-3.33)

$$\alpha_{zz} = \frac{2t^2\mu_{CT}^2}{E_g^3} = \frac{2t^2(\mu_{DA})^2 f^2 Q^2}{(V^2+4t^2)^{3/2}} \tag{4.19}$$

$$\beta_{zzz} = \frac{3t^2\mu_{CT}^3 V}{E_g^5} = \frac{3t^2(\mu_{DA})^3 f^3 Q^3 V}{(V^2+4t^2)^{5/2}} = -\frac{1}{2}\mu\frac{\partial\alpha_{zz}}{\partial V} \tag{4.20}$$

$$\gamma_{zzzz} = \frac{4t^2\mu_{CT}^4(V^2-t^2)}{E_g^7} = \frac{4t^2(\mu_{DA})^4 f^4 Q^4\,(V^2-t^2)}{(V^2+4t^2)^{7/2}} = \frac{1}{3}\mu^2\frac{\partial\beta_{zzz}}{\partial V} \tag{4.21}$$

$$\delta_{zzzzz} = \frac{5t^2\mu_{CT}^5(V^2-3t^2)V}{E_g^9} = \frac{5t^2(\mu_{DA})^5 f^5 Q^5(V^2-3t^2)V}{(V^2+4t^2)^{9/2}} = -\frac{1}{4}\mu^3\frac{\partial\gamma_{zzzz}}{\partial V}. \tag{4.22}$$

In solution one measures the rotationally averaged values of the polarizabilities,

$$\alpha \equiv \langle\alpha\rangle = \frac{1}{3}\left(\alpha_{xx}+\alpha_{yy}+\alpha_{zz}\right), \tag{4.23}$$

$$\mu\beta \equiv \langle\mu\cdot\beta\rangle = \sum_{i,j}\beta_{ijj}\mu_i, \tag{4.24}$$

$$\gamma \equiv \langle\gamma\rangle = \frac{1}{5}(\gamma_{xxxx}+\gamma_{yyyy}+\gamma_{zzzz}+2\gamma_{xxyy}+2\gamma_{yyzz}+2\gamma_{xxzz}). \tag{4.25}$$

Assuming only the z components are nonzero, (4.23)-(4.25) lead to

$$\alpha = \frac{1}{3}\alpha_{zz} = \frac{2t^2\mu_{CT}^2}{3E_g^3} \tag{4.26}$$

$$\beta = \frac{\mu_z\beta_{zzz}}{\mu} = \frac{3t^2\mu_{CT}^3 V}{E_g^5} \tag{4.27}$$

$$\gamma = \frac{1}{5}\gamma_{zzzz} = \frac{4t^2\mu_{CT}^4(V^2-t^2)V}{5E_g^7}. \tag{4.28}$$

All quantities in (4.19)-(4.22) are defined except Q, which is the ratio of the actual solvent-free dipole moment of the CT state to the ideal value assuming that the CT state has one electron transfered from the donor to the acceptor. This can be obtained

by comparing to the absolute value of one of the quantities in (4.19)-(4.22) at some value of ϵ.

4.3 Comparison with Experiment

4.3.1 Application to 1,1 dicyano, 6-(di-butyl amine) hexatriene,(1)

The dots in Figure 4.3.c show the experimental values[3] of the second hyperpolarizability γ for molecule (1) for a variety of solvents [$C_6H_6{-}n{-}C_6H_{14}$ ($\epsilon = 2.087$), Dioxane ($\epsilon = 2.209$), CCl_4($\epsilon = 2.238$), C_6H_6 ($\epsilon = 2.284$), CH_2Cl_2 ($\epsilon = 9.08$), CH_3OH ($\epsilon = 32.6$), and CH_3CN ($\epsilon = 37.5$)]. We will compare the predictions of $VB{-}CT{-}S$ theory with these experimental results.

To compare VB-CT-S theory with experiment, we must evaluate six parameters: t, V_0, S_F, R_{DA}, Q, and k. Using the Universal Force Field[4,5] (UFF) in conjunction with Charge Equilibration theory[6] to predict the charges of Figure 4.1 in vacuum, we obtain

$$R_{DA} = 7.30\text{Å} \tag{4.29}$$

for molecule in Figure 4.1. Similarly UFF[4] leads to

$$k = 773.7kcal/\text{Å}^2 = 33.55\text{eV}/\text{Å}^2 = 5.38mdyn/cm. \tag{4.30}$$

The remaining parameters t, V_0, S_F, and Q are each intrinsic parameters of CT molecules and can be determined directly from experiment.[3]

According to Chapter 3, γ is zero when $|V| = |t|$. Experimentally[3] $\gamma = 0$ for a solvent polarity of $\epsilon = 2.209$, leading to $E_g = 2.648eV$ for this polarity. Thus from $|V| = |t|$ and (7), we obtain

$$t = E_g/\sqrt{5} = 1.184eV. \tag{4.31}$$

V_0 and S_F can be obtained by fitting absorption peaks in two different solvents. We

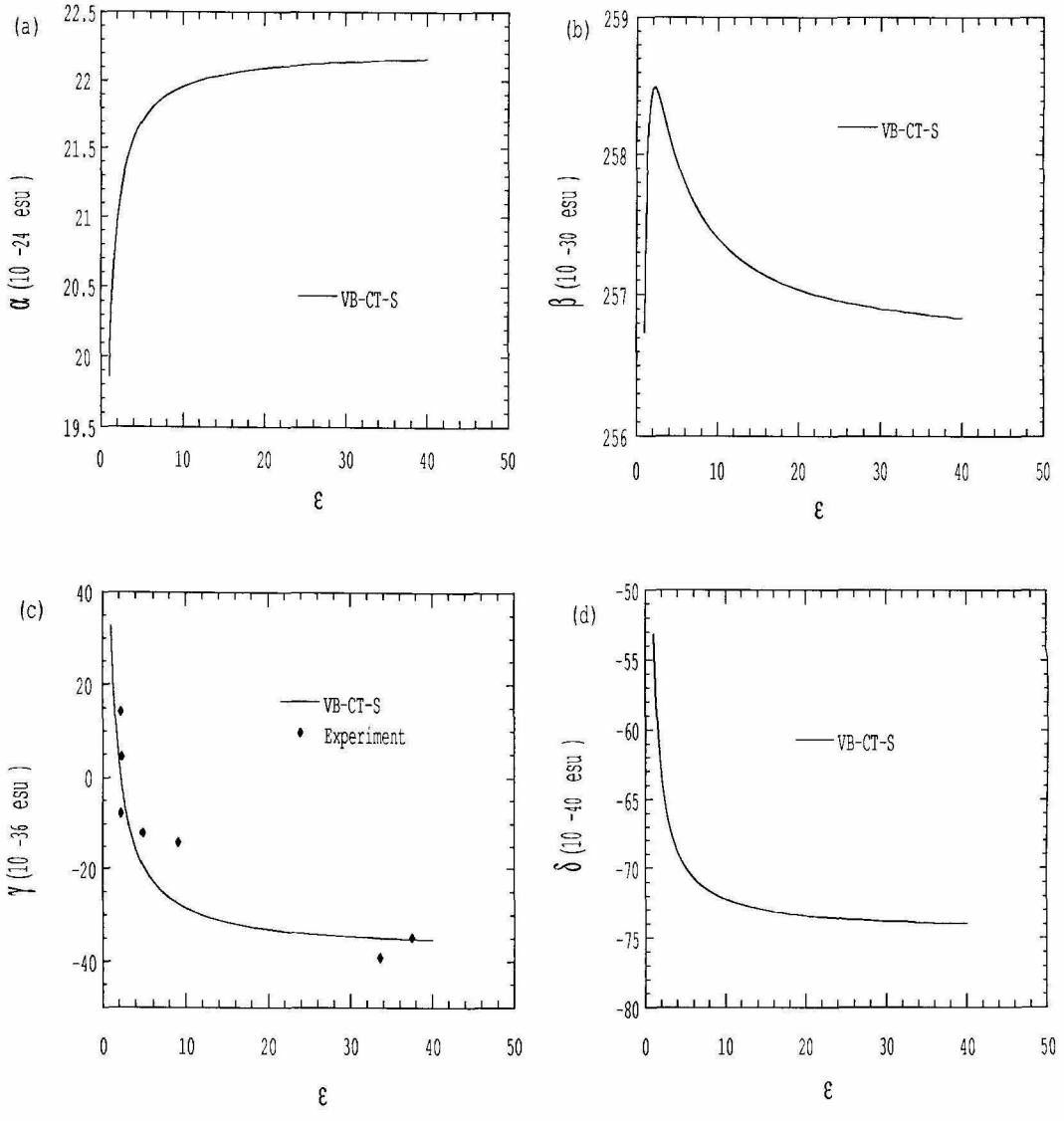

Figure 4.3: The predicted dependence of polarizabilities on solvent polarity (expressed in terms of the static dielectric constant ϵ). (a) Polarizability, α, (b) Hyperpolarizability, β, (c) Second hyperpolarizability, γ, (d) Third hyperpolarizability, δ_{zzzzz}. The values plotted are the static averaged values. The parameters used are: $V_0 = 0.833$ eV, $S_F = 0.0685\text{Å}^{-1}$, $t = 1.184$ eV, $R_{DA} = 7.30$Å, $Q = 0.738$, k =33.55 eV/Å^2. For γ in (c) a comparison is made between theory (solid line) and experiment (dots). Here the experimental results were corrected to static values using (4.39).

choose dioxane ($\epsilon_1 = 2.209$ and[7] absorption energy $E_{g1} = 2.648eV$), and CH_3CN ($\epsilon_2 = 37.5$ and[7] $E_{g2} = 2.604eV$). This leads to the following equations:

$$V_0 + \frac{1}{2}k\left[\left(q_1 - q_{CT}^0\right)^2 - \left(q_1 - q_{VB}^0\right)^2\right] - \frac{e^2}{4\pi\epsilon_0}\left(1 - \frac{1}{\epsilon_1}\right) f_1 Q^2 S_F = \sqrt{{E_{g1}}^2 - 4t^2}, \quad (4.32)$$

$$V_0 + \frac{1}{2}k\left[\left(q_2 - q_{CT}^0\right)^2 - \left(q_2 - q_{VB}^0\right)^2\right] - \frac{e^2}{4\pi\epsilon_0}\left(1 - \frac{1}{\epsilon_2}\right) f_2 Q^2 S_F = \sqrt{{E_{g2}}^2 - 4t^2}, \quad (4.33)$$

where f_i depends on t and E_g [as given in (4.11)] and the BLA coordinate, q_i, can be obtained from (4.7) and (4.8). Solving equations (4.32), and (4.33), leads to

$$Q^2 S_F = 0.0373\text{Å}^{-1} \quad (4.34)$$

and

$$V_0 = 0.833\text{eV} \quad (4.35)$$

To separate out Q from S_F, we can fit to the magnitude of γ at some ϵ. We choose to do this for CH_3CN ($\epsilon = 37.5$). The experimental value[3] is $\gamma_{static} = -35$ esu whereas the calculated value would be $\gamma = -118$ esu for $Q = 1$. This leads to

$$Q^4 = 0.297, \quad (4.36)$$

or

$$Q = 0.738. \quad (4.37)$$

Substituting into (4.34) leads then to

$$S_F = 0.0685\text{Å}^{-1}. \quad (4.38)$$

Given t, V_0, S_F, Q, R_{DA}, and k from (4.29 - 4.38), we can calculate α, β, γ, and δ for all solvent polarities, ϵ. The resulting averaged values are shown in Figure 4.3.

Currently only γ is available from experiment, Figure 4.3.c. We see that VB-CT-S fits reasonably well with experiment[3] despite the simplicity of this model. It will be valuable to measure the α and β for this molecule in various solvents in order to

further test the model.

4.3.2 Frequency Dependent Correction for Hyperpolarizations

In Figure 4.3.c the experimental THG results are corrected to the static values by using the following formula

$$\frac{\gamma_{THG}}{\gamma_{static}} = \frac{1}{4}\left(\frac{E_g^3}{(E_g-3\omega)(E_g-2\omega)(E_g-\omega)} + \frac{E_g^3}{(E_g+3\omega)(E_g+2\omega)(E_g+\omega)} + \frac{E_g^3}{(E_g+\omega)(E_g+2\omega)(E_g-\omega)} + \frac{E_g^3}{(E_g+\omega)(E_g-2\omega)(E_g-\omega)}\right) \tag{4.39}$$

where E_g is the bandgap and ω is the frequency used in the experiment ($\omega = 0.65eV$). Similarly when experiments are available, the α and β will be corrected by using

$$\frac{\beta_{SHG}}{\beta_{static}} = \frac{E_g^4}{(E_g^2-4\omega^2)(E_g^2-\omega^2)}, \tag{4.40}$$

and

$$\frac{\alpha_\omega}{\alpha_{static}} = \frac{E_g^2}{E_g^2-\omega^2}. \tag{4.41}$$

4.4 Discussion

4.4.1 Summary of VB-CT-S

The VB-CT-S model is quite simple. It involves

1. two properties (k and R_{DA}) which can be obtained from the force field (spectroscopy or theory)

2. three electronic parameters (V_0, t, Q) characteristic of the isolated molecule that can be derived from theory or experiment on the isolated molecule or from experiment in solution [as illustrated in Section 4.3.1]

3. one solvent independent parameter, S_F, which must be obtained from an experimental value of the α, β, or γ in a polar solvent.

Given these six parameters one can predict the properties [λ_{max}, α, β, γ, δ, and q_{opt}] as a function of solvent polarity.

4.4.2 Estimation of Molecular Based Properties

In designing new nonlinear materials, one might consider replacement of the donor, of the acceptor, or of the linker. The value for V_0 should depend strongly on the ionization potential (IP) of donor (D) and the electron affinity (EA) of acceptor (A) which might be related to the change in redox potentials for some solvent. Similarly the differential charge transfer, Q, can be estimated from IP_D and EA_A. The effect of changing the length of the linker or of replacing the polyene linker in (1) with other polymers is more difficult. In an earlier paper,[8] we discussed the dependence of λ_{max}, α, β, and γ on polymer chain length based on a valence-bond charge-transfer-exciton (VB-CTE) model of the polymer chain. The combination of the VB-CT-S description of donor accepter systems with the VB-CTE model for polymer linker character and length leads to a three state description that is no longer analytic. This will be considered in a later paper.[9]

4.4.3 Estimation of Solvent Properties

In comparing to experiment we used the *static* dielectric constant for the solvent. This assumes that the relaxation time of the solvent is much longer than the time scale of charge transfer (that is, of the excitation process). This is true in polar solvents where the dielectric contribution is dominated by the orientation of the polar molecule. For non-polar solvents, the contribution of the induced electronic dipole moment to the total dielectric constant is not negligible, and its response to the change of electric field may have a time scale similar to the charge transfer. In this case we should use the frequency dependent dielectric constant, ϵ_ω. This may account for the poorer fit of γ to experiment[3] for the nonpolar solvents.

4.4.4 Estimation of Solvation Energy

In estimating the effect of solvent on the energy separation V_S [equations (4.12)-(4.18)], we employed the Marcus solvent model used for predicting electron transfer rates[2]. This leads to the specific form (4.18) for the geometric parameter S_F in which r_A and r_D should be about the size of the van der Waals radii of the donor and the acceptor. Assuming that $r_A = r_D$, equation (4.38) leads to $r_A = 4.87$Å for molecule in Figure 4.2. This is a plausible value, but we may also treat S_F as a characteristic shape parameter of the CT molecule. The induced dipole density of the solvent is proportional to $\frac{1}{\epsilon}$. Therefore, ΔV_S in (4.17) should be proportional to $\left(1 - \frac{1}{\epsilon}\right)$ and f regardless of the structure of solvent molecule. Hence equation (4.17) may be generalized to an arbitrary geometry of the CT molecule (rather than Figure 4.2).

More rigorous ways to calculate solvation effects are available. Thus Warshel *et al.* [10] used an explicit representation of the solvent (the SCAAS model, surface constrained all atom solvation) to treat the effect of solvent on the empirical valence bond (EVB) description of an S_N2 reaction. To treat S_N1 ionic dissociation in a liquid, Kim and Hynes[11] used a nonlinear Schrödinger equation formulation. Alternatively, the solvation energy could be evaluated with the DelPhi Poisson-Boltzmann continuum solvent procedure of Honig *et al.* [12]. The charges for such calculations could be obtained using Charge Equilibration (QEq)[6]. Indeed, Friesner *et al.* [13] have developed an interface between Jaguar[14] and DelPhi[12] that does the quantum mechanics self-consistently within the self-consistent reaction field of the solvent[13].

4.5 Summary

We find that the simple $VB{-}CT{-}S$ model provides a quantitative explanation of the dependence of hyperpolarizabilities β and γ on solvation. The theory agrees well with the experimental results by Marder, *et al.*[3] for the γ of molecule in Figure 4.1, the only system for which a hyperpolarizability has been measured for a wide range of solvents. The VB-CT-S theory employs a continuous dielectric description of the solvent and leads to analytic formula for λ_{max}, α, β, and γ in different solvents.

Because of its simplicity, this theory should be of use in designing new nonlinear optical materials.

4.6 References

1. Lu, D.; Chen, G.; Perry, J. W.; Goddard, W. A. III, *J.Am.Chem.Soc.* **116**, 10679 (1994).

2. Marcus, R. A., *J. Chem. Phys.* **24**, 996 (1956).

3. Marder, S. R.; Perry, J. W.; Bourhill, G.; Gorman, C. B.; Tiemann, B. G., **Science 261**, 186 (1993).

4. Rappé, A. K.; Casewit, C. J.; Colwell, K. S.; Goddard, W. A. III; W. M. Skiff, W. M., **J. Am. Chem. Soc. 114**, 10024 (1992).

5. Force field calculations were carried out with POLYGRAF from Molecular Simulation Inc. (Burlington, Massachusetts).

6. Rappé, A. K.; Goddard, W. A. III, *J. Phys. Chem.* **95**, 2260 (1991).

7. Personal correspondence with Dr. Bourhill and Dr. Perry of JPL.

8. Lu, D.; Chen, G.; Goddard, W. A. III, *J. Chem. Phys.*, **101**,4920 (1994).

9. Lu, D.; Chen, G.; Goddard, W. A. III, work in progress.

10. Warshel, A.; Weiss, R. M., *J. Am. Chem. Soc.* **102**, 6218 (1980); Hwang, J. K.; King, G.; Creighton, S.; Warshel, A., *J. Am. Chem. Soc.* **110**, 5297 (1988).

11. Kim, H. J.; Hynes, J. T., *J. Am. Chem. Soc.* **114**,10508 (1992); ibid, **114**,10528 (1992).

12. Jean-Charles, A.; Nicolls, A.; Sharp, K.; Honig, B.; Tempczyk, A.; Hendrickson, T. F.; Still, W. C., *J.Am.Chem.Soc.* **113** 1454 (1991).

13. Tannor, D. J.; Marten, B.; Murphy, R.; Friesner, R. A.; Nicholls, A.; Honig, B.; Ringnalda, M., "Accurate First Principles Caculations of Molecular Charge Distributions and Solvation Energies from Ab Initio Quantum Mechanics and Continuum Dielectric Theory," *J. Am. Chem. Soc.*, submitted.

14. Langlois, J. -M.; Muller, R. P.; Coley, T. R.; Goddard, W. A. III; Ringnalda, M. N.; Won, Y.; Friesner, R. A., J.Chem.Phys. **92**, 7488 (1990). Greeley, B. H.; Russo, T. V.; Mainz, D. T.; Friesner, R. A.; Langois, J. -M.; Goddard, W. A. III; Donnelly, R. E. Jr.; Ringalda, M. N., "New Pseudospectral Algorithms for Electronic Structure Caculations: Length Scale Separation and Analytical Two-Electron Integral Corections," *J. Am. Chem. Soc.*, submitted.

15. This is available as Jaguar/Solvate from Schrödinger Inc. (Pasadena, California).

Chapter 5 The Temperature Dependence For Nonlinear Optical Properties of Donor Acceptor Push-Pull Organic Molecules

5.1 Introduction

Extensive theoretical studies[1–13] have been done on the hyperpolarizabilities of organic materials. Most studies are for the ideal case of an isolated molecule in a vacuum at its equilibrium geometry (absolute temperature of zero). However, most measurements of hyperpolarizabilities are at room temperature and in solvent. In order to compare the theoretical calculations with the experiment, it is important to consider the temperature dependence and solvation effects on the hyperpolarizabilites of these molecules.

We recently proposed the valence-bond charge-transfer (VB-CT) model[14] to predict hyperpolarizabilities of donor acceptor push-pull conjugated molecules, such as (1). In order to predict the effect of solvation on the hyperpolarizabilities of these molecules, we developed the VT-CT-S model.[15] Both studies ignored the effect of temperature. In this paper, we use the VB-CT model to consider the electronic and vibrational contributions to hyperpolarizabilities at finite temperature. This leads to analytical expressions for describing the temperature dependence of the hyperpolarizabilities.

5.2 Theory

The highest hyperpolarizabilities for organic systems are obtained in push-pull donor acceptor organics which exhibit two dominant resonant structures differing by a charge transfer from the donor to the acceptor.[16–17] We assume as a model the typical example 1,1 dicyano,6-(di-butyl amine) hexatriene (Figure 4.1). In this system two

low energy vibrational modes are likely to play a role in thermal effects on nonlinear optical (NLO) properties. The vibrational mode q distorts the resonance structure of a into b in Figure 4.1 and is critical in determining the hyperpolarizability. Motion in the torsional mode t modifies the π overlap and hence the coupling of the states in Figure 4.1. Thus motions in both q and t might modify the polarizabilities. We write the ground state energy at finite temperature as

$$E = E_v(q, \phi) + E_t(\phi) \tag{5.1}$$

where $E_t(\phi)$ is the torsional energy and $E_v(q, \phi)$ describes the vibrational energy of the resonance system (Figure 4.1).

We describe the vibrational energy of this system as in the VB-CT model,

$$E_v(q) = \frac{1}{2}V(q) + \frac{1}{2}\lambda\left(q - q_{VB}^0\right)^2 - \frac{1}{2}\sqrt{V^2(q) + 4t^2(\phi)} \tag{5.2}$$

where

$$V(q) = V_0 + \frac{1}{2}\lambda\left[\left(q - q_{CT}^0\right)^2 - \left(q - q_{VB}^0\right)^2\right] \tag{5.3}$$

and λ is the force constant. However, we now allow the transition matrix element, t, between VB state and CT state to depend on the torsional angle ϕ,

$$t = t(\phi). \tag{5.4}$$

The torsional energy, $E_t(\phi)$, can be expanded to a Fourier series

$$E_t(\phi) = -\sum_{m=0}^{\infty} E_m \cos(m\phi). \tag{5.5}$$

There are two contributions to the polarizability and hyperpolarizabilities: electronic and vibrational. From reference 14, 19, 20, and 21, the polarizability and hyperpolarizabilities have the forms

$$\alpha^e = \frac{2t^2\mu^2}{\Delta^3} \tag{5.6}$$

$$\beta^e = \frac{3t^2\mu^3 V}{\Delta^5} \tag{5.7}$$

$$\gamma^e = \frac{4t^2\mu^4\left[V^2 - t^2\right]}{\Delta^7} \tag{5.8}$$

$$\alpha^v = \alpha^e\overline{\alpha} = \alpha^e\frac{2t^2\lambda(q^0_{CT} - q^0_{VB})^2}{\Delta^3} \tag{5.9}$$

$$\beta^v = \beta^e\overline{\beta} = \beta^e\frac{6t^2\lambda(q^0_{CT} - q^0_{VB})^2}{\Delta^3} \tag{5.10}$$

$$\gamma^v = \gamma^e\overline{\gamma} = \gamma^e(1 + \frac{9V^2}{8(V^2 - t^2)}). \tag{5.11}$$

Here $\Delta = \sqrt{V^2 + 4t^2}$ and we omit the z subscripts where z is the direction along the linker.

Hence, the total polarizability and hyperpolarizabilities are

$$\alpha = \alpha^e + \alpha^v = \frac{2t^2\mu^2}{\Delta^3}(1 + \frac{2t^2\lambda(q^0_{CT} - q^0_{VB})^2}{\Delta^3}) \tag{5.12}$$

$$\beta = \beta^e + \beta^v = \frac{3t^2\mu^3 V}{\Delta^5}(1 + \frac{6t^2\lambda(q^0_{CT} - q^0_{VB})^2}{\Delta^3}) \tag{5.13}$$

$$\gamma = \gamma^e + \gamma^v = \frac{4t^2\mu^4(V^2 - t^2)}{\Delta^7}(2 + \frac{9V^2}{8(V^2 - t^2)}). \tag{5.14}$$

The average value of a property p [either the polarizability (α) or hyperpolarizabilities (β, and γ] of the molecule is given by

$$< p >= \frac{1}{Z}\int_{-\infty}^{+\infty} dq \int_{-\pi}^{\pi} d\phi\, p(\phi, q) exp\left[-\frac{E_v(q,\phi) + E_t(\phi)}{kT}\right] \tag{5.15}$$

where Z is the partition function

$$Z = \int_{-\infty}^{+\infty} dq \int_{-\pi}^{\pi} d\phi\, exp\left[-\frac{E_v(q,\phi) + E_t(\phi)}{kT}\right]. \tag{5.16}$$

Since the vibrational and torsional energies are much higher than the thermal energy, the first order approximation to (5.15) and (5.16) leads to [see (A-14) of

Appendix A]

$$< p >= p(q_0, \phi_0) + \left[\frac{1}{2\lambda_q} \frac{\partial^2 p(q_0, \phi_0)}{\partial^2 q} + \frac{1}{2E_\phi} \frac{\partial^2 p(q_0, \phi_0)}{\partial^2 \phi} \right] kT \tag{5.17}$$

where

$$\lambda_q = \lambda \left\{ 1 - \frac{2t^2(\phi_0)\lambda \left(q^o_{VB} - q^o_{CT}\right)^2}{\left[V^2(q_0) + 4t^2(\phi_0)\right]^{\frac{3}{2}}} \right\} \tag{5.18}$$

and

$$E_\phi = E_{t1} - \frac{2t_1 t(\phi_0)}{\sqrt{V^2(q_0) + 4t^2(\phi_0)}}. \tag{5.19}$$

Here q_0 and ϕ_0 are the optimum vibrational coordinate and torsional angle, while t_1 and E_{t1} are the second derivatives of $t(\phi)$ and $E_t(\phi)$ evaluated at ϕ_0.

5.3 Application to 1,1 dicyano, 6-(di-butyl amine) hexatriene

We illustrate the application of (5.17)-(5.19) by applying the theory to the molecule 1,1 dicyano,6-(di-butyl amine) hexatriene, Figure 4.1. The values of some of the parameters were fitted to the experimental data in reference 15:

$$\begin{aligned} t_0 &= 1.184 \text{ eV}, \\ V_0 &= 0.833 \text{ eV}, \\ \frac{\mu}{|e|} &= 5.39 \text{ Å}, \text{ and} \\ \lambda &= 33.55 \text{ eV/Å}^2. \end{aligned} \tag{5.20}$$

Here t_0 is the charge transfer matrix element, V_0 is the difference in energy between the valence bond state and the charge transfer state, μ is dipole moment, and λ is the force constant.

Using the universal force field[18](UFF), we expand the torsional potential in the

form of

$$E_t(\phi) = E_t(\phi_0) + \frac{1}{2}V_0(\phi - \phi_0)^2 \tag{5.21}$$

where $\phi_o = 0$ and $V_0 = 0.434eV$. The matrix element t can be written in the form of

$$t = t_0 \cos\phi \tag{5.22}$$

where $t_0 = 1.184eV$. The matrix element V can be written in the form of

$$V = V_0 + \frac{1}{2}\lambda(q - q_0)^2 \tag{5.23}$$

where the equilibrium position[15] $q_0 = -0.0577$ Å.

Thus, the total energy has the form

$$E(\text{eV}) = -0.6362 + 12.16\,[q + 0.0577]^2 + 0.953\phi^2. \tag{5.24}$$

Substituting (5.6 - 5.14) and (5.24) into (5.15 - 5.16) leads to

$$\alpha^e = (19.84 + 0.00028\ T)\ 10^{-24}\ \text{esu} \tag{5.25}$$

$$\beta^e = (256.81 - 0.0173\ T)\ 10^{-30}\ \text{esu} \tag{5.26}$$

$$\gamma^e = (32.88 - 0.046\ T)\ 10^{-36}\ \text{esu} \tag{5.27}$$

$$\alpha^v = (5.47 + 0.00072\ T)\ 10^{-24}\ \text{esu} \tag{5.28}$$

$$\beta^v = (212.07 - 0.0067\ T)\ 10^{-30}\ \text{esu} \tag{5.29}$$

$$\gamma^v = (254.48 - 0.079\ T)\ 10^{-36}\ \text{esu} \tag{5.30}$$

$$\alpha = (25.31 + 0.0010\ T)\ 10^{-24}\ \text{esu} \tag{5.31}$$

$$\beta = (468.88 - 0.024\ T)\ 10^{-30}\ \text{esu} \tag{5.32}$$

$$\gamma = (287.36 - 0.125\ T)\ 10^{-36}\ \text{esu}. \tag{5.33}$$

Here α and γ are the average values. Thus at $T = 300$ K, we obtain

$$\alpha = 25.61 \times 10^{-24}\ \text{esu}, \tag{5.34}$$

$$\beta = 461.68 \times 10^{-30}\ \text{esu}, \tag{5.35}$$

$$\gamma = 249.86 \times 10^{-36}\ \text{esu}. \tag{5.36}$$

In Figure 1 we compare the values from equation (5.31 - 5.33) (dash line) with numerical evaluation of equation (5.17) (solid line). We see that these two curves agree very well at temperatures up to $T = 500$ K. The increased discrepancy for higher temperatures may arise partly from the higher order terms.

As the temperature increases from $0K$ to $300K$, α increases by 1%, β decreases by 1.7%, and γ decreases by 10%. Thus for a donor acceptor push-pull molecule, temperature has only a very small effect on α, β and γ.

5.4 Discussion

5.4.1 Electronic and Vibrational Hyperpolarizabilities

In Figure 1, we plot the contributions from electronic hyperpolarizabilities (line with cross), and vibrational hyperpolarizabilities (line with triangle). As the temperature increases from $0K$ to $300K$, α^e increases by 0.5%, α^v increases by 3%, β^e decreases by 2.1%, β^v decreases by 1.3%, γ^e decreases by 50%, and γ^v decreases by 8%.

The sensitivity of γ^e to temperature occurs because molecule (1) was designed to have a large β^e, causing γ^e near the zero crossing point (see Figure 2 of reference 14).

5.4.2 Macroscopic Hyperpolarizabilities

The experimentally measured hyperpolarizabilities are the average of microscopic hyperpolarizabilities over a statistical distribution of molecular orientations. For the

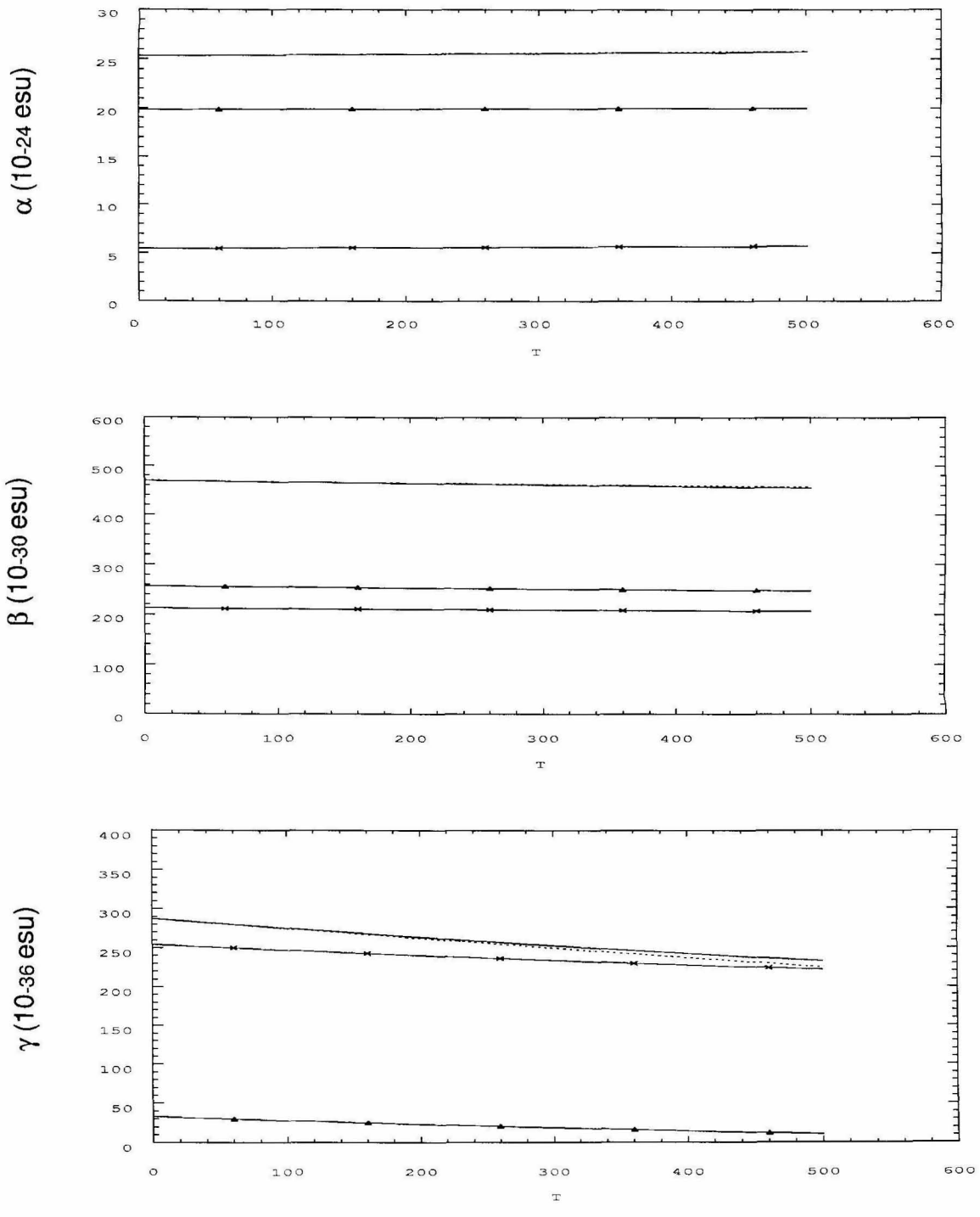

Figure 5.1: Temperature dependence of the polarizability (α), and hyperpolarizabilities (β, and γ) for 1,1 dicyano,6-(di-butyl amine) hexatriene (1). The dash lines (analytical) are from the formula (5.31 - 5.33). The solid lines are from the numerical evaluation of (5.17). The crosses are the vibrational contributions. The triangles are the electronic contributions.

isotropic average,

$$\begin{aligned}
\bar{\alpha} &= <\alpha> + \frac{\mu^2}{3kT} = \frac{1}{3}(\alpha_{xx} + \alpha_{yy} + \alpha_{zz}) + \frac{\mu^2}{3kT} \\
\bar{\beta} &= 0 \\
\bar{\gamma} &= <\gamma> + \frac{\mu \cdot \beta}{5kT} \\
&= \frac{1}{5}(\gamma_{xxxx} + \gamma_{yyyy} + \gamma_{zzzz} + 2\gamma_{xxyy} + 2\gamma_{xxzz} + 2\gamma_{yyzz}) + \frac{\mu \cdot \beta}{5kT}.
\end{aligned} \tag{5.37}$$

Here $\bar{\alpha}, \bar{\beta}$, and $\bar{\gamma}$ indicate the macroscopic hyperpolarizabilities. Considering temperature effects, the above equations become

$$\bar{\alpha} = <\alpha_0> + A_\alpha kT + \frac{\mu^2}{3kT} \tag{5.38}$$

$$\bar{\gamma} = <\gamma_0> + \frac{\mu A_\beta}{5} + A_\gamma kT + \frac{\mu \cdot \beta_0}{5kT}. \tag{5.39}$$

Here A_α, A_β, and A_γ are the temperature coefficients in (8) while α_0, β_0, and γ_0 indicate the values at $T = 0K$. In most cases, the modification is negligible. However, for the cases discussed in Section 5.4.1, the temperature effects can be significant.

5.5 Summary

We extended the VB-CT model to treat the effects of temperature on hyperpolarizabilities. We find that temperature has a little effect on hyperpolarizabilities. The result is an analytic description which may be useful in predicting the effects of temperature and in analyzing the results from experiment.

5.6 References

1. Prasad, P. N.; Williams, D. J. Eds, *Introduction to Nonlinear Optical Effects in Molecules and Polymers*; Wiley: New York, 1991.

2. Kuhn, H.; Robillard, J. Eds, *Nonlinear Optical Materials*; CRC Press, Inc. 1992.

3. Perry, J. W.; Mansour, K.; Lee, I. *et al.*, *Science.* 1996, **273**, 1533

4. Rumi, M.; Zeribi, G.; and Mullen, K., *J. Chem. Phys.* 1998, **108**, 685

5. Shuai, Z.; Bredas, J. L.; Saxena, A.; Bishop, A. R., *J. Chem. Phys.* 1998, **109**, 572.

6. Maroulis, G., *J. Chem. Phys.* 1998, **108**, 5432.

7. Jacquemin, D.; Champagne, B.; Kirtman, B., *J. Chem. Phys.* 1997, **107**, 5076.

8. Champagne, B., *Chem. Phys. Lett.* 1998, **287**, 185.

9. Ohta, K.; Sakaguchi, T.; Hamada, K.; Fukumi, T., *Chem. Phys. Lett.* 1997, **274**, 306.

10. Norman, P.; Luo, Y.; Jonsson, D.; Agren, H., *J. Chem. Phys.* 1997, **106**, 8788.

11. Lauderdale, W. J.; Coolidge, M. B., *J. Phys. Chem.* 1995, **99**, 9368.

12. Matsuzawa, N.; Ata, M.; Dixon, D. A., *J. Phys. Chem.* 1995, **99**, 7698.

13. Kirtman, B.; Luis, J. M.; Bishop, D. M., *J. Chem. Phys.* 1998, **108**, 10008.

14. Lu, D.; Chen, G.; Perry, J.; Goddard, W. A. III., *J. Am. Chem. Soc.* 1994, **116**, 10679.

15. Chen, G.; Lu, D.; Goddard, W. A. III., *J. Chem. Phys.* 1994, **101**, 5860.

16. Marder, S. R.; Perry, J. W.; Bourhill, G.; Gorman, C. B.; Tiemann, T. G.; Mansour, K., *Science.* 1993, **261**, 186.

17. Marder, S. R.; Torruellas, W. E.; Blancharddesce, M.; Ricci, V. *et al.*, *Science,* 1997, **276**, 1233.

18. Rappé, A. K.; Casewit, C. J.; Colwell, K. S.; Goddard, W. A. III; Skiff, W. M., *J. Am. Chem. Soc.* 1992, **114**, 10024.

19. Kim, H.; Cho, M.; Jeon, S., *J. Chem. Phys.* 1997, **107**, 1936.

20. Castiglioni, C.; Del Zoppo, M.; Zerbi, G. *Phys. Rev. B*, 1996, **53**, 13319.

21. Bishop, D.; Champagne, B.; Kirtman, B., *J. Chem. Phys.* 1998, **109**, 9987.

Chapter 6 Saturation of the Second Hyperpolarizability for Polyacetylenes

6.1 Introduction

It is well known[4-7] that for polyenes, $-(-CH=CH-)_N-$, α and γ increase rapidly with N for smaller N but saturate to increase only linearly with N above some value, N_{sat} ($\beta = 0$ since the molecule is centrosymmetric). For polythiophenes (which have a polyene backbone), it was established[4-7] that α saturates at $N = 10$ double bonds (a C_{20} polyene) whereas γ saturates at $N = 18$ double bonds (C_{36}). For the parent compound, polyacetylene (PA), experiment[18] shows that $N^{\gamma}_{sat} > 16$ and theory[16] shows that $N^{\gamma}_{sat} > 22$. However, it has not been possible to study sufficiently large N to establish N^{γ}_{sat} experimentally (because of difficulties with synthesis) or theoretically (because of expense). Of two recent reports on long chain polyenes in Science, experiment[8] on a substituted, imperfect PA leads to $N^{\gamma}_{sat} \approx 125$ (C_{250}) whereas (semiempirical) theory[9] leads to $N^{\gamma}_{sat} = 20$ (C_{40}), see Figure 6.1.

6.2 Calculations

The largest previously *ab initio* theoretical calculations[16] were on $N = 22$ (C_{44}), far too small to test for saturation. We have developed a new *ab initio* quantum mechanical program (Jaguar/NLO)[11-13] which allows predictions of hyperpolarizabilities for large molecules 10 to 20 times faster than previously possible. We report here *ab initio* Hartree-Fock (HF) calculations (6-31G basis set)[14] on α and γ with N up to 49 (C_{98}). The geometry was obtained from the optimized structure[15] of $C_{22}H_{24}$ (HF with a 6-31G basis), using the central unit to determine the geometry of all PA polymers. (This led to $C=C = 1.450$ Å, $C-C = 1.338$ Å and a bond angle of 124.3°.) We

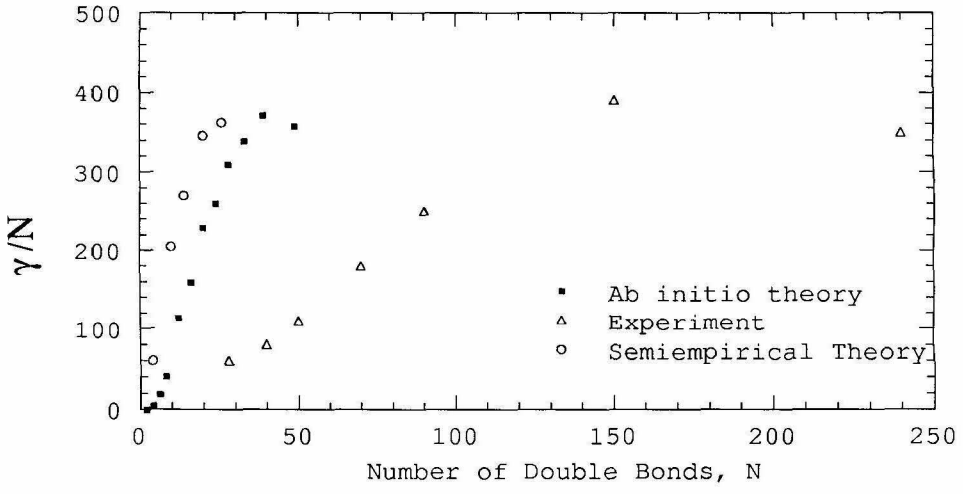

Figure 6.1: Recent results on the saturation of γ/N for polyacetylenes (PA). The open squares are from the experient (reference 8) on a substituted, imperfect PA. The open circles are from semiempirical theory (reference 9).The filled squares are from the current calculation.

tested the geometry by calculating the energy of $C_{48}H_{50}$ with bond lengths changed by $\pm$ 0.003 Å and found that the above structure has the lowest energy.

The α and γ were obtained by calculating $\mu(\mathcal{E})$ with three finite fields (sufficient because of the inversion symmetry). We used electric fields along the chain direction to obtain α_{zz} and γ_{zzzz}.

There are two contributions to the errors.

1. Higher order terms in (1.1). By using a fourth electric field for $C_{78}H_{80}$, we found that neglect of higher order terms leads to less than 0.01% error for α and to about 0.4% error for γ.

2. Errors in the calculation of the dipole moment (due to lack of convergence or other errors in the wavefunction). By examining the changes of α and γ with convergence, we estimate that the error from this source is less than 0.01% for α and less than 3% for γ.

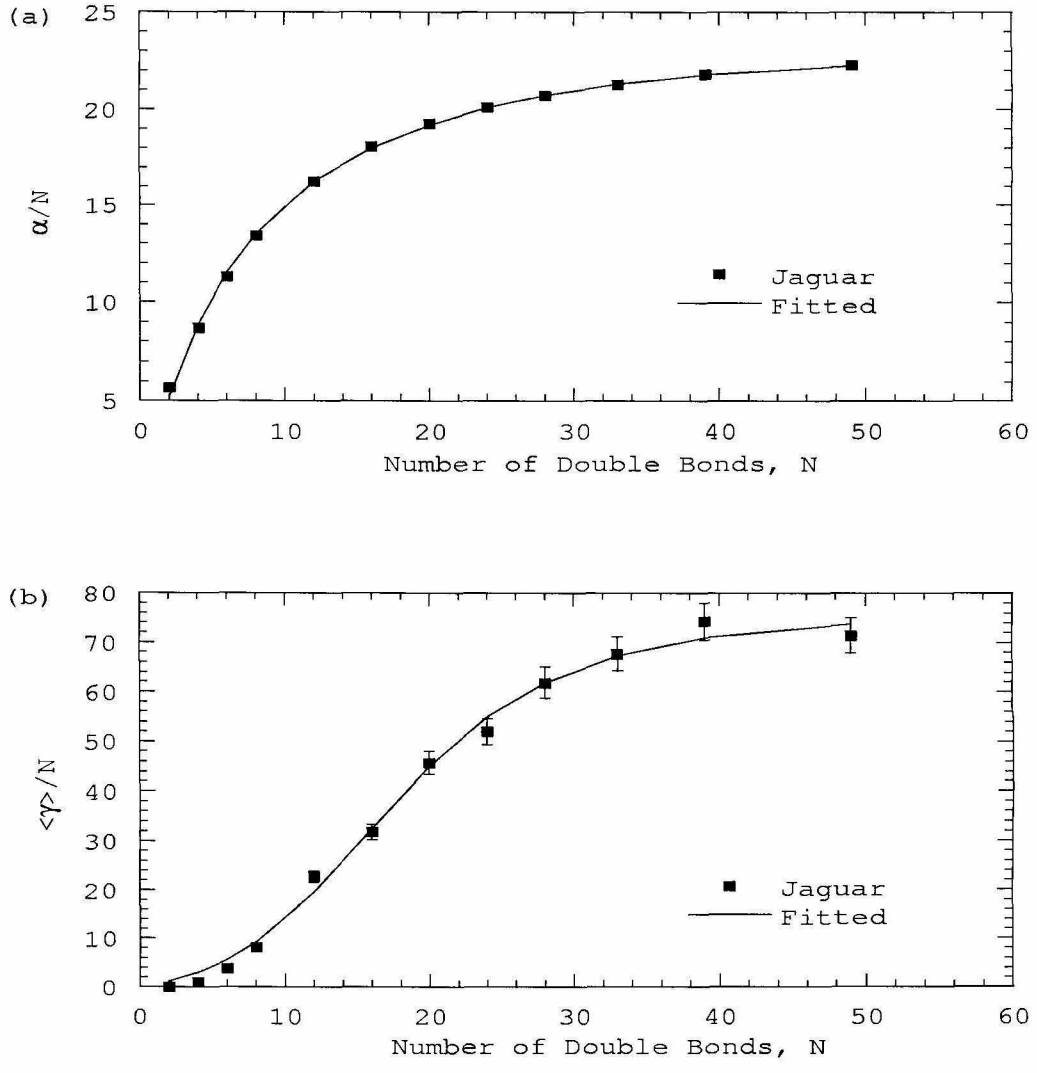

Figure 6.2: (**a**) Polarizability of polyacetylenes chains from *ab initi o* calculations (Jaguar/NLO). The filled squares are from the current *ab initio* HF calculations. The open circles are for VB-CT using $t = 0.83eV$ and $V = 1.0eV$. The solid line is a fit to an equation like (6.3). The parameters are $\alpha_\infty = 22.6 \times 10^{-24}$esu , $A_\alpha = 0.249$, $B_\alpha = 0.84$, and $C_\alpha = 0.08$. (**b**) Second hyperpolarizability of polyacetylenes chains from *ab initio* calculations (Jaguar/NLO). The line is a fit to equation (6.3). The parameters are $\bar{\gamma}_\infty = 380 \times 10^{-36}$ esu, $A_\gamma = 0.073$, $B_\gamma = 11.4$, and $C_\gamma = 0.182$.

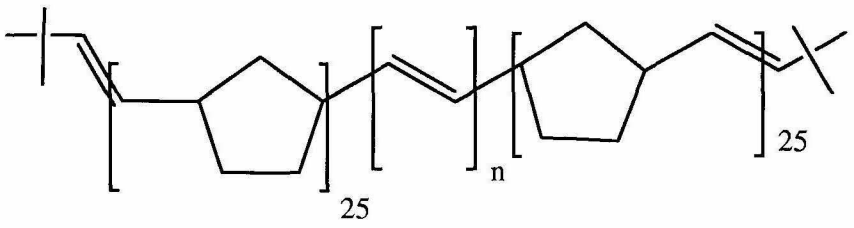

Figure 6.3: Molecule used in experiment (reference 8)

Figure 6.2.a shows the results for α (filled squares), where we see that

$$N_{sat}^{\alpha} = 25 \pm 2 \ (C_{50}). \tag{6.1}$$

Figure 6.2.b shows results for $< \gamma >= \gamma_{zzzz}/5$ where we see that

$$N_{sat}^{\gamma} = 45 \pm 5 \ (C_{90}). \tag{6.2}$$

These values are obtained by fitting α/N and γ/N to smooth curves and setting N_{sat} to 95% of the limiting value. For large N we expect

$$\bar{\gamma}_N = \frac{\gamma}{N} = \bar{\gamma}_{\infty} \left(\frac{1 - exp(-AN)}{1 + Bexp(-CN)} \right). \tag{6.3}$$

The solid lines in Figure 6.2 represent the fits to such a function.

6.3 Discussion

Direct experimental measurements on γ for polyenes has been made by Craig *et al.*[18] who synthesized polymer (Figure 6.3) with N from 4 to 13. The resulting values of γ (in THF) are included in Figure 6.3 (filled triangles). The N dependence from theory and experiment agree well[20].

Previous *ab initio* calculations[16] (HF with 6-31G basis) considered only N up to 22. These results (open squares in Figure 6.3) are in excellent agreement with the current results (circle in Figure 6.3).

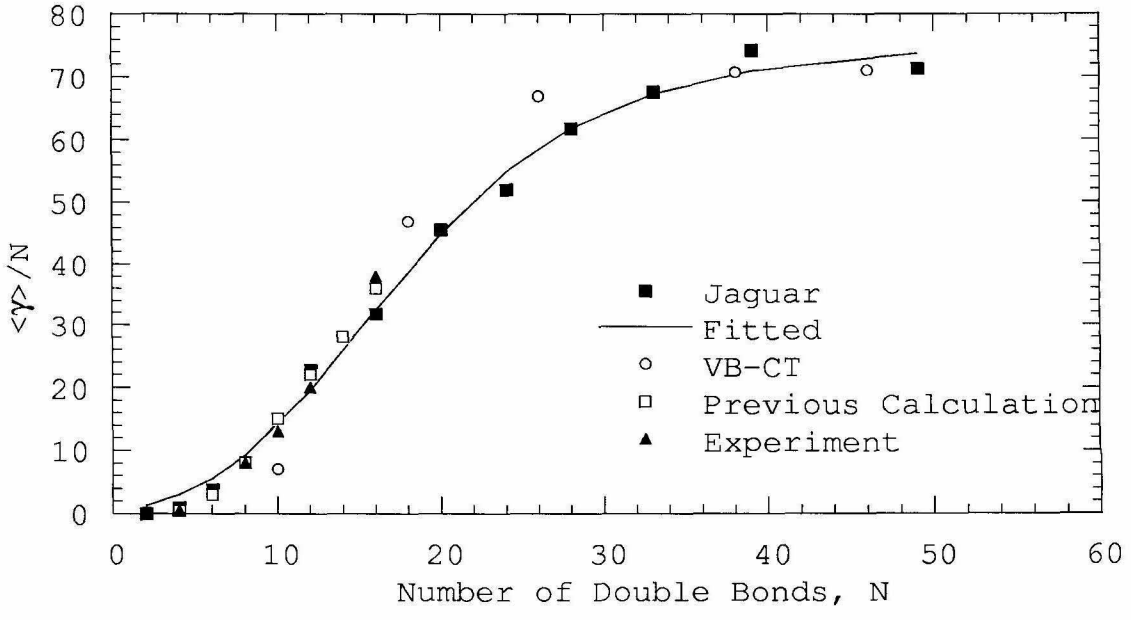

Figure 6.4: Second hyperpolarizability of polyacetylenes chains. The filled squares are from the current *ab initio* HF calculations while previous *ab initio* results (reference 14) are shown with open squares. The open circles are for VB-CT using $t = 0.83eV$ and $V = 1.0eV$. Direct experimental results (reference 16) are shown with filled triangles.

Mukamel and coworkers[9] predicted the N dependence of γ using an electron-hole model (based on semiempirical PPP π electron calculations) to describe polarization. Their results (crosses in Figure 6.2) lead to saturation at $N_{sat}^{\gamma} = 20$ (C_{40}). This is substantially smaller than the *ab initio* results ($N_{sat}^{\gamma} = 45$). The difference is probably due to approximation in the semiempirical and electron-hole descriptions.

Previously[5–7] we developed a simple theoretical model, valence bond-charge transfer (VB-CT), for predicting polymer length dependence of α and γ. This method involves two parameters (t and V) which can be fitted to either experiment or theory. [The bandgap and valence bandwidth and their dependence can be used on N.] Using $t = 0.83eV$ and $V = 1.0eV$ for VB-CT leads to good agreement with the *ab initio* results on α (as shown in Figure 1, open circles). The VB-CT results for γ in Figure 6.3 (open circles, scaled by a factor of 0.457) leads to $N_{sat}^{\gamma} = 45$, in excellent agreement with the *ab initio* calculations.

6.4 Summary

Summarizing, the *ab initio* theoretical studies lead to $N_{sat}^{\alpha} = 25 \pm 2$ and $N_{sat}^{\gamma} = 45 \pm 5$.

These theoretical results are in strong disagreement with recent experimental results[8], which led to $N_{sat}^{\gamma} = 125$. However, these experiments did *not* involve pure all-trans polyenes. The synthetic method[19] led to about a 50-50% mixture of the species in Figure 6.5. We find (vide infra) that such disorder can increase N_{sat}^{γ}. In addition, there appears to be other structural defects[8,19] in the chains that might modify the saturation length. Also the measurement of chain length was indirect[8], leading to additional uncertainties.

Given the limitations in the experiments, *we believe that the current estimate of* $N_{\gamma}^{sat} = 45 \pm 5$ *is the most reliable estimate.*

In order to examine the role that disorder plays in α and γ, we used VB-CT theory with the t and V parameters discussed above but randomly changed V (the site energy) by $\pm 0.4eV$. The result is shown in Figure 6.6 along with that for pure all-trans polyethylene. We find two effects:

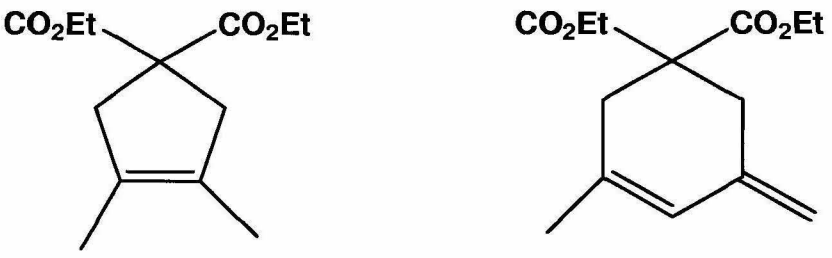

Figure 6.5: Solvent used in experiment (reference 19)

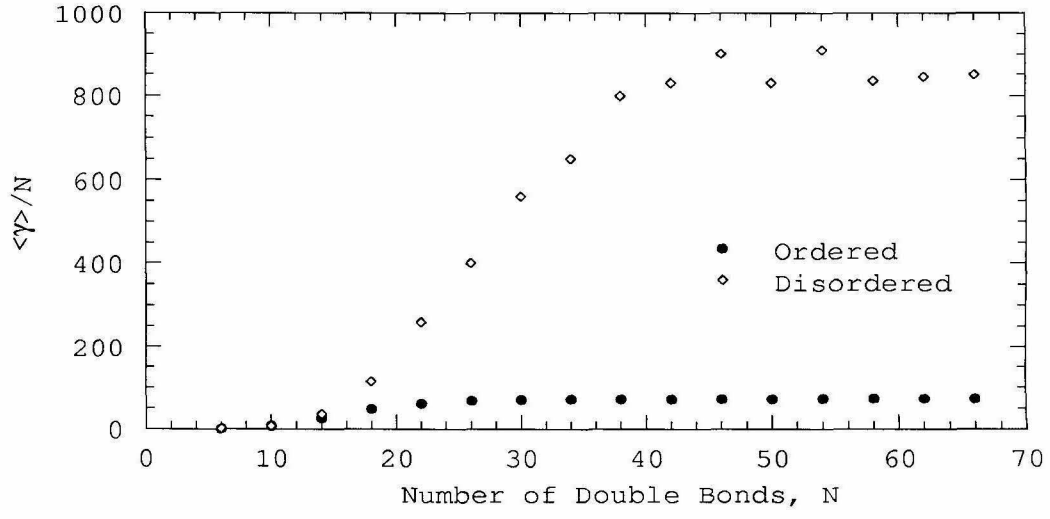

Figure 6.6: Effect of disorder in second hyperpolarizability based on VB-CT with $t = 0.83eV$ and $V = 1.0eV$. Filled circles indicates the ordered polyene while open circles are with a random disorder of $V_i = V \pm 0.4eV$.

1. N_{sat}^{γ} increases by a factor of about 1.4.

2. The *magnitude* of γ for a given N also increases by a factor of about 5.

This suggests that deliberate inclusion of disorder may be advantageous. One might do this by including monomers with CH_3, Cl, or F substituents. Such monomers might lead to increased solubility in various solvents, allowing synthesis of longer chains. In addition one might achieve the alignment needed for high nonlinear performance by using substituents that can be photolytically or thermally cross linked in the applied electric field.

6.5 References

1. For a recent survey see Chemistry and Engineering News, February 20, 1995, page 28.

2. Arizmendi, L.; Agullolope, F., MRS Bulletin, **19**(3), 32-38(1994).

3. Marder, S. R. *et al.*, *Science* **263**, 511(1994).

4. Thinpont, H.; Rikken, G. L.; Meijer, E. W.; tan Hoeve, W.; Hynberg, H., *Phys. Rev. Lett.* **65**, 2141 (1990).

5. Chen, G.; Lu, D.; Goddard, W. A. III, *J. Chem. Phys.* **101**, 5860 (1994).

6. Lu, D.; Chen, G.; Goddard, W. A. III, *J. Chem. Phys.* **101**, 4920 (1994).

7. Lu, D.; Chen, G.; Perry, J. W.; Goddard, W. A. III, *J. Am. Chem. Soc.* **116**, 10679 (1994).

8. Samuel, I. D. W.; Ledoux, I.; Dhenaut, C.; Zyss, J.; Fox, H. H.; Schrock, R. R.; Silbey, R. J., *Science* **265**, 1070 (1994).

9. Mukamel, S.; Tahahashi, A.; Wang, H. X.; Chen, G., *Science* **266**, 250 (1994).

10. Hurst, G. J. B.; Dupuis, M.; Clementi, E., *J. Chem. Phys.* **89**, 385 (1988).

11. Ringnalda, M. N.; Langlois, J.-M.; Greeley, B. H.; Murphy, R. B.; Russo, T. V.; Cortis, C.; Muller, R. P.; Marten, B.; Donnelly, R. E. Jr.; Mainz, D. T.; Wright, J. R.; Pollard, W. T.; Cao, Y.; Won, Y.; Miller, G. H.; Goddard, W. A. III; Friesner, R. A., Jaguar v2.01, Schrödinger, Inc., Pasadena, California, 1994.

12. Lu, D.; Marten, B.; Cao, Y.; Ringnalda, M. N.; Freisner, R. A.; Goddard, W. A. III, *Chem. Phys. Lett.*, **242**, 543 (1995).

13. Marten, B.; Cao, Y.; Friesner, R. A.; Lu, D.; Goddard, W. A. III, J. Chem. Phys., submitted.

14. The 6-31G basis set gives accurate predictions for such systems. For example, in reference 10 we calculated the hyperpolarizabilities of Julolidinyl-n-isoxazolone using the 6-31G basis set for $n = 1$ to 6. Adding polarization functions increases γ uniformly by about 10%. Thus the dependence of γ on N was not affected and led to excellent agreement with experiment. At the HF level the magnitude of β was systematically about half the experimental value.

15. Villar, H. O.; Dupuis, M.; Watts, J. D.; Hurst, G. J. B.; Clementi, E., *J. Chem. Phys.* **88**, 1003 (1988).

16. Kirtman, B.; Toto, J. L.; Robins, K. A.; Hasen, M., *J. Chem. Phys.* **102** 5350 (1995).

17. Mukamel, J.; Wang, H. X., *Phys. Rev. Lett.* **69**, 65 (1992).

18. Craig, G. S.; Cohen, R. E.; Schrock, R. R.; Silbey, R. J.; Puccetti, G.; Ledoux, I.; Zyss, J., *J. Am. Chem. Soc.* **115**, 860 (1993).

19. Fox, H. H.; Wolf, M. O.; O'Dell, R.; Lin, B. L.; Schrock, R. R.; Wrighton, M. S., *J. Am. Chem. Soc.* **116**, 2827 (1994).

20. Because of the correlation effect, the presence of solvent and end groups, and the non-zero frequency, it is difficult to compare the absolute values between the theory and experiment. Consequently, in Figure 6.4 we divided the reported experimental value of γ by a factor of 6.

Chapter 7 ab initio Predictions of Large Hyperpolarizability Push-Pull Polymers: Julolidinyl-n-isoxazolone and Julolidinyl-n-N, N'-diethylthiobarbituric acid

7.1 Introduction

For telecommunications (electrooptic switches), optical information processing, and sensor applications, it is useful to develop organic chromophores with very large first hyperpolarizabilities, β. A major step forward in developing such materials was made recently by Marder *et al.*[1] who succeeded in developing the highest β organics currently known, Julolidinyl-6-isoxazolone [Figure 7.1.a with $n = 6$] and Julolidinyl-6-N, N'-diethylthiobarbituric acid [Figure 7.1.b with $n = 6$]. These push-pull organic materials lead to $\mu \cdot \beta(0) = 13,600 \times 10^{-48}$ esu and $14,920 \times 10^{-48}$ esu, respectively.

Although semiempirical and *ab initio* level calculations of hyperpolarizabilities of various molecules have been reported recently[2–6], *ab initio* level calculations have not been previously reported for molecules of the size of molecules in Figure 7.1 with $n = 6$. We have developed a new *ab initio* Quantum Mechanical program (Jaguar/NLO)[7,8] which provides predictions of hyperpolarizabilities for such molecules far faster than previously possible and have applied it to predicting the hyperpolarizabilities for molecules in Figure 7.1.a with $n = 0$, 1, 2, 3, and 6, for molecules in Figure 7.1.b with $n = 6$.

7.2 Results

Hartree-Fock(HF) calculations using the 6-31G basis leads to the results in Table 7.1 and Figure 7.2. Here we see that the comparison between theory (in vacuum) and experiment (in chloroform) is good; in particular, the trend with n is excellent.

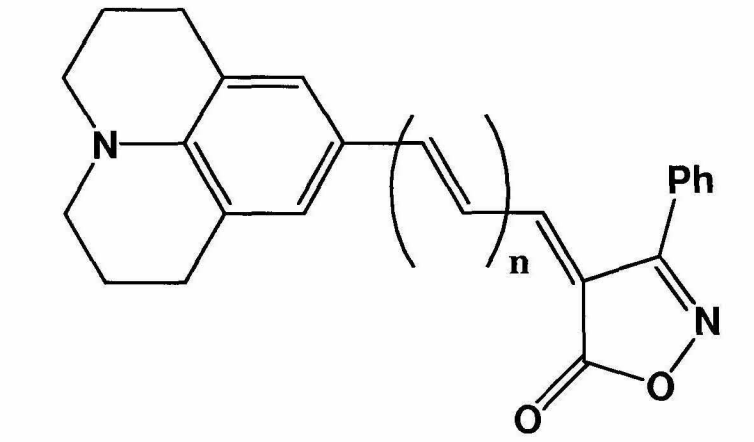

(a)

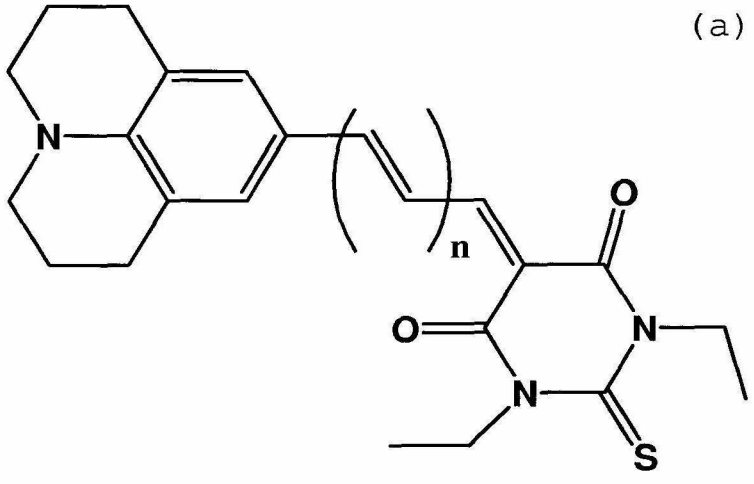

(b)

Figure 7.1: (a) Julolidinyl-n-isoxazolone and (b) Julolidinyl-n-N, N'-diethylthiobarbituric acid

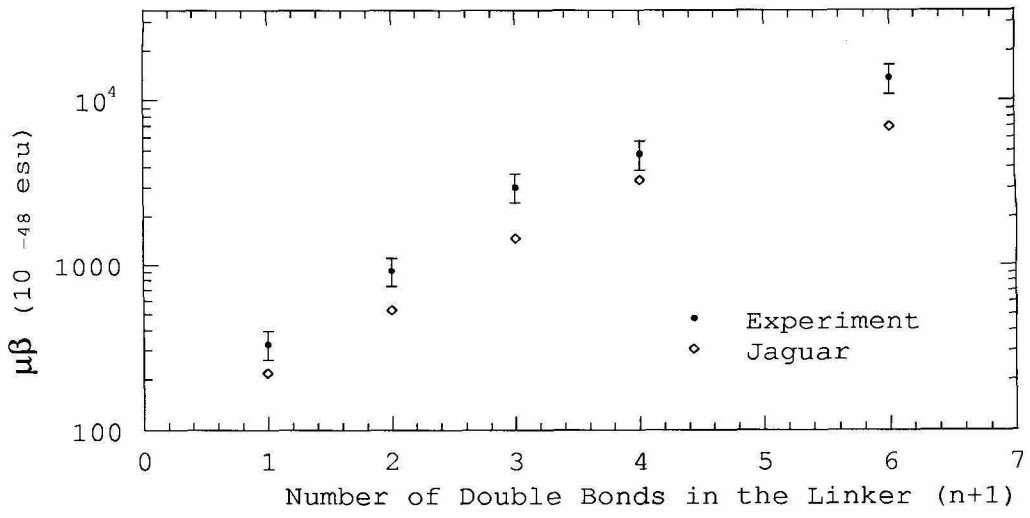

Figure 7.2: The dependence of hyperpolarizability $\mu \cdot \beta$ (0) for Jololidine-n-isoxazolone on $N = n + 1$, the number of double bonds in the linker.

The excellent agreement between theory and experiment suggests that theory can be used as an effective tool in developing new nonlinear optical materials. For Julolidinyl-6-isoxazolone the total CPU time to obtain $\mu, \alpha, \beta, \mu \cdot \beta$, γ is 10 hours (on an HP 735 workstation). This is much faster than the processes of synthesizing and purifying the compounds and then running the experiments to measure the moments and hyperpolarizabilities.

Taking x as the direction of the linker and xz as the plane of the linker leads to the components in Table 7.2. As expected, the major contribution to β is from β_x. For example, for molecule in Figure 7.1.a with $n = 6$, we calculate $\beta_x/\beta_y = 146$ and $\beta_x/\beta_z = 7.2$.

Table 7.1 shows that the theoretical dipole moment μ for moleclue in Figure 7.1.a changes smoothly with n (as expected). However, experiment[1] does not. The experimental values of μ are obtained from the changes of the capacitance of the vessel with molecules (Figure 7.1.a) in chloroform solvent. We believe that this discrepancy is mainly experimental.

The EFISH experiment[1] measures $\mu \cdot \beta$ rather than β. Since there is no data on the relation between the μ and β vectors, the experimental value of $\beta(0)$ is extracted

Molecule Class	n	$\mu \cdot \beta(0)$ Exp.	Jaguar	μ Exp.	Jaguar	$\beta(0)$ Exp.	Jaguar	θ Jaguar
1	0	328 ± 65	218	9.5	10.71	34 ± 7	31	49
1	1	919 ± 180	529	9.1	12.47	100 ± 20	60	45
1	2	3000 ± 600	1466	9.0	15.49	339 ± 70	117	36
1	3	4753 ± 950	3311	9.8	16.65	485 ± 100	232	31
1	6[a]	13600 ± 2720	6960	16	17.67	849 ± 100	442	27
2	6[a]	14920 ± 3000	6877	-	15.25	-	456	9

Table 7.1: Hyperpolarizabilities for the Julolidinyl-n-isoxazolone class and Julolidinyl-n-N,N'-diethylthiobarbituric acid class. Here μ is the dipole moment, $\beta(0)$ is the static hyperpolarizability, and θ is the angle between $\vec{\mu}$ and $\vec{\beta}$. The units are 10^{-48} esu for $\mu \cdot \beta(0)$, 10^{-18} esu for μ, and 10^{-30} esu for $\beta(0)$. The experiments used $CHCl_3$ solvent whereas theory considered molecules in the gas phase.

from $\mu \cdot \beta$, assuming that μ and β are parallel. However, the calculations (Table 7.1) show that the angle between μ and β of Figure 7.1.a ranges from 27° to 49°, and the angle for Figure 7.1.b is 9° for $n = 6$. Thus the theory is useful in extracting the experimental value of β from $\mu \cdot \beta$.

Experimental values were not reported for α (polarizability) and γ (second hyperpolarizability). We show in Figure 7.3 the calculated α, β, γ as a function of number of double bonds (N) in the linker for Figure 7.1.a. The lines in the log-log plots of Figure 7.3 lead to $\alpha = \alpha_0 N^{0.70}$, $\beta = \beta_0 N^{1.44}$, and $\gamma = \gamma_0 N^{2.65}$. The components of α, β and γ are listed in Table 7.2.[9]

The experiments were carried out for molecules in chloroform whereas the results reported above were for gas phase molecules. In order to determine the effects of solvent, we used Jaguar/Solvent[10–12] program which uses DelPhi[15] to evaluate the reaction field using a continuous Poisson-Boltzmann description of the solvent self consistently with using Jaguar to calculate the wavefunctions in the reaction field. Table 7.3 shows the calculated hyperpolarizabilities of molecules in Figure 7.1.a with $n = 0, 1, 2$ in chloroform ($\epsilon = 4.806$). Here we see that α is the same in the gas phase and in solvent, β changes less than 10%, and γ decreases less than 40% in solvent.

n	0	1	2	3	6^a	6^b
μ_x	9.66	11.12	14.29	15.35	16.71	15.20
μ_y	-1.04	-0.35	0.14	-0.73	-0.42	0.09
μ_z	4.50	-5.65	-5.97	-6.42	-5.72	1.12
α_{xx}	59.40	82.87	113.4	141.02	228.9	242.6
α_{yy}	23.40	19.38	18.91	20.71	24.2	28.0
α_{zz}	36.43	41.53	45.06	40.16	51.4	56.7
α_{xy}	-0.59	-1.69	-2.63	2.92	-1.8	0.8
α_{xz}	10.65	8.66	5.86	3.16	4.0	13.4
α_{yz}	0.27	-3.44	-0.02	7.37	2.9	-1.5
β_{xxx}	27.38	52.78	108.75	206.44	400.48	406.4
β_{xyy}	-1.17	0.74	2.44	14.26	16.39	20.9
β_{xzz}	2.24	3.86	2.69	14.97	20.91	27.5
β_x	28.45	57.38	113.88	229.24	437.77	454.8
β_{yxx}	-0.35	0.44	0.08	13.18	2.78	1.0
β_{yyy}	0.01	0.09	0.12	0.51	-1.11	-0.07
β_{yzz}	0.14	0.23	0.14	0.26	1.41	-0.07
β_y	-0.20	0.76	0.34	13.94	3.07	0.9
β_{zxx}	12.17	18.04	27.24	31.69	59.23	-26.7
β_{zyy}	-0.32	0.03	0.28	-0.22	0.19	-2.9
β_{zzz}	0.74	0.89	-0.71	-1.63	2.02	-4.4
β_z	12.59	18.96	26.81	29.84	61.44	-34.0
γ_{xxxx}	21.31	99.84	290.37	640.70	3736.7	4269.9
γ_{yyyy}	0.51	0.418	-0.80	-0.08	15.5	4.0
γ_{zzzz}	3.09	2.203	7.22	6.81	38.3	45.6

Table 7.2: Dipole moment μ, polarizability α, hyperpolarizabilities β and γ for Julolidinyl-n-isoxazolone class and Julolidinyl-n-N, N'-diethylthiobarbituric acid class. The units are 10^{-18} esu for μ, 10^{-24} esu for α, 10^{-30} esu for β, and 10^{-36} esu for γ.[a] Molecule in Figure 7.1.a with $n = 6$. [b] Molecule in Figure 7.1.b with $n = 6$.

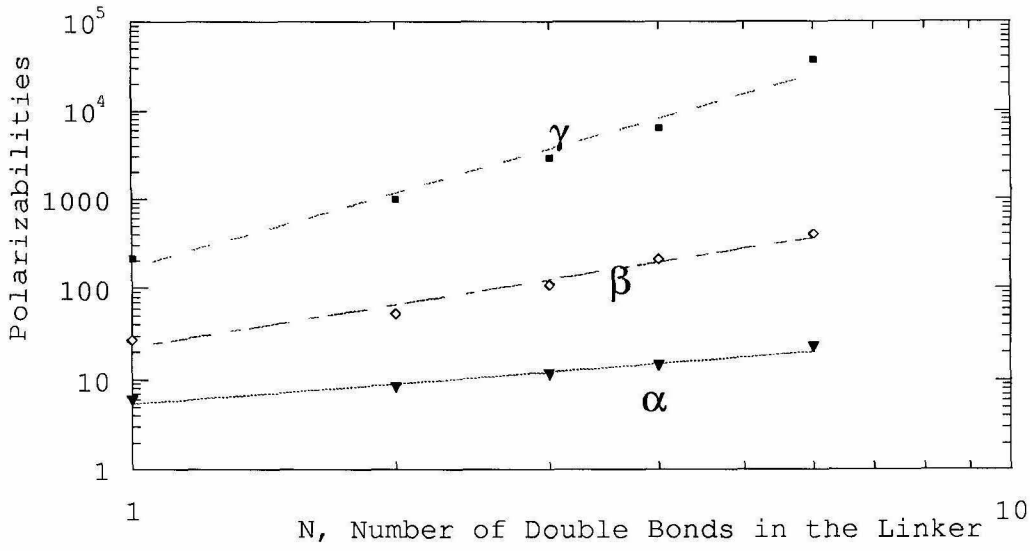

Figure 7.3: The dependence of α_{xx}, β_{xxx}, and γ_{xxxx} on $N = n + 1$, the number of double bonds in the linker. The solid lines are the least squares fit to the calculated values. The units are 10^{-23} esu for α_{xx}, 10^{-30} esu for β_{xxx}, and 10^{-37} esu for γ_{xxxx}.

n	0		1		2	
	no solvent	solvent	no solvent	solvent	no solvent	solvent
α_{xx}	59.40	60.88	82.87	82.85	113.4	111.0
α_{zz}	36.43	36.54	41.53	41.35	45.06	44.93
β_x	28.45	33.18	57.38	60.28	113.88	110.09
β_z	12.59	15.04	18.96	18.79	26.81	23.91
γ_{xxxx}	21.31	13.06	99.8	76.7	290.37	242.14

Table 7.3: Hyperpolarizabilities of molecules in Figure 7.1.a with $n = 0, 1, 2$. *no solvent* indicates a standard gas phase calculation using Jaguar, *solvent* indicates Jaguar/Solvate calculation using chloroform, the solvent used in the experiments. The units are 10^{-24} esu for α, 10^{-30} esu for β, and 10^{-36} esu for γ.

Basis Sets	6-31G	6-31G**
α_{xx}	82.87	83.73
α_{zz}	41.53	42.19
β_x	57.38	57.35
β_z	18.96	17.95
γ_{xxxx}	99.8	108.5

Table 7.4: Hyperpolarizabilities of molecules in Figure 7.1.a with $n = 1$ with different basis sets, 6-31G, 6-31G** (including polarization functions), and 6-31G++ (including diffuse functions). The units are 10^{-24} esu for α, 10^{-30} esu for β, and 10^{-36} esu for γ.

7.3 Calculational Details

7.3.1 Basis Sets

All calculations in Table 7.1 and Figure 7.2 were at the Hartree-Fock(HF) level using the 6-31G basis set with Jaguar (v2.01) program[8]. The results in Table 7.4 show that adding polarization functions to the basis (6-31G**) affects the results by 1% to 8%.

7.3.2 Geometry

Crystal structures have been reported[1] for molecules in Figure 7.1.a with $n = 2$ and 3. In estimating the structure for the other molecules, we used the geometries of the donor and acceptor from the crystal structure of $n = 3$. The bond lengths for the linker polyene were estimated from the structural data of $n = 2, 3$. We assumed that the polymer linker involves a resonance of the two valence bond (VB) configurations with an average bond length of 1.385Å and an average alternation of δr_n. The experiments lead to $\delta r_2 = 0.037$Å and $\delta r_3 = 0.049$Å, respectively, and we use[13] $\delta r = 0.11$Å for $n = +\infty$. Fitting these results leads to $\delta r_1 = 0.023$ Å and $\delta r_6 = 0.071$ Å; we assumed $\delta r_0 = 0.0$ Å.

For molecules in Figure 7.1.b, we assumed that the donor and linker have the same geometry as for those in Figure 7.1.a. The geometry of the acceptor of molecule

in Figure 7.1.b was obtained by geometry optimization at the HF/3-21G level.

We assumed that molecules in the gas phase and in the solid state have the same bond length. This is reasonable since the environment in a molecular crystal is far less polarized than in a polar solvent. For the solvation calculations, we also used the same geometry as for the gas phase. For a polar solvent, this could cause increased errors because of changes in the bond lengths of the linker. To estimate this effect, we used the VB-CT-S model[14,15] coupled with the experimental data. For molecule in Figure 7.1.a with $n = 3$, VB-CT-S estimates that δr_3 changes from 0.049Å to 0.040Å and β decreases by 7% [the parameters used were: $t = 0.88eV$, $V = 0.79eV$, $Q = 0.43$, $r_D = 3$Å, $r_A = 3$Å, $r_{DA} = 16$Å].

7.3.3 Hyperpolarizabilities

The polarizabilities were obtained by solving for the HF wavefunction in finite fields, $\vec{\mathcal{E}}$, and calculating the dipole moments, $\vec{\mu}$. Considering only the x components, this leads to

$$\mu(\mathcal{E}) = \mu(0) + \alpha\mathcal{E} + \beta\mathcal{E}^2 + \gamma\mathcal{E}^3 + \delta\mathcal{E}^4 + ... \tag{7.1}$$

The 5 point calculation uses the values $\mathcal{E} = 0, \pm\mathcal{E}_1, \pm\mathcal{E}_2$ with $\mathcal{E}_2 = 2\mathcal{E}_1$. This leads to

$$\alpha = \frac{2}{3\mathcal{E}_1}\left[\mu\left(\mathcal{E}_1\right) - \mu\left(-\mathcal{E}_1\right)\right] - \frac{1}{12\mathcal{E}_1}\left[\mu\left(\mathcal{E}_2\right) - \mu\left(-\mathcal{E}_2\right)\right] + O(\mathcal{E}_1^4), \tag{7.2}$$

$$\beta = \frac{2}{3\mathcal{E}_1^2}\left[\mu\left(\mathcal{E}_1\right) + \mu\left(-\mathcal{E}_1\right)\right] - \frac{1}{24\mathcal{E}_1^2}\left[\mu\left(\mathcal{E}_2\right) + \mu\left(-\mathcal{E}_2\right)\right] - \frac{5}{4}\frac{\mu(0)}{\mathcal{E}_1^2} + O(\mathcal{E}_1^4), \tag{7.3}$$

$$\gamma = -\frac{1}{6\mathcal{E}_1^3}\left[\mu\left(\mathcal{E}_1\right) - \mu\left(-\mathcal{E}_1\right)\right] + \frac{1}{12\mathcal{E}_1^3}\left[\mu\left(\mathcal{E}_2\right) - \mu\left(-\mathcal{E}_2\right)\right] + O(\mathcal{E}_1^2). \tag{7.4}$$

The magnitudes of the finite field were chosen to minimize the error in β. We used $\mathcal{E}_1 = 0.0024$ a.u. for $n = 6$, $\mathcal{E}_1 = 0.0048$ a.u. for $n = 1, 2, 3$, and $\mathcal{E}_1 = 0.0098$ a.u. for $n = 0$. To test the accuracy, we did two extra points $\pm\mathcal{E}_3$ with $\mathcal{E}_3 = 0.0192$ a.u. for molecule in Figure 7.1.a with $n = 1$. The β_{xxx} values for calculations with three points, five points, and seven points are 52.99×10^{-30} esu, 52.78×10^{-30} esu, and 52.58×10^{-30} esu respectively. This indicates that the numerical error in β is

less than 1%.

We also tested the accuracy by calculating the hyperpolarizabilities of various molecules and comparing with the results using Gaussian 92[16] (which uses analytic methods). The agreement between these two methods is excellent. Examples include: p-nitrobenzene, $\beta_{zzz} = -111$ a.u.(Gaussian 92) and $\beta_{zzz} = -111$ a.u. (Jaguar); and orthonitroaniline, $\beta_{zzz} = 189$ a.u.(Gaussian 92) and $\beta_{zzz} = 192$ a.u. (Jaguar). Additional details of the hyperpolarizability calculations will be published elsewhere.[7]

We also tested the accuracy by calculating the γ of benzene. The EFISH experiment[17] yields $\gamma = 1.5 \times 10^{-36}$ esu. Jaguar calculations at the HF/6-31G level lead to $\gamma = 1.1 \times 10^{-36}$ esu, in reasonable agreement with experiment.

7.4 References

1. Marder, S. R. *et al.*, *Science* **263**, 511 (1994).

2. Meyers, F.; Brédas, J. L.; Zyss, J., *J. Am. Chem. Soc.* **114**,2914 (1992).

3. Chopra, P.; Carlacci, L.; King, H. F.; Prasad, P. N., *J. Phys. Chem.* **93**, 7120 (1989).

4. Clays, K.; Hendrickx, E.; Triest, M.; Verbiest, T.; Persoons, A.; Dehu, C.; Brédas, J. L., *Science*, **262**, 1419 (1993).

5. Hurst, G. J. B.; Dupuis, M.; Clementi, E.,*J. Chem. Phys.* **89**, 385 (1988).

6. Sim, F.; Chin, S.; Dupuis, M.; Rice, J. E., *J. Phys. Chem.* **97**, 1158 (1993).

7. Marten, B.; Lu, D.; Cao, Y.; Ringnalda, M. N.; Goddard, W. A. III; Friesner, R. A., in preparation.

8. Ringnalda, M. N.; Langlois, J.-M.; Greeley, B. H.; Murphy, R. B.; Russo, T. V.; Cortis, C.; Muller, R. P.; Marten, B.; Donnelly, R. E. Jr.; Mainz, D. T.; Wright, J. R.; Pollard, W. T.; Cao, Y.; Won, Y.; Miller, G. H.; Goddard, W.

A. III; Friesner, R. A., Jaguar v2.01, Schrödinger, Inc., Pasadena, California, 1994.

9. We did not calculate the $\gamma_{xxyy}, \gamma_{xxzz}$ and γ_{yyzz} components because the electric fields were applied only along the chain direction. Since the dominant contribution to γ is from γ_{xxxx}, the other components can be neglected.

10. Tannor, D.; Marten, B.; Murphy, R.; Friesner, R. A.; Sitkoff, D.; Nicholls, A.; Ringnalda, M.; Goddard, W. A. III; Honig, B., *J. Am. Chem. Soc.* **116**, 11875 (1994).

11. Marten, B.; Sitkoff, D.; Kim, K.; Murphy, R.; Ringnalda, M.; Friesner, R. A.; Honig, B.; in preparation.

12. Nicholls, A.; Honig, B., *J Comput. Chem.* **12**, 435-445 (1991).

13. Villar, H. O.; Dupuis, M.; Watts, J. D.; Hurst, G. J. B.; Clement i, E., *J. Chem. Phys.*, **88**, 1003 (1987).

14. Lu, D.; Chen, G.; Perry, J.; Goddard, W. A. III, *J. Am. Chem. Soc.*, **116**, 10679 (1994).

15. Chen, G.; Lu, D.; Goddard, W. A. III, *J. Chem. Phys.*, **101**, 5860 (1994).

16. Frisch, M. J.; Trucks, G. W.; Schlegel, H. B.; Gill, P. M. W.; Johnson, B. G.; Wong, M. W.; Foresman, J. B.; Robb, M. A.; Head-Gordon, M.; Replogle, E. S.; Gomperts, R.; Andres, J. L.; Raghavachari, K.; Binkley, J. S.; Gonzalez, C.; Martin, R. L.; Fox, D. J.; Defrees, D. J.; Baker, J.; Stewart, J. P.; Pople, J. A., Gaussian, Inc., Pittsburgh, PA, 1993.

17. Karna, S. P.; Talapatra, G. B.; Prasad, P. N., *J.Chem.Phys.*, **95**,5873 (1991).

Appendix A Evaluation of Matrix Elements

To illustrate the evaluation of (2.6) and (2.7), consider the butadiene monomer (Figure A.1), where

$$\Theta_p^{LUMO} = \sum_{i=1}^{4} C_{ip}^{LUMO} \chi_i^p = 0.602\chi_1^p - 0.372\chi_2^p - 0.372\chi_3^p + 0.602\chi_4^p \tag{A.1}$$

$$\Theta_p^{HOMO} = \sum_{i=1}^{6} C_{ip}^{HOMO} \chi_i^p = 0.602\chi_1^p + 0.372\chi_2^p - 0.372\chi_3^p - 0.602\chi_4^p \tag{A.2}$$

and χ_1^p are the four atomic orbitals on monomer p.

For electron hops this leads to

$$\langle \phi_{pq} | \mathcal{H} | \phi_{p,q+1} \rangle = \langle \theta_{p+q}^{LUMO} | h | \theta_{p+q+1}^{LUMO} \rangle = \langle 0.602\chi_4^p | H | 0.602\chi_1^{p+1} \rangle = -0.36\beta \tag{A.3}$$

where β is the resonance integral between two adjacent sp^2 carbon centers. Thus (2.3) becomes

$$t = 0.36\beta. \tag{A.4}$$

For excitation to adjacent sites we obtain

$$\begin{aligned} &\langle \phi_{p0} | \mathcal{H} | \phi_{p1} \rangle \\ &\quad = \langle \theta_p^{HOMO} \theta_p^{HOMO} | \mathcal{H} | \frac{\left(\theta_p^{HOMO} \theta_{p+1}^{LUMO} + \theta_{p+1}^{LUMO} \theta_p^{HOMO} \right)}{\sqrt{2}} \rangle \\ &\quad = \frac{-2}{\sqrt{2}} * 0.36\beta \\ &\quad = -\sqrt{2}t. \end{aligned} \tag{A.5}$$

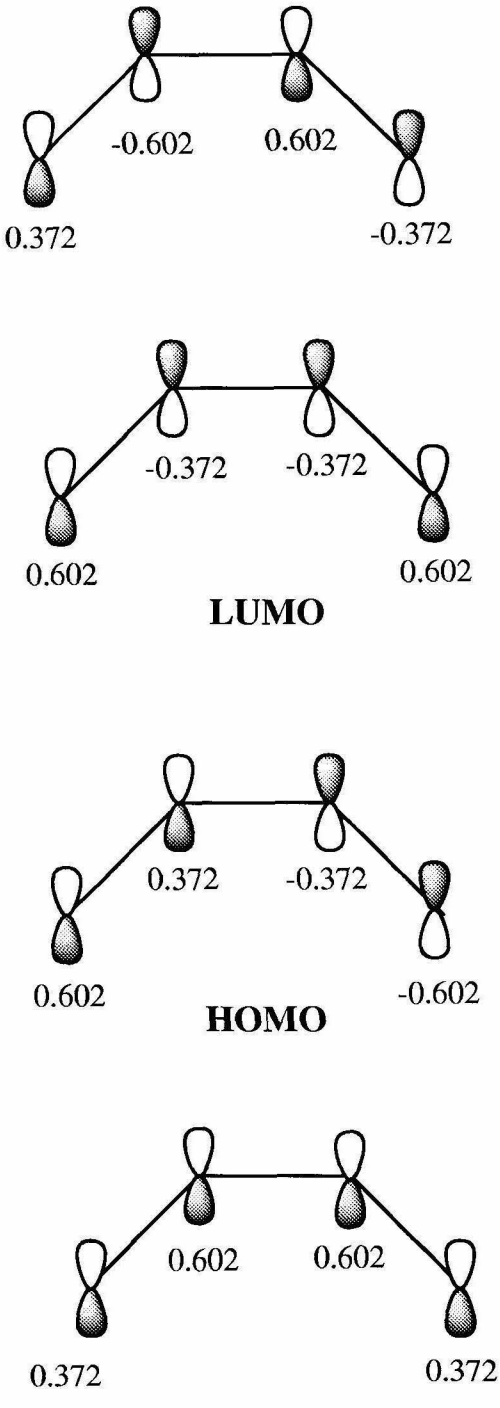

Figure A.1: The MO of butadiene. The wavefunction of LUMO is $0.602\chi_1 + 0.372\chi_2 - 0.372\chi_3 - 0.602\chi_4$. The wavefunction of HOMO is $0.602\chi_1 - 0.372\chi_2 - 0.372\chi_3 + 0.602\chi_4$, where χ_i are the four atomic orbitals.

Similarly

$$\langle \phi_{p0} | \mathcal{H} | \phi_{p,-1} \rangle = \sqrt{2}t. \tag{A.6}$$

Thus (2.5) leads to

$$a = \sqrt{2}. \tag{A.7}$$

More generally we can write the coefficient of the outer orbital on θ^{LUMO} as C_l and on θ^{HOMO} as C_h to obtain

$$t = \left(C_l^2 + C_h^2\right)\beta, \tag{A.8}$$

$$at = \sqrt{2}C_l C_h \beta. \tag{A.9}$$

Thus

$$a = \frac{\sqrt{2}C_l C_h}{(C_l^2 + C_h^2)}. \tag{A.10}$$

If $C_l = C_h$, then

$$a = \sqrt{2}. \tag{A.11}$$

A simple approximation is $C_l \approx 1/\sqrt{M}$ and $C_h \approx 1/\sqrt{M}$ where M is the number of atoms ($M = 4$ for butadiene) so that

$$a \approx \sqrt{2}. \tag{A.12}$$

Even if $C_l = 2C_h$, we obtain $a = 0.8\sqrt{2}$.

Appendix B Application of Perturbation Theory

The ground state energy E^0 can be decomposed as follows:

$$E^0 = \sum_{i=0}^{\infty} \Delta_i \tag{B.1}$$

where

$$\Delta_0 = E_0 \tag{B.2}$$

$$\Delta_1 = \langle 0|W|j\rangle \tag{B.3}$$

$$\Delta_2 = \sum_{j\neq 0} \frac{|\langle 0|W|0\rangle|^2}{E_0 - E_j} \tag{B.4}$$

$$\Delta_3 = \sum_{j\neq 0} \langle 0|W|j\rangle\langle j|0;2\rangle \tag{B.5}$$

$$\Delta_n = \sum_{j\neq 0} \langle 0|W|j\rangle\langle j|0;n-1\rangle - \sum_{\nu=2}^{n-2} \Delta_\nu \langle 0|0;n-\nu\rangle \tag{B.6}$$

Here we use the notation

$$\langle 0|0;1\rangle = 0 \tag{B.7}$$

$$\langle l|0;1\rangle = \frac{\langle l|W|0\rangle}{E_0 - E_l} \qquad (l \neq 0) \tag{B.8}$$

$$\langle 0|0;2\rangle = -\frac{1}{2}\sum_j \langle j|0;1\rangle^2 \tag{B.9}$$

$$\langle l|0;2\rangle = -\sum_j \frac{\langle l|W|j\rangle\langle|0;1\rangle}{E_l - E_0} - \frac{\langle l|W|0\rangle\langle 0|W|0\rangle}{(E_l - E_0)^2} \qquad (l \neq 0) \tag{B.10}$$

$$\langle 0|0;n\rangle = -\frac{1}{2}\sum_{\nu=1}^{n-1}\sum_j \langle j|0;\nu\rangle\langle j|0;n-\nu\rangle \tag{B.11}$$

$$\langle l|0;n\rangle = -\sum_j \frac{\langle l|W|j\rangle\langle|0;n-1\rangle}{E_l - E_0} + \sum_{\nu=1}^{n-1} \frac{\Delta_\nu \langle l|0;n-\nu\rangle}{E_l - E_0} \qquad (l \neq 0). \tag{B.12}$$

Substituting (B.1), (B.2), and (B.3) into (2.19)-(2.21) leads to

$$\alpha_{zz} = \frac{4a^2e^2R_0^2\eta^2}{V} \sum_{i=0}^{\infty} A_{2i}\eta^{2i} \tag{B.13}$$

$$\beta_{zzz} = 0 \tag{B.14}$$

$$\gamma_{zzzz} = \frac{8a^2e^4R_0^4\eta^2}{V^3} \sum_{i=0}^{\infty} G_{2i}\eta^{2i} \tag{B.15}$$

where

$$\eta = \frac{t}{V} \tag{B.16}$$

$$\begin{aligned}
A_0 &= 1 \\
A_2 &= 11 - 8a^2) \approx -5 \\
A_4 &= 80 - 144a^2 + 60a^4 \approx 32 \\
A_6 &= 490 - 1488a^2 + 1456a^4 - 448a^6 \approx -396 \\
A_8 &= 2730 - 1194a^2 + 19260a^4 - 13440a^6 + 3360a^8 \approx 6608 \\
A_{10} &= 14322 - 82776a^2 + 189816a^4 - 214720a^6 + 118800a^8 - 25344a^{10}) \approx -19934
\end{aligned} \tag{B.17}$$

$$\begin{aligned}
G_0 &= 1 \\
G_2 &= 57 - 18a^2 \approx 21 \\
G_4 &= 1170 - 1104a^2 + 224a^4 \approx -142 \\
G_6 &= 15403 - 27390a^2 + 14760a^4 - 2400a^6 \approx 463 \\
G_8 &= 157564 - 433488a^2 + 420816a^4 - 168960a^6 + 23760a^8 \approx 2332 \\
G_{10} &= 1368796 - 5233928a^2 + 7684768a^4 - 5372640a^6 + 1777776a^8 - 224224a^{10} \approx -71860
\end{aligned}$$

$$G_{12} = 10602592 - 52717056a^2 + 106140480a^4 - 110176640a^6 + 61850880a^8 - 17751552a^{10} + 2050048a^{12} \approx 1084778. \tag{B.18}$$

In each case we have substituted $a \approx \sqrt{2}$.

The above coefficients are for long chains. If the chain length is small, the coefficients are different. For perturbation theory in which V_n is not constant, we find that the expressions for A_0, G_0 are just functions of t, V_1, the expressions for A_2, G_2 are functions of t, V_1, V_2, the expressions for A_4, G_4 are functions of t, V_1, V_2, V_3, etc. When the order of expansion increases, the coefficients in the Hamiltonian matrix involved in the expression expand gradually along the diagnal. Thus we can consider that A_0, G_0 are contributions from charge transfer to the nearest neighbor site, A_2, G_2 are contributions from charge transfer to the second nearest neighbor sites, etc. The convergence length of the polynomial should correspond to the saturation length. In order to get the accurate values of $\alpha_{zz}, \gamma_{zzzz}$ from the polynomial, we must calculate to the N terms where $2N$ is the saturation length.

Appendix C The Evaluation of t and V

We can estimate the values of t and V from the bandgap and the conduction bandwidth. The eigenvalues E of the Hamiltonian matrix (2.1) satisfy the difference equation:

$$-tb_{n-1} + (V_n - E)b_n - tb_{n+1} = 0 \tag{C.1}$$

When n is large, V_n approaches the constant value $IP - EA$. In this case (C.1) becomes a homogeneous linear difference equation[17] with the solutions

$$b_n = C_1\lambda_1^n + C_2\lambda_2^n \tag{C.2}$$

where λ_1 and λ_2 are solutions of

$$-t\lambda^2 + (V - E)\lambda - t = 0 \tag{C.3}$$

$$\lambda = \frac{V - E}{2t} \pm \sqrt{(\frac{V - E}{2t})^2 - 1} \tag{C.4}$$

when

$$|V - E| < 2t. \tag{C.5}$$

This leads to complex conjugate roots (oscillating b_n). These states correspond to the conduction states, leading to the bandwidth of the conduction band

$$B = 4t. \tag{C.6}$$

The upper bound of the conduction band is $V + 2t$ and the lower bound is $V - 2t$. When n is small, V_n is smaller than V. That will decrease the lower bound $V - 2t$. Because of the coupling between the ground state and excited state, the ground state will lower a little bit ($-\frac{2a^2t^2}{V}$), and the excited state will be elevated a little bit

$(-\frac{2a^2t^2}{V})$. Combining these two effects together, the bandgap is approximately

$$E_g = V - 2t \tag{C.7}$$

and the bandgap is

$$B = 4t. \tag{C.8}$$

Appendix D Evaluation of the Temperature Effect

Suppose that q_0 and ϕ_0 are the optimum vibrational and torsional coordinates (at absolute zero temperature). Since the torsional energy $E_t(\phi)$ and the charge transfer matrix element $t(\phi)$ are even functions of $\phi - \phi_0$, the Taylor expansions of $E_t(\phi)$ and $t(\phi)$ lead to

$$E_t(\phi) = E_t(\phi_0) + \frac{1}{2}E_{t1}(\phi - \phi_0)^2 + O((\phi - \phi_0)^4) \tag{D.1}$$

$$t(\phi) = t(\phi_0) + \frac{1}{2}t_1(\phi - \phi_0)^2 + O((\phi - \phi_0)^4) \tag{D.2}$$

The vibrational energy becomes

$$\begin{aligned}
E_v(q,\phi) &= \frac{1}{2}V(q) + \frac{1}{2}\lambda\left(q - q_{VB}^0\right)^2 - \frac{1}{2}\sqrt{V^2(q) + 4t^2(\phi)} \\
&= \frac{1}{2}V(q) + \frac{1}{2}\lambda\left(q - q_{VB}^0\right)^2 - \frac{1}{2}\sqrt{V^2(q) + 4t^2(\phi_0) + 4t_1t(\phi_0)(\phi - \phi_0)^2 + O\left[(\phi - \phi_0)^4\right]} \\
&= \frac{1}{2}V(q) + \frac{1}{2}\lambda\left(q - q_{VB}^0\right)^2 - \frac{1}{2}\sqrt{V^2(q) + 4t^2((\phi_0))}\left[1 + \frac{4t_1t(\phi_0)(\phi - \phi_0)^2}{V^2(q) + 4t^2(\phi_0)}\right]^{\frac{1}{2}} \\
&\qquad + O\left[(\phi - \phi_0)^4\right] \\
&= \frac{1}{2}V(q) + \frac{1}{2}\lambda\left(q - q_{VB}^0\right)^2 - \frac{1}{2}\sqrt{V^2(q) + 4t^2(\phi_0)} - \frac{t_1t(\phi_0)(\phi - \phi_0)^2}{\sqrt{V^2(q) + 4t^2(\phi_0)}} \\
&\qquad + O\left[(\phi - \phi_0)^4\right]
\end{aligned} \tag{D.3}$$

The first three terms describe the ground state energy *without* torsional contributions. Taking the Taylor expansion of these three terms about $q - q_0$ leads to

$$E_v(q) = E_v(q_0) + \frac{1}{2}\lambda_q(q - q_0)^2 + O\left[(q - q_0)^4\right] \tag{D.4}$$

where q_0 is the equilibrium position

$$q_0 = \frac{1}{2}(q^0_{VB} + q^0_{CT}) + \frac{1}{2}\left(q^0_{VB} - q^0_{CT}\right)\frac{V}{\sqrt{V^2 + 4t^2(\phi_0)}} \tag{D.5}$$

and

$$\lambda_q = \frac{\partial^2 E_v(q)}{\partial^2 q}\,|_{q=q_0} = \lambda\left\{1 - \frac{t^2(\phi_0)\lambda\left(q^o_{VB} - q^o_{CT}\right)^2}{\left[V^2(q_0) + t^2(\phi_0)\right]^{\frac{3}{2}}}\right\}. \tag{D.6}$$

Thus

$$\begin{aligned} E_v(q,\phi) = E_v(q_0) + \frac{1}{2}\lambda_q\,(q-q_0)^2 - \frac{t_1 t(\phi_0)(\phi-\phi_0)^2}{\sqrt{V^2(q_0) + 4t^2(\phi_0)}} \\ + O\left[(\phi-\phi_0)^4 + (q-q_0)^4 + (\phi-\phi_0)^2(q-q_0)^2\right]. \end{aligned} \tag{D.7}$$

The total energy becomes

$$\begin{aligned} E &= E_v(q,\phi) + E_t(\phi) \\ &= E_v(q_0) + E_t(\phi_0) + \frac{1}{2}\lambda_q\,(q-q_0)^2 + \frac{1}{2}\left[E_{t1} - \frac{2t_1 t(\phi_0)}{\sqrt{V^2(q_0) + 4t^2(\phi_0)}}\right](\phi-\phi_0)^2 \\ &\quad + O\left[(\phi-\phi_0)^4 + (q-q_0)^4 + (\phi-\phi_0)^2(q-q_0)^2\right] \\ &= E_v(q_0) + E_t(\phi_0) + \frac{1}{2}\lambda_q\,(q-q_0)^2 + \frac{1}{2}E_\phi(\phi-\phi_0)^2 \\ &\quad + O\left[(\phi-\phi_0)^4 + (q-q_0)^4 + (\phi-\phi_0)^2(q-q_0)^2\right]. \end{aligned} \tag{D.8}$$

Here

$$E_\phi = E_{t1} - \frac{2t_1 t(\phi_0)}{\sqrt{V^2(q_0) + 4t^2(\phi_0)}} \tag{D.9}$$

The high order terms can be ignored since we assume the vibrational energy and rotational barrier are much higher than the thermal energy kT. This leads to

$$< p > = \frac{1}{Z}\int_{-\infty}^{+\infty} dq \int_{-\pi}^{\pi} d\phi p(\phi, q) exp\left[-\frac{E}{kT}\right]$$

$$= \frac{1}{Z}\int_{-\infty}^{+\infty} dq \int_{-\pi}^{\pi} d\phi \left[p(\phi_0, q_0) + \frac{\partial p}{\partial q}(q - q_0) + \frac{\partial p}{\partial \phi}(\phi - \phi_0) + \right.$$
$$\left. \frac{1}{2}\frac{\partial^2 p}{\partial^2 q}(q - q_0)^2 + \frac{\partial^2 p}{\partial q \partial \phi}(q - q_0)(\phi - \phi_0) + \frac{1}{2}\frac{\partial^2 p}{\partial^2 \phi}(\phi - \phi_0)^2 \right] exp\left[-\frac{E}{kT} \right]. \tag{D.10}$$

Evaluating each term in the above equation leads to

$$\frac{1}{Z}\int_{-\infty}^{+\infty} dq \int_{-\pi}^{\pi} d\phi p(\phi_0, q_0) exp\left[-\frac{E}{kT} \right] = p(\phi_0, q_0) \tag{D.11}$$

$$\frac{1}{Z}\int_{-\infty}^{+\infty} dq \int_{-\pi}^{\pi} d\phi [\frac{\partial p}{\partial q}(q - q_0) + \frac{\partial p}{\partial \phi}(\phi - \phi_0)] exp\left[-\frac{E}{kT} \right] = 0 \tag{D.12}$$

$$\frac{1}{Z}\int_{-\infty}^{+\infty} dq \int_{-\pi}^{\pi} d\phi \frac{\partial^2 p}{\partial q \partial \phi}(q - q_0)(\phi - \phi_0) exp\left[-\frac{E}{kT} \right] = 0 \tag{D.13}$$

$$\frac{1}{Z}\int_{-\infty}^{+\infty} dq \int_{-\pi}^{\pi} d\phi \, \frac{1}{2}\frac{\partial^2 p}{\partial^2 q}(q - q_0)^2 exp\left[-\frac{E}{kT} \right] = \frac{\int_{-\infty}^{+\infty} dq \frac{1}{2}\frac{\partial^2 p}{\partial^2 q}(q - q_0)^2 exp\left[-\frac{\lambda_q (q - q_0)^2}{2kT} \right]}{\int_{-\infty}^{+\infty} dq \, exp\left[-\frac{\lambda_q (q - q_0)^2}{2kT} \right]}. \tag{D.14}$$

Letting

$$x = \sqrt{\frac{\lambda_q}{2kT}}(q - q_0) \tag{D.15}$$

the above equation becomes

$$\frac{\frac{1}{2}\frac{\partial^2 p}{\partial^2 q}(\frac{2kT}{\lambda_q})^{\frac{3}{2}} \int_{-\infty}^{+\infty} dx \, x^2 e^{-x^2}}{(\frac{2kT}{\lambda_q})^{\frac{1}{2}} \int_{-\infty}^{+\infty} dx \, e^{-x^2}} = \frac{kT}{2\lambda_q}\frac{\partial^2 p(q_0, \phi_0)}{\partial^2 q}. \tag{D.16}$$

Similarly,

$$\frac{1}{Z}\int_{-\infty}^{+\infty} dq \int_{-\pi}^{\pi} d\phi \frac{1}{2}\frac{\partial^2 p}{\partial^2 \phi}(\phi - \phi_0)^2 e^{-\frac{E}{kT}} = \frac{kT}{2E_\phi}\frac{\partial^2 p(q_0, \phi_0)}{\partial^2 \phi}. \tag{D.17}$$

The average value of p then becomes

$$< p >= p(q_0, \phi_0) + \left[\frac{1}{2\lambda_q}\frac{\partial^2 p(q_0, \phi_0)}{\partial^2 q} + \frac{1}{2E_\phi}\frac{\partial^2 p(q_0, \phi_0)}{\partial^2 \phi} \right] kT \tag{D.18}$$

which was used in (5.17).